TRIBHUVAN UNIVERSITY
INSTITUTE OF ENGINEERING
PULCHOWK CAMPUS

Design and Fabrication of a Phase Change Material (PCM) Based Heat Storage Setup

By:

Gaurav Bhattarai (076BME013)

Gaurav Kattel (076BME014)

Onyx Dhakal (076BME026)

Sagar Neupane (076BME035)

A FINAL YEAR PROJECT REPORT SUBMITTED TO THE DEPARTMENT OF MECHANICAL AND AEROSPACE ENGINEERING IN PARTIAL FULFILLMENT OF THE REQUIREMENT FOR THE BACHELOR'S DEGREE IN MECHANICAL ENGINEERING

DEPARTMENT OF MECHANICAL AND AEROSPACE ENGINEERING
LALITPUR, NEPAL

April, 2024

COPYRIGHT

TRIBHUVAN UNIVERSITY

INSTITUTE OF ENGINEERING, PULCHOWK CAMPUS

DEPARTMENT OF MECHANICAL AND AEROSPACE ENGINEERING

The undersigned certify that they have read, and recommended to the Institute of Engineering for acceptance, a project report entitled "DESIGN AND FABRICATION OF PCM HEAT STORAGE SETUP" submitted by Gaurav Bhattarai, Gaurav Kattel, Onyx Dhakal and Sagar Neupane in partial fulfillment of the requirements for the degree of Bachelor of Mechanical Engineering.

Supervisor, Navin Kumar Jha

Assistant Professor

Department of Mechanical and Aerospace Engineering

IOE, Pulchowk Campus

External Examiner, Er. Rudra Mani Ghimire

Deputy Manager

Civil Aviation Authority of Nepal

Tribhuvan University
Institute of Engineering
Department of Mechanical and Aerospace Engineering
Pulchowk Campus

Committee Chairperson, Dr. Sudip Bhattrai

Assistant Professor

Head, Department of Mechanical and Aerospace Engineering

IOE, Pulchowk Campus

Date: 2024/04/09

ABSTRACT

This report outlines a significant project focused on developing and testing two different methods to store heat using special materials called phase change materials (PCMs) within heat exchangers. Initially, the project started with basic designs for heat exchangers such as double pipe and shell & tube configurations. As the project progressed, advanced features like radial fins and PCM integration were incorporated to improve heat exchange efficiency and storage capacity.

Using ANSYS Fluent, detailed computational fluid dynamics (CFD) and thermal simulations were conducted to understand how heat transfers within these systems. These simulations provided valuable insights into heat transfer dynamics, guiding the refinement of designs. Subsequently, one of the shell & tube PCM heat storage setups was fabricated and tested to validate theoretical models. The experimental results closely matched predictions, confirming the effectiveness of the design approach.

Comparing the two configurations, similar rates of heat storage were found, with the shell & tube design offering advantages in simplicity and cost-effectiveness. These findings have important implications for various practical applications, including solar power generation, HVAC systems, and industrial processes, highlighting the scalability and adaptability of the designs.

Looking ahead, future efforts will focus on optimizing these systems to maximize heat storage efficiency and integrating them with renewable energy sources to enhance energy utilization and grid stability. Overall, this project represents a significant advancement in thermal energy storage technologies, laying the groundwork for further progress in sustainable energy solutions.

ACKNOWLEDGEMENT

We would like to express our sincere gratitude to the Department of Mechanical and Aerospace Engineering, Pulchowk Campus, and specifically to Dr. Sudip Bhattarai, the Head of the Department, for giving us this invaluable opportunity to learn more about the project-based and practical aspects of mechanical engineering through our project on design and fabrication of PCM-based heat storage setup.

We express our sincere appreciation to Mr. Navin Kumar Jha, our project supervisor, for his unwavering support and invaluable guidance throughout this endeavor. His wealth of knowledge, steadfast support, and constructive feedback have significantly contributed to the growth and enhancement of our expertise in this specialized area. We are deeply grateful for his dedication and mentorship, which have been instrumental in steering our project towards success.

Furthermore, we would like to extend our thanks to all our classmates and seniors for their collaborative efforts and insights, which have enriched our learning experience. The collaborative environment within the department has fostered a sense of camaraderie and mutual support, significantly shaping our comprehension of the subject matter and reinforcing the importance of teamwork in achieving common goals. Additionally, we express our gratitude to the Incubation Centre at IOE Pulchowk Campus for providing the necessary facilities and space required for the experimentation phase of our project. Their support has been invaluable in facilitating our hands-on learning and practical exploration within a conducive environment.

TABLE OF CONTENTS

LIST OF FIGURES

LIST OF TABLES

ABBREVIATIONS

CAD	Computer Aided Design
CFD	Computational Fluid Dynamics
DPHE	Double pipe heat exchanger
HTF	Heat transfer fluid
HVAC	Heating Ventilating and Air Conditioning
LHTES	Latent heat thermal energy storage
LMTD	Logarithmic Mean Temperature Difference
LPM	Liters per Minute
MWCNT	Multi-walled carbon nanotubes
NEPCM	Nanoparticle Enhanced Phase Change Material
PCM	Phase Change Material
RT	Rubitherm

SYMBOLS

h	Convective Heat Transfer Coefficient
ρ	Density
μ	Dynamic Viscosity
Gr	Grashof Number
Q	Heat Transfer Rate
ν	Kinematic Viscosity
L_f	Latent Heat of Fusion
Nu	Nusselt Number
U	Overall Heat Transfer Coefficient
Pr	Prandtl Number
ΔP	Pressure drop
Ra	Rayleigh Number
Re	Reynolds Number
C_p	Specific Heat Capacity
k	Thermal Conductivity
α	Thermal Diffusivity
β	Thermal Expansion Coefficient

CHAPTER ONE: INTRODUCTION

1.1 Background

Heat exchange systems play a vital role in managing thermal energy efficiently across different fields and applications. As industries aim to cut down on energy use, boost process efficiency, and reduce environmental impact, the demand for effective heat exchange systems has grown. These systems transfer heat between different mediums, enabling crucial functions like heating, cooling, and temperature control in various processes and equipment. One popular example is the double pipe heat exchanger, which consists of two pipes where hot fluid flows through one and cold fluid flows through the other. Heat moves from the hot fluid to the cold one through the pipe walls, allowing for efficient heat transfer. Double pipe heat exchangers are used widely in HVAC systems, chemical processes, and power generation due to their effectiveness.

Apart from heat exchange systems, there's also a rising need for heat storage in industries and systems requiring a reliable heat source. Heat storage systems can store thermal energy, ensuring it's available when needed. This is especially useful in areas like residential heating, industrial processes, and renewable energy systems. Technologies like Phase Change Materials (PCMs) have been developed to improve heat storage efficiency. PCMs can store and release heat during phase transitions. By combining heat exchangers with PCM-based heat storage systems, industries can manage heat supply effectively, reduce energy waste, and improve overall system performance.

1.1.1 Heat exchangers

Heat exchangers are devices that move heat between fluids at different temperatures without them mixing. They're used a lot in HVAC systems and industries. Their main job is to move thermal energy from one fluid to another.

This transfer happens through convection between the fluids and conduction through the walls between them. The walls are made of heat-conductive material and keep the fluids separate. Usually, the fluids flow through metal tubes or plates.

A double-pipe heat exchanger is the simplest kind. One fluid goes through a small pipe (usually hot fluid), and the other (cold) goes between two pipes. There are two types based on how the fluids move: parallel flow and counterflow. In parallel flow, both fluids go in the same direction, while in counterflow, they go in opposite directions.

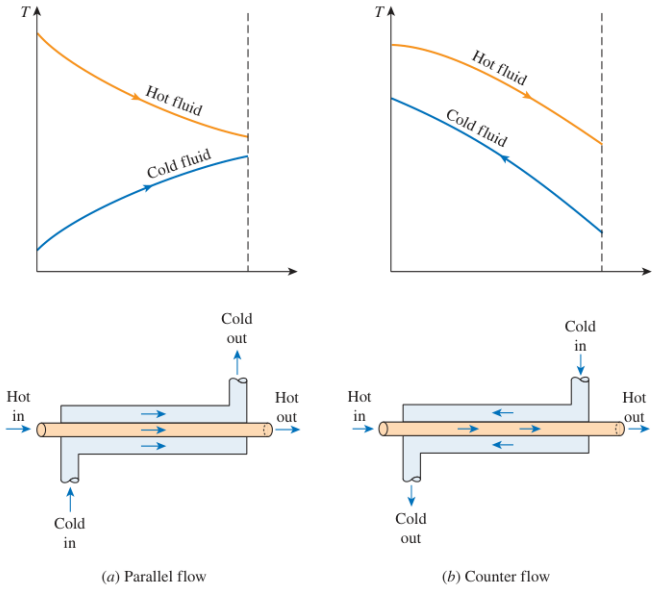

Figure 1.1: Types of double pipe heat exchanger (Yunus A Çengel, 2019)

1.1.2 Heat storage technology

In many different fields and applications, heat storage technology is essential for the effective management and use of thermal energy. Heat storage encourages energy conservation and reduces reliance on conventional energy sources. It involves capturing and storing excess heat for later use. Three fundamental approaches for the heat storage are:

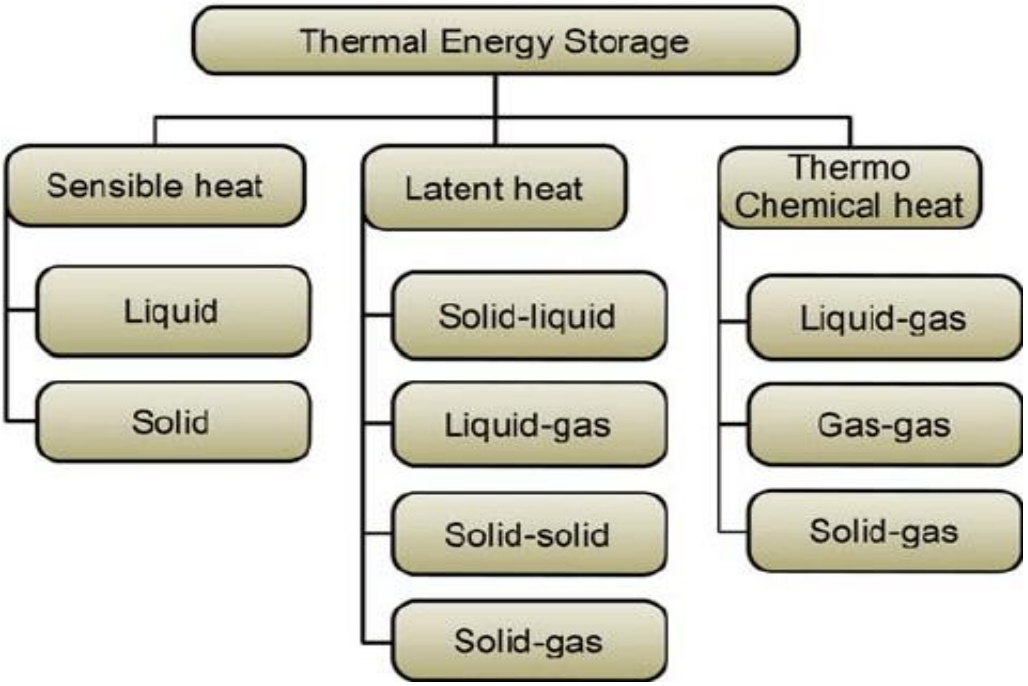

Figure 1.2: Types of heat storage technologies (Lavinia Socaciu, 2012)

1.1.2.1 Sensible Heat Storage

Sensible heat storage involves the storage of thermal energy by increasing the temperature of a material. This technology relies on the principle that the amount of heat stored in a substance is directly proportional to its mass and the change in its temperature. Common materials used for sensible heat storage include water, rocks, concrete.

1.1.2.2 Latent Heat Storage

Latent heat storage aims to capture the energy brought on by a material's phase transitions. A substance absorbs or releases a considerable amount of energy while transitioning from one phase to another, such as from solid to liquid or from liquid to gas, while maintaining a steady temperature. Latent heat storage systems utilize phase change materials like paraffin wax or salt hydrates.

1.1.2.3 Thermochemical Storage

Heat gets stored using reversible chemical reactions in a process called thermochemical storage. In this process, a material reacts with a heat source, soaking up or letting out heat. Later on, this stored heat can be released by undoing the chemical reaction. Thermochemical storage is good because it can store a lot of energy in a small space and keep it for a long time without losing much. Metal hydrides, metal oxides, and salts are some materials often used for this type of storage.

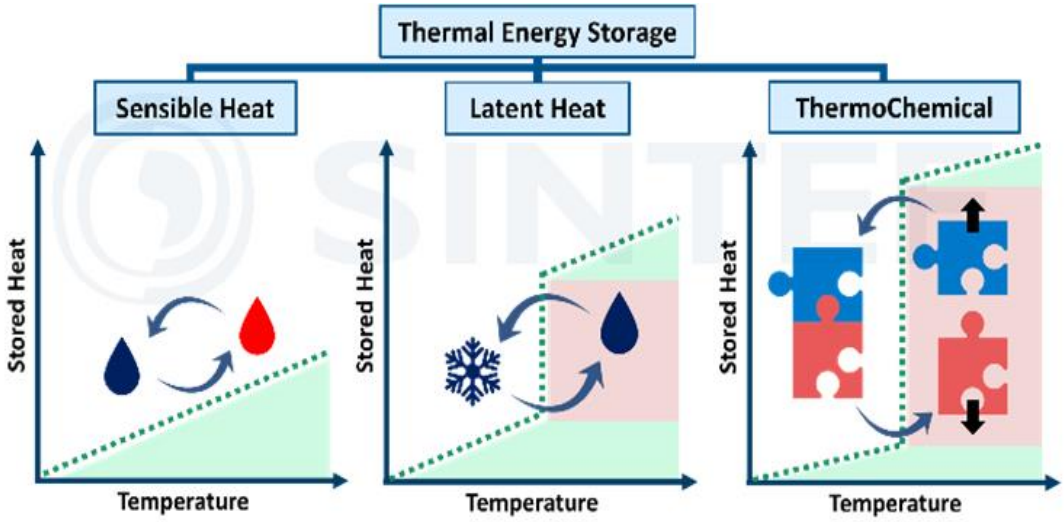

Figure 1.3: Classification of thermal energy storage (TES) systems and the heat stored with temperature variation (Jorge Salgado Beceiro, 2022)

1.1.3 Latent Heat Storage using Phase Change Materials (PCM)

The latent heat storage system, also referred to as a phase change heat storage system, is based on the idea of storing and releasing thermal energy during a material's phase transition. In these systems, the phase change material (PCM) switches between solid and liquid states, or between liquid and gas states, absorbing or releasing latent heat in the process. A typical latent heat system operates as follows:

a) Charging (Heat absorption)

Initially, the PCM material is in a solid state in low temperatures. A heat source, such as a hot liquid or an electrical heater, transfers heat to the PCM. As the PCM's temperature rises, it finally achieves its phase change temperature and begins transitioning to liquid phase.

b) Phase change

The PCM transforms from a solid to a liquid once it reaches its melting point. During the phase change, the PCM material absorbs a significant amount of heat energy. The temperature of the material remains almost constant throughout the phase change process. The heat absorbed in this process is known as latent heat.

c) Storage of latent heat

Until the PCM completely changes to a liquid form, it continues to absorb heat without a significant rise in temperature. It stores the latent heat energy that was absorbed during the phase change. It can store a large quantity of energy in a small space thereby acting as a thermal energy reservoir.

d) Discharging (Heat release)

The process of extracting heat from PCM material is known as discharge process. Heat from the latent heat system is typically extracted by flowing a cooler fluid or air over the PCM layer. As the PCM releases the stored latent heat, its temperature decreases, and it begins to solidify. This latent heat release and phase change process from liquid to solid also happens at an almost constant temperature. The heat released can be utilized for various applications such as space heating, water heating and so on.

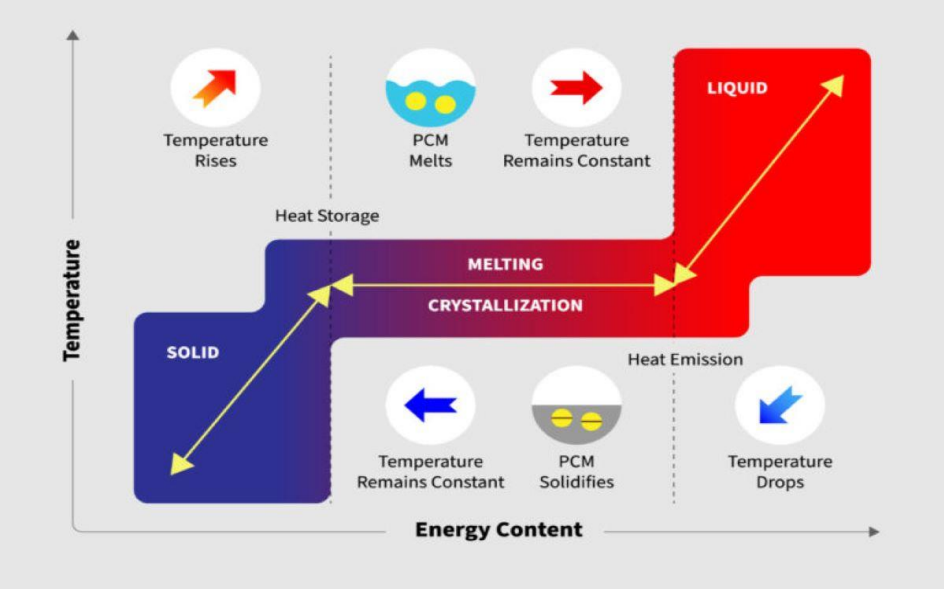

Figure 1.4: Heat storage and heat release mechanism in PCMs (https://thermtest.com/phase-change-material-pcm, 2023)

Figure 1.5: Phase change material (PCM) (https://en.wikipedia.org/wiki/Phase-change_material, 2023)

1.2 Problem Statement

Efficiently storing and using heat energy is a big challenge in many areas and homes because old methods have some problems. These problems include not having enough places to store heat, not being able to move heat around well, and losing heat energy. This all ends up costing more money and hurting the environment.

The introduction of Phase Change Materials (PCMs) provide a good solution. PCMs are special because they can store and let out a lot of heat energy when they change from one phase to another, like from solid to liquid. They can keep heat at a steady temperature until they change phase, which helps store and release heat effectively. PCMs are used in solar energy systems, keeping buildings warm, and reusing wasted heat from factories. They make things more energy efficient, reduce harm to the environment, and save money. So, using PCMs helps fix the problems with old methods and makes storing and using heat better.

1.3 Objectives

1.3.1 Main Objective

The main goal of this project is to compare the performance of concentric tube and shell and tube arrangement for latent heat storage using phase change material (PCM) and design and fabricate the best setup.

1.3.2 Specific Objectives

a) To design a conventional double pipe heat exchanger and a shell and tube heat exchanger with fins
b) To integrate PCM in the design for heat storage
c) To perform CAD modeling for visualization and simulation for verification.
d) To fabricate a prototype of the best heat storage setup.

CHAPTER TWO: LITERATURE REVIEW

2.1 Phase Change Materials (PCMs)

PCM is a Latent heat thermal energy storage (LHTES) material that stores energy by changing its phase. These are the substances with a ability of storing and releasing large amounts of thermal energy during a phase change, such as melting or solidification, while keeping their temperature almost constant. Their ability to store and release heat makes them useful in a variety of applications, including temperature control, energy storage, and thermal management, as well as augmentation of heat transport. Phase change materials helps in maximizing energy efficiency.

Thermal	**Physical**	**Chemical**	**Economics**
High specific heat	High density	Chemically stable	Cost effective
High latent heat of fusion	Slight volume change with phase change	Reversible melting and cooling cycle	Abundant
High thermal conductivity	Low vapor pressure at operating conditions	Nontoxic, inflammable	Large scale production
Desired melting temperature	–	–	–

Table 2.1: Desirable properties of PCM (Uttam Roy, 2020)

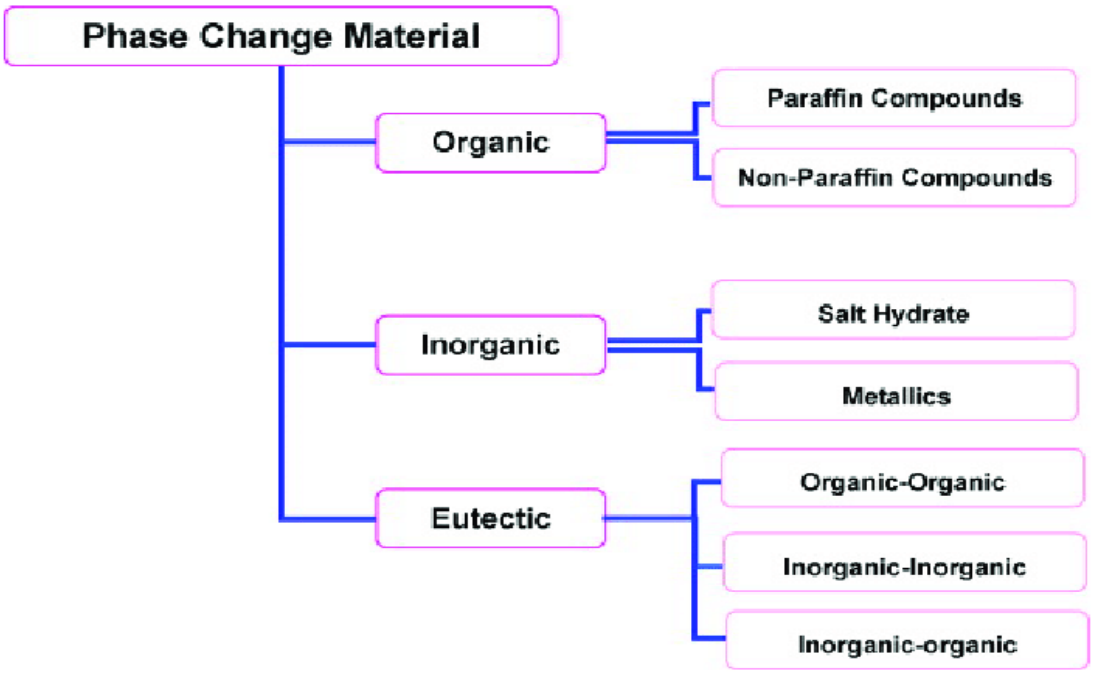

Figure 2.1: Types of PCM (Ahmed Hassan et al., 2016)

Organic PCMs are composed of organic compounds, such as paraffins or fatty acids and they have high latent heat capacity, meaning they can store a significant amount of thermal energy during the phase transition but their thermal conductivity is low. Inorganic PCMs are typically made of salts, metals, or metal alloys and they have high thermal conductivity, making them suitable for applications where efficient heat transfer is required. Eutectic PCMs are created by combining two or more substances to form a mixture with a lower melting point than the individual components.

Figure 2.2: Organic, inorganic, eutectic PCMs (Uttam Roy, 2020)

Compound	Melting point (°C)	Specific heat (kJ/(kg K))		Thermal conductivity ($W m^{-1} K$)		Melting enthalpy (kJ/kg)	Density (kg/m^3)
		Solid	Liquid	Solid	Liquid		
Paraffin wax	0–88	2.9	2	0.22	–	817–898	0–7
Acetamide	82	2	3	0.4	0.20	260	942
Lauric acid	45	2.02	2.16	0.20	0.17	219	1007
Maleic acid	141	1.17	3.08	0.29	–	–	1592
Urea	134	1.70	2.17	0.70	0.50	240	1319
Acetic acid	19	1.67	2.14	0.24	0.17	981	190
D-Mannitol	164	1.30	2.35	0.19	0.10	298	1489
Erythritol	118	2.24	2.60	0.70	0.32	330	1450
Stearic acid	54	1.78	2.26	0.28	0.15	156.9	1001

Table 2.2 Properties of Organic PCMs (Uttam Roy, 2020)

2.2 PCM Heat Exchangers

PCM heat exchangers can be divided into two types: shell and tube heat exchanger and triple concentric tube heat exchanger. Shell and tube heat exchanger can further be broken down into three types: cylindrical model, pipe model and multi-tube model. In a cylindrical model heat exchanger, PCM is placed in the shell while the fluid flows in the tube. In a pipe model heat exchanger, PCM is placed in the inner tube and fluid is flown in the shell whereas in a multi-tube model heat exchanger, there are multiple pipes through which fluid can flow for heat transfer.

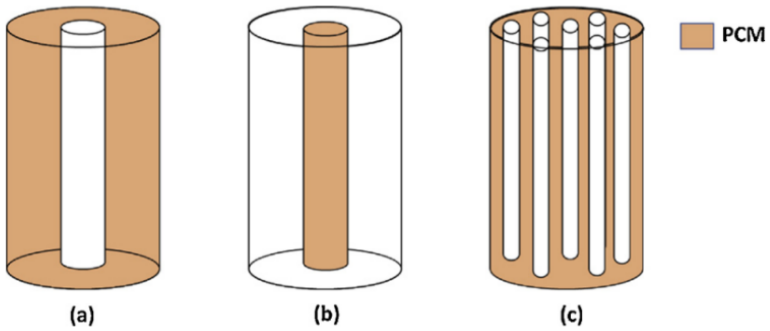

Figure 2.3: Types of shell and tube heat exchanger: a) Cylindrical model b) Pipe model c) Multi-tube model (Kalapala and Devanuri, 2018)

Based on the orientation of heat exchangers, they can be classified as horizontal and vertical heat exchangers.

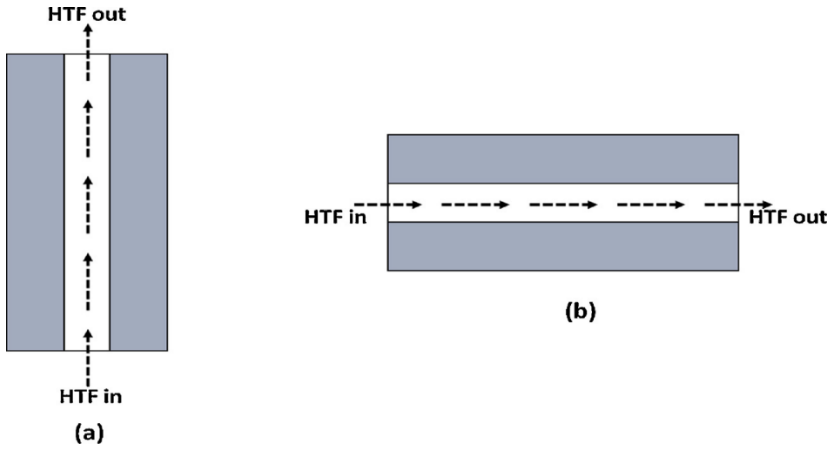

Figure 2.4: Shell and tube heat exchanger a) Horizontal configuration b) Vertical configuration (Kalapala and Devanuri, 2018)

Hosseini, M. J. et al. used paraffin RT50 as a PCM inside a horizontal shell and tube heat exchanger and found that increasing the hot fluid temperature from 70 c to 80 c increased the thermal efficiency during both charging and discharging.

Trp, A. et al. studied a vertical shell and tube LHTES system which used water as a heat transfer fluid and technical grade paraffin RT30 and found out that mass flow rate had negligible effect in the heat transfer rate in laminar region.

A triple concentric tube heat exchanger consists of three tubes of varying cross-sectional area. Usually, hot fluid is flown in the tube which has the smallest diameter, the next layer is occupied by PCM and cold fluid is flown in the outermost tube. Heat is transferred from the hot fluid to the PCM layer and then to the cold fluid.

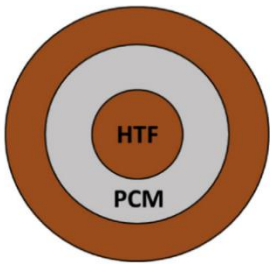

Figure 2.5: Triple concentric tube heat exchanger (Kalapala and Devanuri, 2018)

2.3 Use of fins in PCM heat exchangers

PCMs have the capability to store large amounts of thermal energy through the phase change process, which takes place at nearly constant temperature of the storage material. The essential challenge of using PCMs is their low thermal conductivities, this lead to increase the time needed to store and release thermal energy. Using fins to improve the poor performance of PCM systems is a highly desirable solution due to its effectiveness, low construction cost, and ease of fabrication.

Fins are used to increase the surface area available for heat transfer. By increasing the contact area between the PCM and the surrounding fluid, fins enhance the heat transfer rate and improve overall efficiency. The presence of fins in a PCM heat exchanger speeds up heat transfer. Fins boost the heat exchanger's thermal conductivity, allowing for faster heat exchange between the PCM and the surrounding liquid. (Nie et al., 2020) found that increasing the fin number and length accelerated the heat storage/release rate and the total heat storage and release time reduced about 67.9% when fin number increased from 2 to 10. The fins arranged in the lower part when the fin number was less than or equal to 6, or uniformly distributed when fin number was greater than 6, could improve the melting of PCM (Deng et al., 2019).

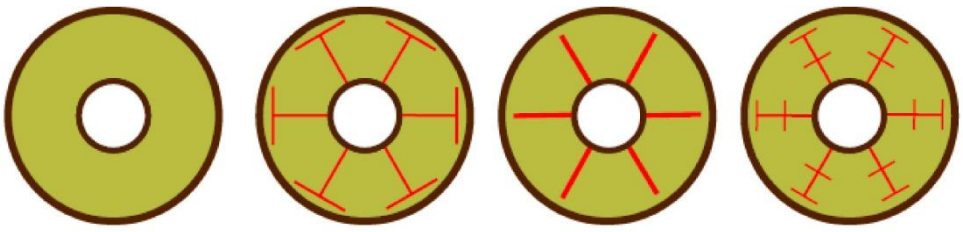

Figure 2.6: Different fins configurations in heat exchanger: (a) without fins, (b) tee fins, (c)Longitudinal fins, (d) tree fins (A. Nowakowski, 2021)

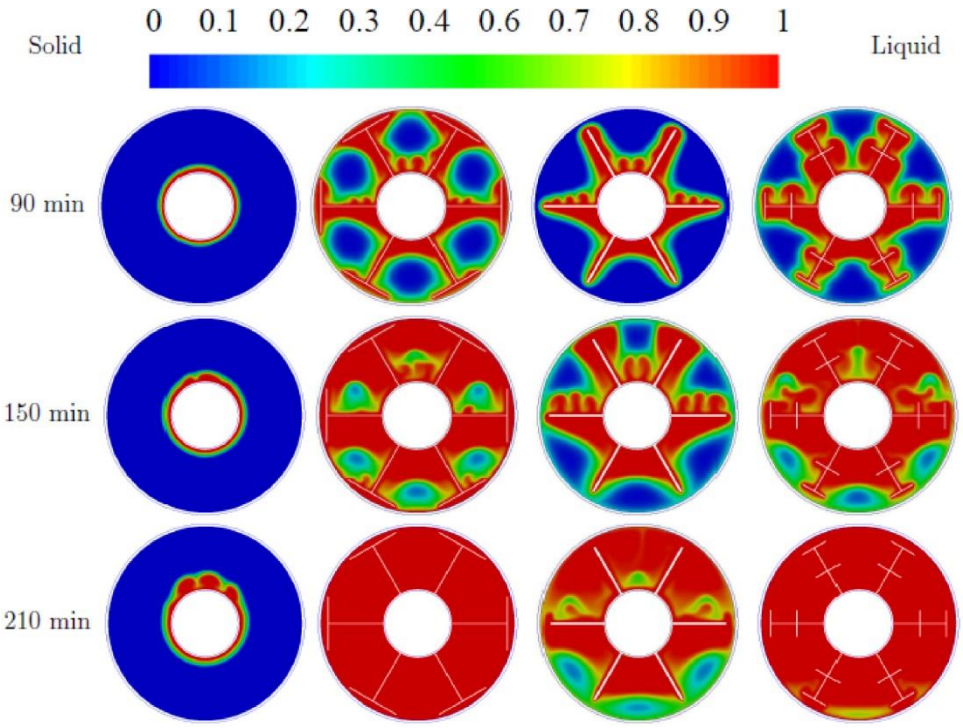

Figure 2.7: Liquid fraction contours at different times for melting process comparison for various fins shapes. From left: first without fins, second tee fins, third longitudinal fins, and fourth tree fins. (A. Nowakowski, 2021)

CHAPTER THREE: METHODOLOGY

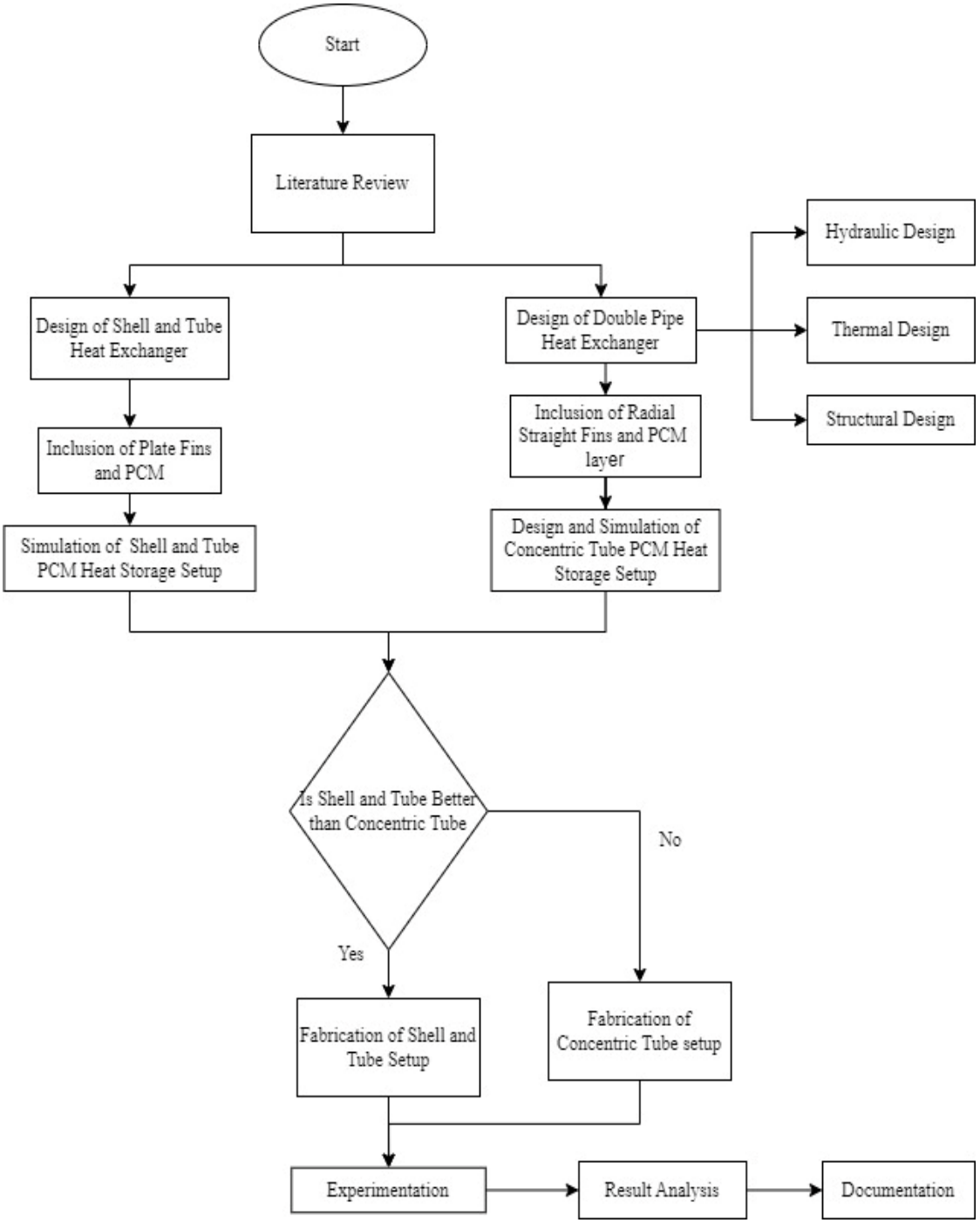

Figure 3.1: Methodology Flowchart

3.1 Literature Review

During the literature review, we did a thorough search to find the newest research on heat exchangers, PCM heat storage, and studies about counter flow heat exchangers. We carefully looked at all the information to see where there are gaps, problems, and chances to make things better in this area. This review helped us understand the current theories, ideas, and progress in designing heat exchangers and using PCMs.

3.2 Design of Double Pipe Heat Exchanger (Thermal and Hydraulic Design)

The double pipe heat exchanger's thermal and hydraulic design was done using different principles and equations. The required heat transfer area, overall heat transfer coefficient, and temperature patterns inside the heat exchanger were calculated. Diameter of the pipe was also optimized to further enhance the efficiency of our system.

3.3 Inclusion of Fins and PCM in Design of Double Pipe Heat Exchanger

To enhance the heat transfer efficiency, various fin geometries and materials were analyzed for their suitability in the double pipe heat exchanger design. The inclusion of fins improved the overall performance of the heat exchanger and reduced the length of heat exchanger needed. Additionally, suitable PCM materials and their integration within the design were studied to incorporate them into our heat exchanger design.

3.4 Design and Simulation of Concentric Tube PCM Heat Storage Setup

Various design and computational software such as SOLIDWORKS and ANSYS FLUENT were used for the design and simulation of the setup. Using this software, the CAD modelling and simulation were performed.

3.5 Design of Shell and Tube Heat Exchanger

When designing the shell and tube heat exchanger, we paid attention to two main things: moving heat and moving fluids. We used calculations to see how much heat could move well and how the fluid should flow through the system. This helped us make the design better so it could move heat effectively and keep the fluid flowing smoothly. By looking at both parts together, we wanted to make a heat exchanger that worked well and used energy efficiently.

3.6 Inclusion of Plate Fins and PCM

Adding plate fins and PCM (Phase Change Material) to the double pipe heat exchanger design improved heat transfer efficiency. We explored various fin shapes and materials to enhance heat transfer surfaces and investigated PCM options to boost heat storage capacity. By selecting the right fins and PCM, we aimed to enhance the overall performance of the heat exchanger.

3.7 Simulation of Shell and Tube PCM Heat Storage Setup

For simulating the shell and tube PCM heat storage setup, we utilized design and computational software like SOLIDWORKS and ANSYS FLUENT. Through these tools, we optimized the design and studied the thermal behavior of the setup. This involved analyzing factors such as heat transfer, fluid flow, and PCM phase change within the shell and tube configuration.

3.8 Decision

The decision between concentric pipe and shell and tube configurations was made after thorough consideration of factors such as efficiency, economy, and feasibility. After performing detailed analysis, it was determined that the fabrication of the shell and tube configuration offered higher effectiveness compared to the concentric pipe design.

3.9 Fabrication, Experimentation, and Validation

The shell and tube heat exchanger design, with added fins and PCM, was built according to set parameters and materials. We set up experiments to measure temperature, flow rates, and pressure drop. We then compared our experimental results with simulation results to check the accuracy of our experiment.

3.10 Documentation

A report was written documenting the experimental setup, steps that were followed, and the data was collected. Different graphs, tables, and analysis were included to help understand how well the system worked.

CHAPTER FOUR: RESULT AND DISCUSSION

4.1 Design of a Double Pipe Heat Exchanger

4.1.1 Material Selection

The pipe material for the double pipe heat exchanger was chosen carefully to meet various needs like cost-effectiveness, practicality, structural integrity, and heat transfer efficiency. Five options were evaluated which were:

- mild steel,
- carbon steel,
- copper,
- aluminum, and
- stainless steel.

Each material was rated from 1 to 5 on criteria such as:

- thermal conductivity,
- cost,
- mechanical strength,
- resistance to corrosion, and
- weight.

Each criterion was given a weight factor to show its importance. Cost was the most important, with a weight of 5, followed by thermal conductivity (4), strength (3), corrosion resistance (2), and weight (1). To find the best material, we multiplied each criterion score by its weight factor and added them up to get the Total Weighted Score using this formula:

Total Weighted Score = Σ (individual criterion score * corresponding weight factor)

		Weight factor of					
		Thermal Conductivity	Cost	Strength	Corrosion Resistance	Light Weight	Total Weighted Score
		5	5	3	2	1	
Materials	Stainless Steel	0.2	1.9	2.2	5	2	28.9
	Mild Steel	0.6	5	4	2	3	46.4
	Carbon Steel	0.6	4	3.3	1	4	38.3
	Copper	5	0.7	2	4	1	38.5
	Aluminum	2.9	1.6	1	3	5	33.6

Table 4.1: Decision matrix for material selection

After carefully analyzing options using the decision matrix, we found mild steel to be the best choice with a top score of 46.4. It performed well in key areas like cost, strength, and practicality.

Cost was prioritized in our decision-making process, and mild steel stood out because of its availability and properties like high durability and high heat conductivity, making it ideal for our heat exchanger design.

The operation of a heat exchanger is dependent on what fluid it uses. Water was picked because of the following reasons:

1. Water can soak up and hold a lot of heat, which is super important for a heat exchanger. It helps the system transfer heat efficiently.
2. Water is cheap and easy to find, making it a smart choice for the heat exchanger. It saves money.
3. Water is safe for people, food, and the environment. It doesn't harm anyone or anything.
4. Water can handle a wide range of temperatures, making it useful for lots of different jobs.

4.1.2 Hydraulic Design

In the hydraulic design phase of the double pipe heat exchanger project, the goal was to determine the optimal diameter. This diameter needed to strike a balance between cost of material and cost of power loss due to head loss.

The frictional head loss for various pipe diameters was calculated using the Darcy-Weisbach equation. This equation helps understand how head loss changes as the diameter of the pipe varies.

Head loss per unit length (H/L) = $\frac{8*f*\dot{m}_h^2}{\pi*g*\rho_h*d_h^5}$

where,

f = friction factor

$\dot{m}_h$ = mass flow rate of hot fluid

g = acceleration due to gravity

ρ_h = density of hot fluid at average temperature

d_h = diameter of hot fluid pipe

Using Haaland's equation to calculate friction factor,

$$f = \frac{0.3086}{[\log_{10}\{\frac{6.9}{Re}+\left(\frac{e}{3.7d_h}\right)^{1.11}\}]^2}$$

where,

absolute roughness for mild steel (e) = 0.055 mm

Relative roughness (e/d) = 0.055/d

Head loss per unit length (H/L) = $\frac{8*f*\dot{m}^2}{\pi^2*g*\rho*d^5}$

Head loss for length L (H) = (H/L) * L

The fluid flow power equation was then utilized to convert the head loss into power loss. After that, the cost of each diameter's power loss was calculated using the formula listed below.

Energy loss in time t (E) = (ρ*g*H*Q)*t

Cost of power loss = E* cost per kwh

Taking cost of electricity = Rs 12 per kwh

Diameter (d)(mm)	**Reynold's number**	**Relative roughness (e/d)**	**Friction factor**	**Head loss per unit length**	**Head loss for 5m long pipe(m)**	**Power loss(W)**	**Energy loss(kwh)**	**Cost of energy loss(Rs)**
20	19393.77	0.002750	0.0309	22.439	112.196	183477.34	366.95	4403.46
21	18470.25	0.002619	0.0309	17.582	87.910	143762.22	287.52	3450.29
22	17630.70	0.002500	0.0309	13.943	69.715	114006.33	228.01	2736.15
23	16864.14	0.002391	0.0310	11.178	55.892	91401.96	182.80	2193.65
24	16161.47	0.002292	0.0310	9.052	45.259	74012.76	148.03	1776.31
25	15515.01	0.002200	0.0311	7.397	36.984	60480.63	120.96	1451.54
26	14918.28	0.002115	0.0312	6.095	30.476	49838.20	99.68	1196.12
27	14365.75	0.002037	0.0313	5.062	25.308	41386.57	82.77	993.28
28	13852.69	0.001964	0.0314	4.233	21.167	34614.18	69.23	830.74
29	13375.01	0.001897	0.0315	3.564	17.820	29142.05	58.28	699.41
30	12929.18	0.001833	0.0316	3.019	15.096	24686.22	49.37	592.47
31	12512.11	0.001774	0.0317	2.572	12.861	21031.75	42.06	504.76
32	12121.10	0.001719	0.0318	2.203	11.016	18014.32	36.03	432.34
33	11753.80	0.001667	0.0319	1.897	9.483	15507.20	31.01	372.17
34	11408.10	0.001618	0.0321	1.640	8.201	13411.78	26.82	321.88
35	11082.15	0.001571	0.0322	1.425	7.124	11650.76	23.30	279.62
36	10774.31	0.001528	0.0324	1.243	6.215	10163.05	20.33	243.91
37	10483.12	0.001486	0.0325	1.088	5.442	8900.07	17.80	213.60
38	10207.24	0.001447	0.0326	0.957	4.784	7822.91	15.65	187.75
39	9945.52	0.001410	0.0328	0.844	4.219	6900.19	13.80	165.60
40	9696.88	0.001375	0.0329	0.747	3.734	6106.50	12.21	146.56

41	9460.37	0.001341	0.0331	0.663	3.315	5421.11	10.84	130.11
42	9235.13	0.001310	0.0332	0.590	2.952	4827.03	9.65	115.85
43	9020.36	0.001279	0.0334	0.527	2.636	4310.28	8.62	103.45
44	8815.35	0.001250	0.0335	0.472	2.360	3859.26	7.72	92.62
45	8619.45	0.001222	0.0337	0.424	2.118	3464.36	6.93	83.14
46	8432.07	0.001196	0.0338	0.381	1.906	3117.52	6.24	74.82
47	8252.67	0.001170	0.0340	0.344	1.720	2812.02	5.62	67.49
48	8080.74	0.001146	0.0341	0.311	1.555	2542.15	5.08	61.01
49	7915.82	0.001122	0.0343	0.282	1.408	2303.14	4.61	55.28
50	7757.51	0.001100	0.0344	0.256	1.279	2090.91	4.18	50.18
51	7605.40	0.001078	0.0345	0.233	1.163	1901.99	3.80	45.65
52	7459.14	0.001058	0.0347	0.212	1.060	1733.43	3.47	41.60
53	7318.40	0.001038	0.0348	0.194	0.968	1582.69	3.17	37.98
54	7182.88	0.001019	0.0350	0.177	0.885	1447.60	2.90	34.74
55	7052.28	0.001000	0.0351	0.162	0.811	1326.27	2.65	31.83
56	6926.34	0.000982	0.0353	0.149	0.744	1217.09	2.43	29.21
57	6804.83	0.000965	0.0354	0.137	0.684	1118.65	2.24	26.85
58	6687.51	0.000948	0.0356	0.126	0.630	1029.72	2.06	24.71
59	6574.16	0.000932	0.0357	0.116	0.580	949.24	1.90	22.78
60	6464.59	0.000917	0.0359	0.107	0.536	876.28	1.75	21.03
61	6358.61	0.000902	0.0360	0.099	0.495	810.03	1.62	19.44
62	6256.05	0.000887	0.0362	0.092	0.458	749.78	1.50	17.99
63	6156.75	0.000873	0.0363	0.085	0.425	694.88	1.39	16.68
64	6060.55	0.000859	0.0364	0.079	0.394	644.80	1.29	15.48
65	5967.31	0.000846	0.0366	0.073	0.366	599.04	1.20	14.38
66	5876.90	0.000833	0.0367	0.068	0.341	557.17	1.11	13.37
67	5789.18	0.000821	0.0369	0.063	0.317	518.81	1.04	12.45
68	5704.05	0.000809	0.0370	0.059	0.296	483.61	0.97	11.61
69	5621.38	0.000797	0.0372	0.055	0.276	451.27	0.90	10.83
70	5541.08	0.000786	0.0373	0.052	0.258	421.52	0.84	10.12

Table 4.2: Cost of energy loss for pipes of different diameters

At the same time, the cost of materials for each diameter was considered.

Diameter (mm)	Cost per unit length (Rs/m)	Cost of 5 m pipe (Rs)
38.1	324.4750656	1622.375328
50.8	572.5065617	2862.532808
76.2	1217.519685	6087.598425

Table 4.3: Cost of mild steel pipes

Figure 4.1: Obtaining the optimum diameter by plotting the cost of energy loss and cost of material for various diameters of a pipe

As the diameter got bigger, the cost of materials went up because larger pipes are pricier. On the other hand, the cost of power loss went down as the diameter increased. Bigger diameters mean lower head loss and lower power loss.

The important point on the graph was where these two costs met. At about 30 mm diameter, ideal diameter was obtained. Hence, the optimum diameter was obtained.

For hot fluid,

Mass flow rate ($\dot{m}_h$) = 0.166666667 kg/s

Inlet temperature (T_{h1}) = 60°C

Outlet temperature (T_{h2}) = 51°C

Average temperature (T_h) = 55.5°C

Density of hot fluid for average temperature (ρ_h) = 985.01 kg/m^3

Dynamic viscosity of hot fluid for average temperature (μ) = 0.0005003 Ns/m^2

Inner diameter of hot fluid pipe (d_{hi}) = 30 mm

Outer diameter of hot fluid pipe (d_{ho}) = 34 mm

Reynold's number (Re_h) = $\frac{4*\dot{m}_h}{\pi*d_h*\mu}$

$$= \frac{4*0.16667}{\pi*0.005003*30*10^{-3}}$$

= 14138.62288 (Turbulent flow)

For commercial steel pipes (carbon and mild steel),

Average absolute roughness (e) = 0.055 mm

Using Haaland's equation for friction factor (f_h) where $Re_h > 4000$ and $\frac{e}{d} > 10^{-4}$,

$$f_h = \frac{0.3086}{[\log_{10}\{\frac{6.9}{Re}+\left(\frac{e}{3.7d}\right)^{1.11}\}]^2}$$

$$= \frac{0.3086}{[\log_{10}\{\frac{6.9}{14138.62288}+\left(\frac{0.055}{3.7*30}\right)^{1.11}\}]^2}$$

= 0.031035619

Head loss per unit length (H/L) = $\frac{8*f_h*\dot{m}_h^2}{\pi^2*g*\rho_h*d_{hi}^5} = \frac{8*0.031035*0.16667^2}{\pi^2*9.81*985.01*0.03^5} = 0.0030213$

Hence, the frictional head loss per unit length for inner pipe flow is about 0.0030213.

For cold fluid,

The cold fluid mass flow rate ($\dot{m}_c$) is calculated in the following way:

$$Q = \dot{m}_c * (T_{c2} - T_{c1}) = \dot{m}_h * (T_{h1} - T_{h2})$$

$$\dot{m}_c = \frac{\dot{m}_h(T_{h1} - T_{h2})}{(T_{c2} - T_{c1})} = \frac{0.1666667 * (60 - 51)}{(25 - 20)} = 0.3 \text{ kg/s}$$

Inlet temperature (T_{c1}) = 20°C

Outlet temperature (T_{c2}) = 25°C

Average temperature (T_c) = 22.5°C

Density of cold fluid for average temperature (ρ_c) = 997.5 kg/m^3

Dynamic viscosity of hot fluid for average temperature (μ_c) = 0.0009465 Ns/m^2

Inner diameter of cold fluid pipe (d_{ci}) = 80 mm

Outer diameter of cold fluid pipe (d_{co}) = 84 mm

Hydraulic diameter (D_h) = d_{ci} - d_{ho} = (80 – 34) mm = 46 mm

Reynold's number (Re_c) = $\frac{4*\dot{m}_c*D}{\pi*\mu*(d_{ci}^2 - d_{ho}^2)}$

$$= \frac{4*0.3*0.046}{\pi*0.0009465*(0.08^2 - 0.034^2)}$$

= 3540.021533 (Transition flow)

For friction factor, Using Colebrook equation,

$$\frac{1}{\sqrt{f}} = \left\{-2\log_{10}\left[\frac{\left(\frac{e}{D}\right)}{3.7} + \frac{2.51}{Re(f^{0.5})}\right]\right\}^{-2}$$

Iterating until convergence up to 4 decimal places,

f = 0.04252

Head loss per unit length in the annulus region (H/L) = $\frac{f}{2*g*D_h} * \left[\frac{4*\dot{m}_c}{\pi*\rho*(d_{ci}^2 - d_{ho}^2)}\right]^2$

$$= \frac{0.04252}{2*9.81*0.046} * \left[\frac{4*0.3}{\pi*997.5*(0.08^2 - 0.034^2)}\right]^2 = 0.00025122$$

Hence, the frictional head loss per unit length for outer pipe flow is about 0.0002512.

4.1.3 Thermal Design

The thermal design of a double pipe heat exchanger is super important for the efficient transfer of heat. In this part, our focus mainly lies on finding the Logarithmic Mean Temperature Difference (LMTD) and using Nusselt number correlations for calculating convective heat transfer coefficients.

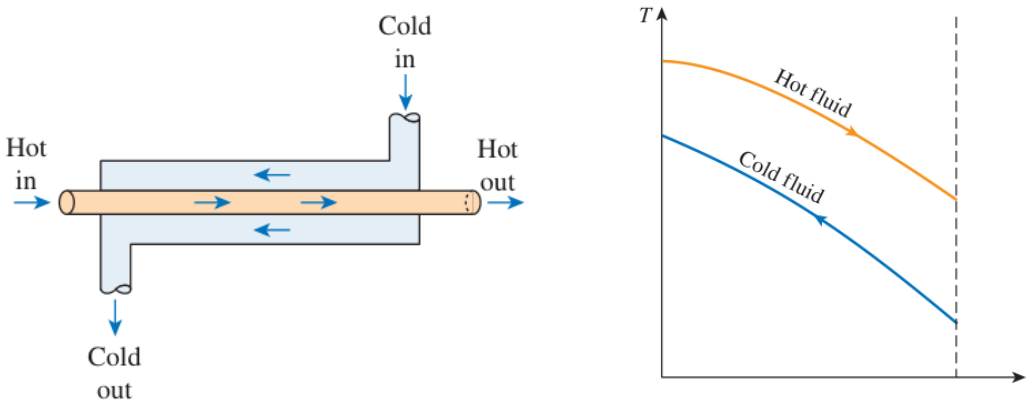

Figure 4.2: Counter-flow heat exchanger temperature profiles
(Yunus A Çengel, 2019)

For hot fluid,

Reynold's number (Re_h) = 14138.62288 (Turbulent flow)

Prandtl's number (Pr_h) = 3.224

Thermal conductivity of water at average temperature (k_h) = 0.6495 W/m.°C

Using Gnielinski correlation to calculate Nusselt number (Nu_h) of hot fluid ($0.5 \leq Pr_h \leq 2000$ and $3000 \leq Re_h \leq 5 * 10^6$),

$$Nu_h = \frac{\left(\frac{f_h}{8}\right)(Re - 1000) * Pr_h}{1 + 12.7 * \left(\frac{f_h}{8}\right)^{0.5} * (Pr_h^{2/3} - 1)}$$

$$= \frac{\left(\frac{0.031035619}{8}\right)*(14138.62288-1000)*3.224}{1+12.7*\left(\frac{0.031035619}{8}\right)^{0.5}*(3.224^{2/3}-1)}$$

= 84.91212371

And,

$Nu_h = \frac{h_h * d_{hi}}{k_h}$, where h_h = convective heat transfer coefficient of hot fluid

So, $h_h = \frac{Nu_h * k_h}{d_{hi}}$ = $\frac{84.91212371*0.6495}{0.03}$ = 1838.347478 W/m^2 °C

For cold fluid,

mass flow rate ($\dot{m}_c$) = 0.3 kg/s

Applying LMTD to calculate the length of heat exchanger required,

$$LMTD = \frac{\Delta T_1 - \Delta T_2}{\ln(\Delta T_1/\Delta T_2)}$$

where, $\Delta T_1 = T_{h1} - T_{c2} = 60 - 25 = 45°C$

$\Delta T_2 = T_{h2} - T_{c1} = 51 - 20 = 31°C$

So, $LMTD = \frac{45-31}{\ln(\frac{45}{31})} = 32.9595°C$

Assuming fully developed flow, the Nusselt's number (Nu_c) corresponding to d_{ci}/d_{hi} = 30/80 = 0.375 on the annular space can be obtained from the table given below by interpolating:

d_{ci}/d_{hi}	Nu_c
0	-
0.05	17.46
0.1	11.56
0.25	7.37
0.5	5.74
1	4.86

Table 4.4: Nusselt number for fully developed laminar flow in a circular annulus with one surface insulated and the other isothermal

So, $Nu_c = 6.555$

And, $h_c = \frac{Nu_c * k_c}{D_h} = \frac{6.555 * 0.6025}{46 * 10^{-3}} = 85.85625\ W/m^2.°C$

Now, the overall heat transfer coefficient (U) is given by:

$$U = \frac{1}{\frac{1}{h_h} + \frac{A_h * \ln\left(\frac{r_{hi} + t}{r_{hi}}\right)}{2 * \pi * k_w * L} + \frac{A_h}{h_c * A_c}}$$

$$= \frac{1}{\frac{1}{h_h} + \frac{\pi * d_{hi} * L * \ln\left(\frac{r_{hi} + t}{r_{hi}}\right)}{2 * \pi * k_w * L} + \frac{\pi * d_{hi} * L}{h_c * \pi * d_{ci} * L}}$$

$$= 201.879\ W/m^2.°C$$

The heat transfer rate ($\dot{Q}$) can then be written as,

$$\dot{Q} = U * A * LMTD$$

$$\dot{Q} = U * \pi * d_{hi} * L * LMTD$$

Solving for L,

$$6300 = 201.879 * \pi * 0.03 * L * 32.9595$$

L = 10.0461m ≈ 10 m

Hence, the length of a straight double pipe heat exchanger is 10 meters.

4.1.4 Structural Design

Making sure the double pipe heat exchanger is strong is crucial for its safe operation. This section explains how to find the highest pressure the pipe can handle inside it using hoop stress and axial stress equations.

To design the structure, stress that the 2mm mild steel pipe can handle is checked. Both hoop stress (around the pipe) and axial stress (along the pipe) are considered. Additional safety factor of 2 is also considered for extra caution. Using the equations, the highest pressure the pipe can handle inside it can be found to ensure that it can work safely. This pressure is compared with the actual pressure expected during operation to confirm the chosen pipe can handle it.

The ratio of inner diameter to the outer diameter $(\frac{d_{hi}}{d_{ho}}) = \frac{30}{34}$= 0.88 < 0.9 which indicates that the pipe is thick walled.

The hoop stress for a thick-walled pipe is given by, $\sigma_H = \frac{p*(d_{hi}^2+d_{ho}^2)}{d_{ho}^2-d_{hi}^2}$

Where, p= Internal pressure in the pipe

For an inner pipe of 30mm diameter and commercially available 2mm wall thickness, d_{hi} = 30 mm = 0.030 m and d_{ho} = 34 mm = 0.034 m

For a mild steel pipe, yield strength = 400 MPa

With factor of safety = 2, Allowable hoop stress (σ_a) = 400/2 = 200 MPa

Maximum allowable pressure (P_{max}) = $\frac{\sigma_a*(d_{ho}^2-d_{hi}^2)}{d_{hi}^2+d_{ho}^2} = \frac{200*10^6*(0.034^2-0.03^2)}{0.03^2+0.034^2}$

= 24.9 MPa

This pressure is higher than the actual internal pressure in the pipe

The axial stress for a thick-walled pipe is given by,

$$\sigma_{ax} = \frac{p * d_{hi}^2}{d_{ho}^2 - d_{hi}^2}$$

Taking allowable axial stress for mild steel pipe = 200 MPa

Maximum allowable pressure (P_{max}) = $\frac{\sigma_{ax} * (d_{ho}^2 - d_{hi}^2)}{d_{hi}^2}$

$$= \frac{200 * (0.034^2 - 0.03^2)}{0.03^2}$$

$$= 56.89 \text{ MPa}$$

This is obviously higher than the actual internal pressure in the pipe.

Therefore, a pipe having a wall thickness of 2mm is appropriate for the intended application.

4.1.5 Design of Insulation

The critical radius of insulation for our double pipe heat exchanger project has been determined in the insulation design section. This critical radius, which denotes the transition point from convective to conductive heat transfer. External convection coefficient was computed. This was accomplished by using the Nusselt number correlation designed for natural convection.

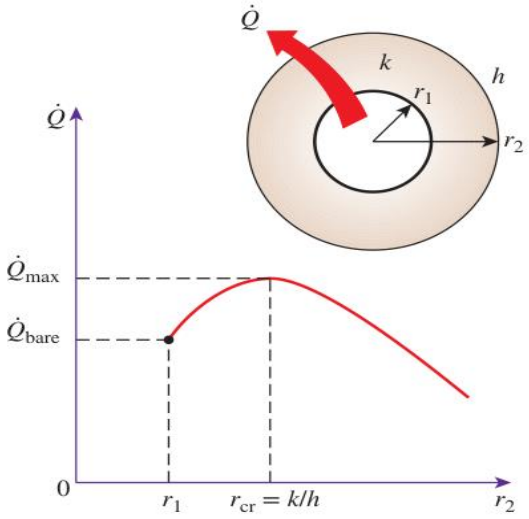

Figure 4.3: Critical radius of insulation (Yunus A Çengel, 2019)

For reducing the rate of heat loss, Outer radius of insulation layer > critical radius of insulation

Insulation Material: EPE black foam insulation

Thermal conductivity of insulation material (k_i) = 0.035 W/m·K

Ambient air temperature (T_∞) = 22˚ C

Outer diameter of cold fluid pipe (D) = 80 mm

Thermal conductivity of wall material (k_w) = 45 W/m·K

Pipe wall thickness (t) = 2 mm

Length of heat exchanger pipe(L) = 5.4095 m

Insulation thickness (t_i) = 10 mm

Convection coefficient of hot water (h_i) = 1838.347 W/m^2.k

Convection coefficient of cold water (h_o) = 78.98775 W/m^2.k

Average temperature of hot fluid (T_h) = 55.5 ˚ C

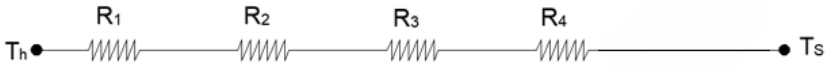

Where, R_1 = Convection resistance of hot water = $\frac{1}{2*\pi*r_{h1}*L*h_h} = \frac{1}{2*\pi*0.015*10*1838.347}$

= 0.00057 °C/W

R_2 = Conduction resistance of inner pipe wall = $\frac{\ln(\frac{r_{h1}+t}{r_{h1}})}{2*\pi*k_w*L} = \frac{\ln(\frac{0..015+0.002}{0.015})}{2*\pi*45*10}$

= 0.0000440644 °C/W

R_3 = Convection resistance of cold water = $\frac{1}{2*\pi*r_{h2}*L*h_c} = \frac{1}{2*\pi*0.017*10*85.85625}$

= 0.00461 °C/W

R_4 = Conduction resistance of outer pipe wall = $\frac{\ln(\frac{r_{c1}+t}{r_{c1}})}{2*\pi*k_w*L} = \frac{\ln(\frac{0.04+0.002}{0.04})}{2*\pi*45*10}$

= 0.000017256 °C/W

Total thermal resistance (R_{th}) = $R_1 + R_2 + R_3 + R_4$ = 0.005248852 °C/W

$T_s = T_h - \dot{Q} * R_{th}$ = 55.5 – 6300 * 0.005248852= 22.43°C

Film temperature (T_f) = $\frac{T_s+T_\infty}{2} = \frac{22.43+22}{2} = 22.215$°C

For natural convection outside the cold fluid pipe,

Rayleigh number (Ra_D) = $Pr * \frac{g*\beta*(T_s-T_\infty)*d_{co}^3}{\nu^2}$

Where, $\beta = \frac{1}{T_f} = \frac{1}{22.215+273} = 0.003387349\ K^{-1}$

ν = kinematic viscosity of air at T_f = 0.0000153639 m^2/s

Pr = Prandtl number of air at T_f = 0.7303

k_a = thermal conductivity of air at T_f = 0.025303992 W/m.K

So, $Ra_D = 0.7303 * \frac{9.81*0.003389349*(22.43-22)*0.084^3}{0.0000153639^2} = 26338.7221$

Nusselt's number (Nu) = $\left\{0.6 + \frac{0.387*Ra_D^{\frac{1}{6}}}{\left[1+\left(\frac{0.559}{Pr}\right)^{\frac{9}{16}}\right]^{\frac{8}{27}}}\right\}^2 = \left\{0.6 + \frac{0.387*26338.7^{1/6}}{\left[1+\left(\frac{0.559}{0.7303}\right)^{\frac{9}{16}}\right]^{\frac{8}{27}}}\right\}^2$

= 5.552

Outside natural convection coefficient (h_a)= $\frac{Nu*k_a}{d_{co}} = \frac{5.552*0.0253}{0.084} = 1.6725$ W/m.K

Critical radius of insulation (r_{cr}) = k_a/h_a = 0.02092 m = 20.92 mm

We have,

Outer radius of insulation layer = outer radius of outer pipe + insulation thickness

= 40+10 = 50 mm > 20.92 mm

This value surpasses the critical radius of insulation. So, there will be a reduction in the rate of heat loss.

4.1.6 Final design & verification via simulation

A comprehensive Computer-Aided Design (CAD) model was created after the calculations related to the design of a conventional double pipe heat exchanger were performed. The CAD model consists of two 10.05-meter-long concentric pipes. The CAD model and it's cross-sectional view is shown in figures below.

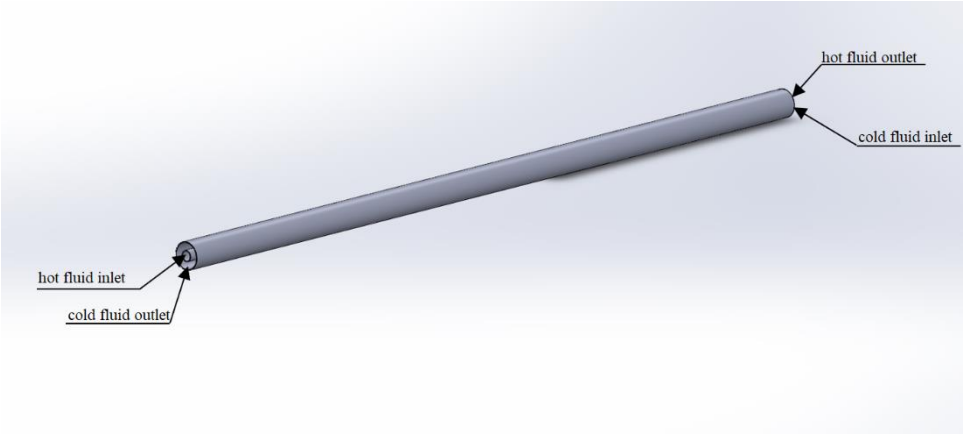

Figure 4.4: CAD model of double pipe heat exchanger

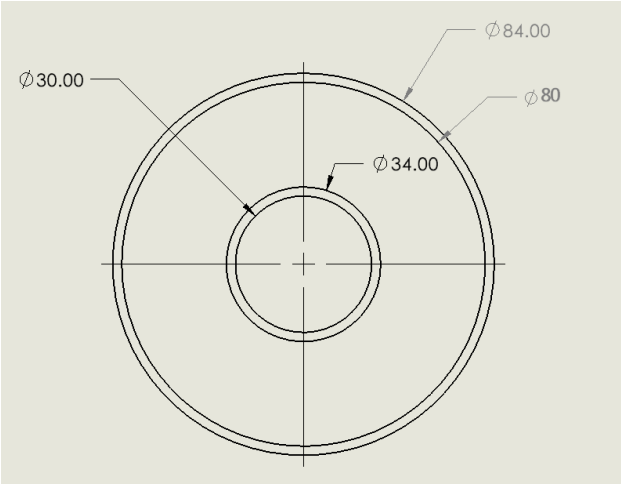

Figure 4.5: Cross-sectional view of double pipe heat exchanger

After creating a CAD model, a Computational Fluid Dynamics (CFD) simulation was conducted to validate the theoretical calculations.

The detailed process of CFD simulation that was performed is explained below:

A) Pre-Processing:

In the pre-processing phase, CAD model was imported into ANSYS and geometry, meshing, and boundary conditions were defined.

- **Geometry Setup:** The CAD model was imported into the simulation software.
- **Mesh Generation:** Meshing is a crucial step in discretizing the geometry into smaller elements for numerical analysis. A structured mesh was generated, defining the computational grid.
- **Boundary Conditions:** Mass flow rates and temperatures of both hot and cold water entering the heat exchanger were specified as boundary conditions. These parameters were selected based on real-world operating conditions.

Specified Parameters	Hot Fluid	Cold Fluid
Inlet Mass flow rate (kg/s)	0.1667	0.3
Inlet temperature (^{o}C)	60	20

Table 4.5: Boundary conditions for the simulation of double pipe heat exchanger

B) Processing:

The processing phase involved solving the governing equations and obtaining numerical solutions for fluid flow and heat transfer.

- **Energy Equation Activation:** To calculate the heat transfer effects, the energy equation model was activated. This allowed the simulation to capture thermal interactions within the fluid.
- **Solver Execution:** The simulation solver was executed to numerically solve the Navier-Stokes equations and the energy equation. This process involved iterating through the computational domain to obtain converged solutions for fluid flow and temperature distribution.

Coordinates: (x,y,z)
Velocity Components: (u,v,w)

Time : t Pressure: p
Density: ρ Stress: τ
Total Energy: Et

Heat Flux: q
Reynolds Number: Re
Prandtl Number: Pr

Continuity:

$$\frac{\partial \rho}{\partial t} + \frac{\partial (\rho u)}{\partial x} + \frac{\partial (\rho v)}{\partial y} + \frac{\partial (\rho w)}{\partial z} = 0$$

X – Momentum:

$$\frac{\partial (\rho u)}{\partial t} + \frac{\partial (\rho u^2)}{\partial x} + \frac{\partial (\rho uv)}{\partial y} + \frac{\partial (\rho uw)}{\partial z} = -\frac{\partial p}{\partial x} + \frac{1}{Re_r}\left[\frac{\partial \tau_{xx}}{\partial x} + \frac{\partial \tau_{xy}}{\partial y} + \frac{\partial \tau_{xz}}{\partial z}\right]$$

Y – Momentum:

$$\frac{\partial (\rho v)}{\partial t} + \frac{\partial (\rho uv)}{\partial x} + \frac{\partial (\rho v^2)}{\partial y} + \frac{\partial (\rho vw)}{\partial z} = -\frac{\partial p}{\partial y} + \frac{1}{Re_r}\left[\frac{\partial \tau_{xy}}{\partial x} + \frac{\partial \tau_{yy}}{\partial y} + \frac{\partial \tau_{yz}}{\partial z}\right]$$

Z – Momentum

$$\frac{\partial (\rho w)}{\partial t} + \frac{\partial (\rho uw)}{\partial x} + \frac{\partial (\rho vw)}{\partial y} + \frac{\partial (\rho w^2)}{\partial z} = -\frac{\partial p}{\partial z} + \frac{1}{Re_r}\left[\frac{\partial \tau_{xz}}{\partial x} + \frac{\partial \tau_{yz}}{\partial y} + \frac{\partial \tau_{zz}}{\partial z}\right]$$

Energy:

$$\frac{\partial (E_T)}{\partial t} + \frac{\partial (uE_T)}{\partial x} + \frac{\partial (vE_T)}{\partial y} + \frac{\partial (wE_T)}{\partial z} = -\frac{\partial (up)}{\partial x} - \frac{\partial (vp)}{\partial y} - \frac{\partial (wp)}{\partial z} - \frac{1}{Re_r Pr_r}\left[\frac{\partial q_x}{\partial x} + \frac{\partial q_y}{\partial y} + \frac{\partial q_z}{\partial z}\right]$$
$$+ \frac{1}{Re_r}\left[\frac{\partial}{\partial x}(u\tau_{xx} + v\tau_{xy} + w\tau_{xz}) + \frac{\partial}{\partial y}(u\tau_{xy} + v\tau_{yy} + w\tau_{yz}) + \frac{\partial}{\partial z}(u\tau_{xz} + v\tau_{yz} + w\tau_{zz})\right]$$

Figure 4.6: Navier-Stokes Equations

(https://www.grc.nasa.gov/www/k-12/airplane/nseqs.html)

C) Post-Processing:

Post-processing included the extraction and interpretation of results from the simulation.

- **Results Extraction:** Results such as outlet temperatures of hot and cold water were extracted. These results were crucial for evaluating the heat transfer efficiency.
- **Temperature & Pressure Contour Plot:** A temperature contour plot was generated to visually represent the temperature distribution within the heat exchanger. This plot played a vital role in defining how the temperature of hot and cold fluids were being varied with length. Similarly, a pressure contour plot was also generated to observe the variation in pressure in the fluid flow.

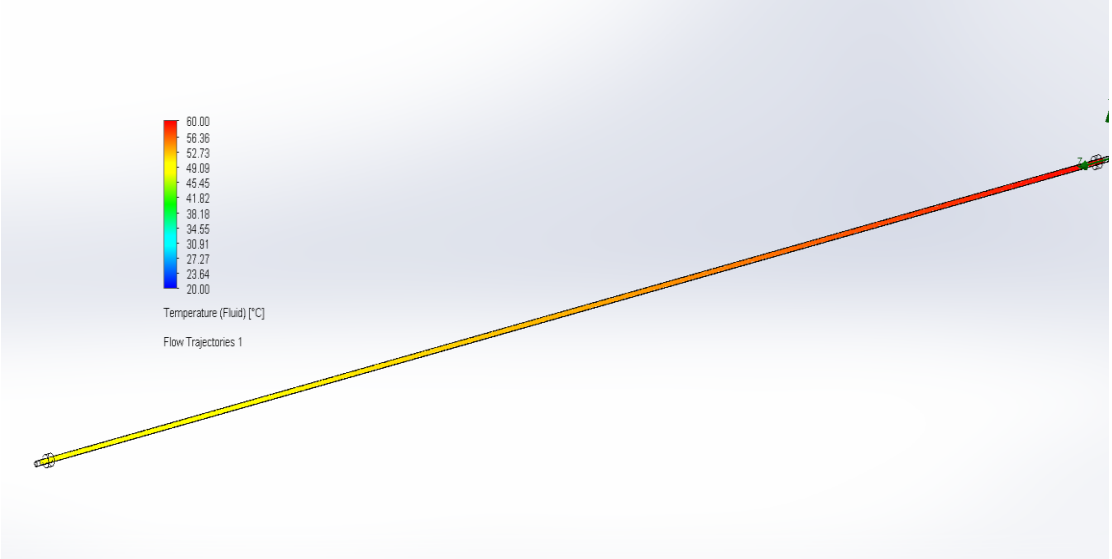

Figure 4.7: Temperature contour for hot fluid in the initial model of double pipe heat exchanger

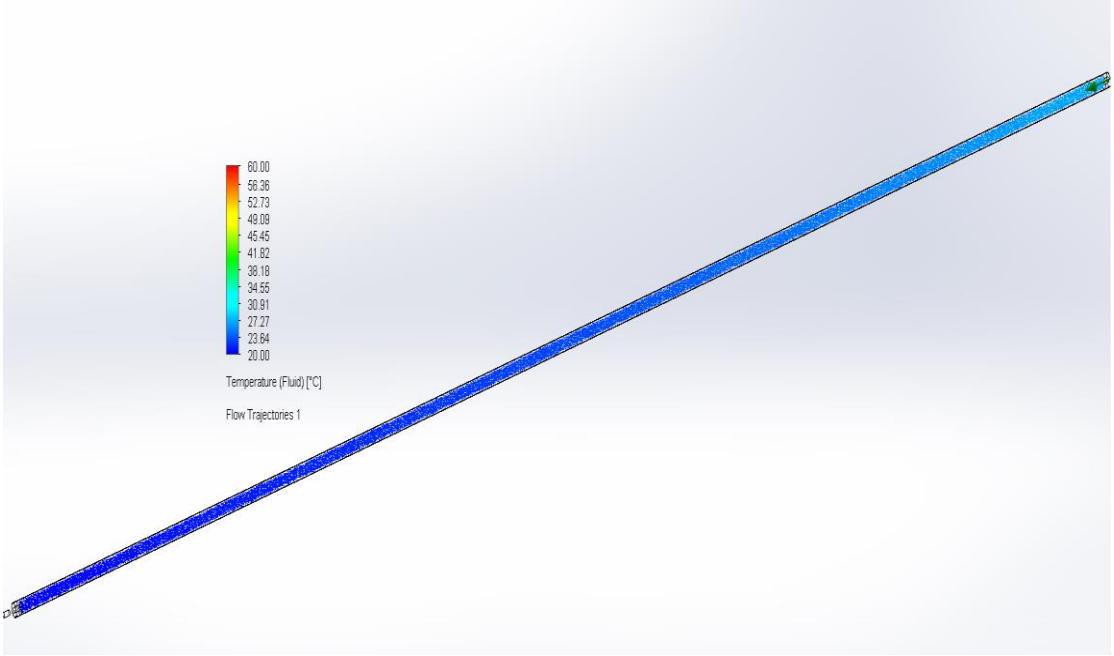

Figure 4.8: Temperature contour for cold fluid in the initial model of double pipe heat exchanger

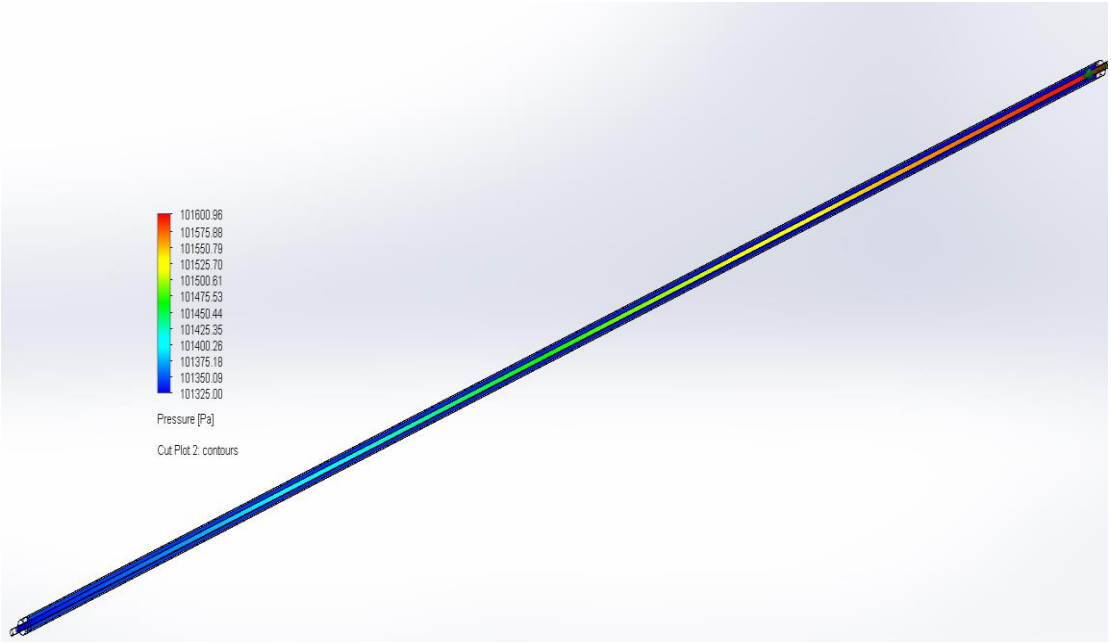

Figure 4.9: Pressure contour for the initial model of double pipe heat exchanger

Since a 10.05-meter-long heat exchanger is impractical in real world, a more feasible CAD model was crafted. This modified design comprises of four hairpins, totaling eight pipes, each with a practical length of 1.352 meters.

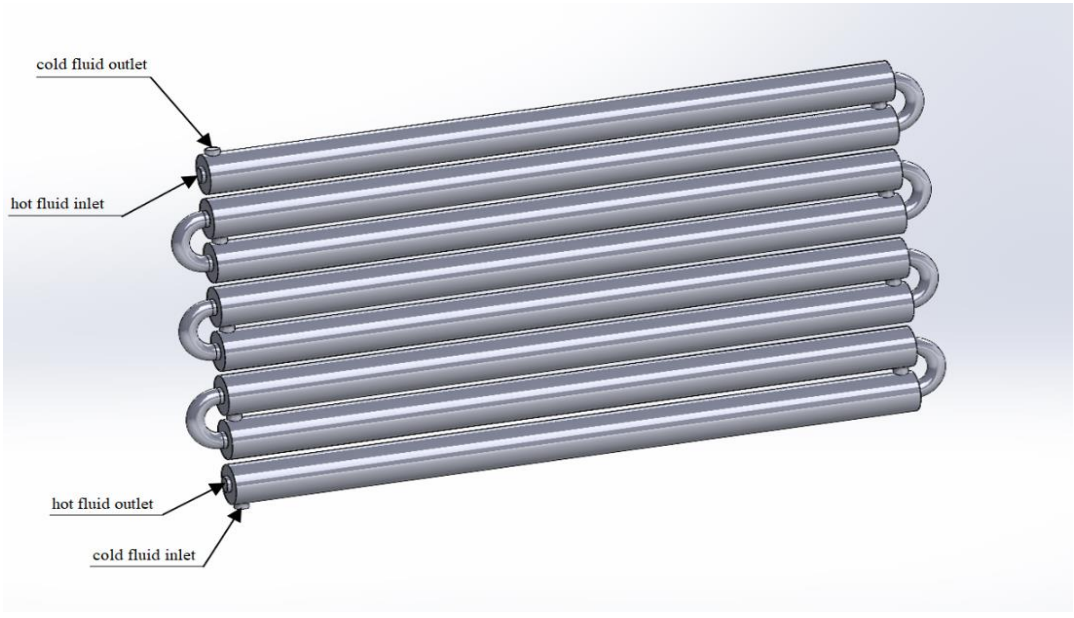

Figure 4.10: Modified CAD model of double pipe heat exchanger

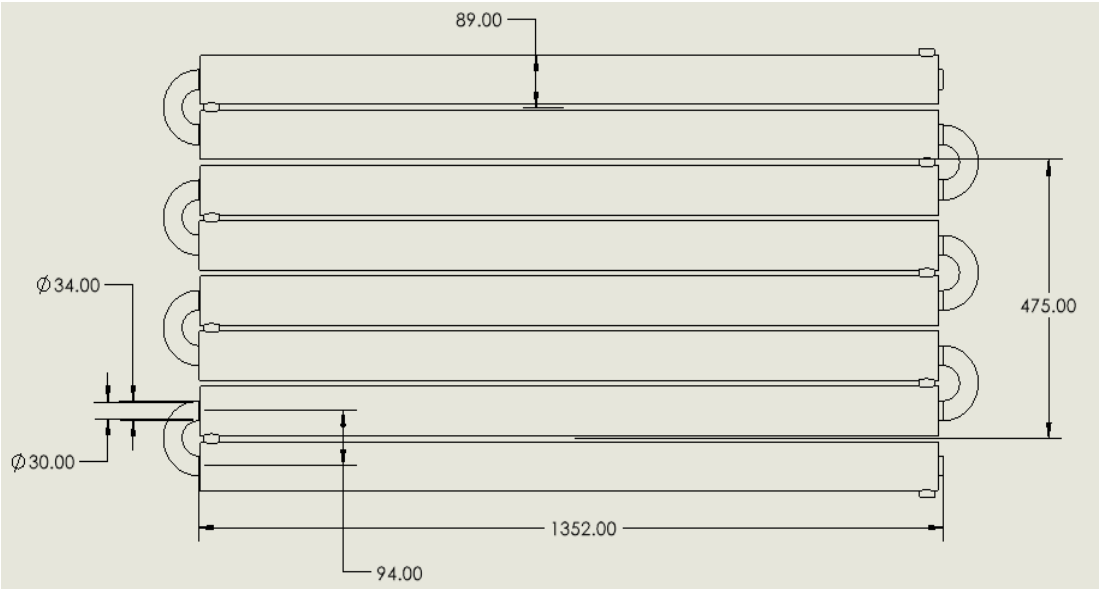

Figure 4.11: Front view of the modified model of double pipe heat exchanger

The modified CAD model of the double pipe heat exchanger also underwent a Computational Fluid Dynamics (CFD) simulation. The results, along with corresponding contour plots, are presented below.

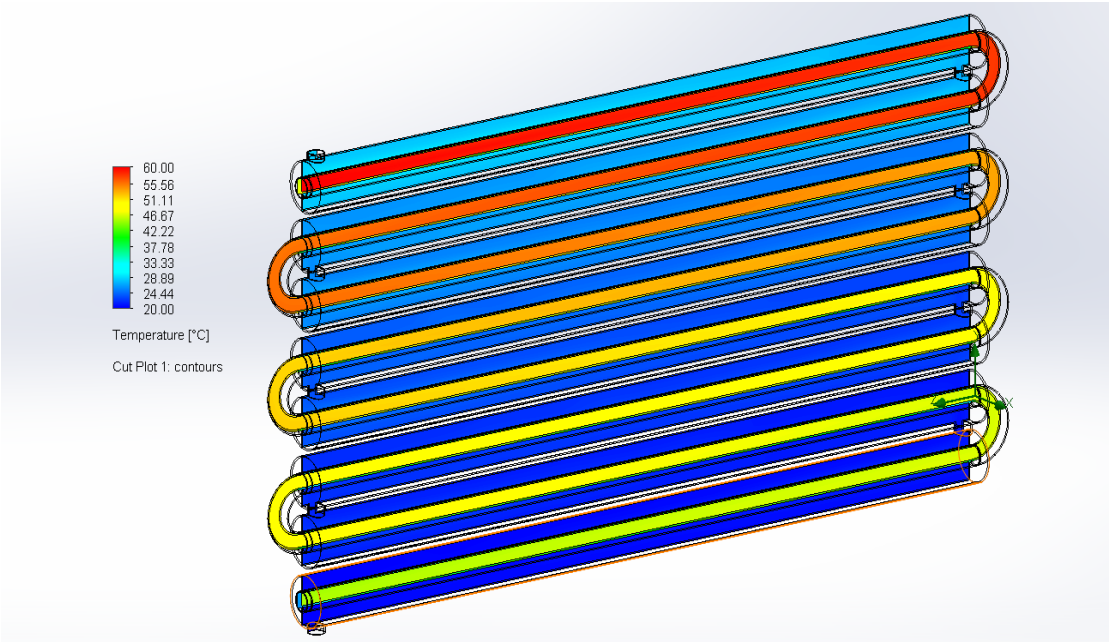

Figure 4.12: Temperature contour of the modified model of double pipe heat exchanger

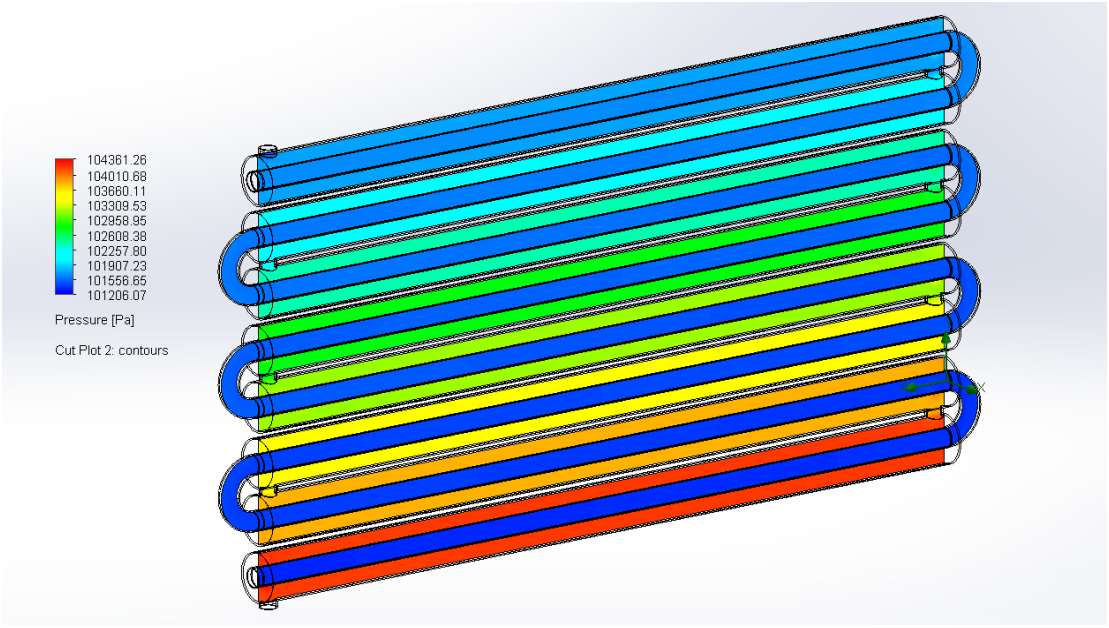

Figure 4.13: Pressure contour of the modified model of double pipe heat exchanger

Comparison of Theoretical and Simulation Results:

A detailed comparison between theoretical calculations and CFD simulation results is presented in the following table:

Sections	Temperature (^oC)		Percentage Error
	Theoretical Calculation	CFD Simulation	
Hot Inlet	60	60 (BC)	--
Cold Inlet	20	20 (BC)	--
Hot Outlet	51	49.94	2.0784
Cold Outlet	25	26.35	5.4

* BC = Boundary Condition

Table 4.6: Theoretical calculation versus CFD simulation results in case of conventional double pipe heat exchanger

The results from the CFD simulation are close to the theoretical calculations. Small deviations are attributed to the finite mesh size employed in the simulation or factors not considered in the theoretical model, such as the effects of turbulence. Overall, the CFD simulation helps to validate the design of our head exchanger.

4.2 Design of Finned Double Pipe Heat Exchanger

To further enhance the heat transfer efficiency, the double pipe heat exchanger was modified to finned double pipe heat exchanger. Straight radial fins were attached to the inner tube to increase the available surface area for heat exchange. Calculations involved determining Nusselt numbers and heat transfer coefficients for the annular space, considering the fin geometry. Fin efficiency was also calculated. Utilizing the finned design helped to further reduce the length of heat exchanger operating within the same conditions as the double pipe design.

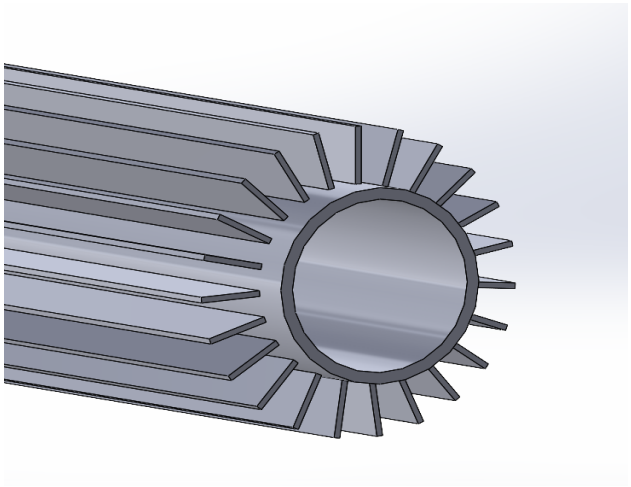

Figure 4.14: Straight radial fins

4.2.1 Necessary Calculations

Fin thickness (δ) = 1 mm

Height of fin (H_f) = 10 mm

Inner diameter of inner pipe (d) = 30 mm

Wall thickness of pipe (t) = 2 mm

Inner diameter of outer pipe (D) = 80 mm

Length of one hairpin section (L_h) = 1 m

Number of fins (N_f) = 23

Thermal conductivity of steel pipe (K_w) = 45 W/m.K

Thermal conductivity of fin (steel) (K_f) = 45 W/m.K

Convective heat transfer coefficient of hot water (h_w) = 1838.347478 W/m^2.K

Wetted perimeter of the annulus (P_w) = $\pi[D + (d + 2t)] + 2\,H_f\,N_f$

$= \pi\,[0.08 + 0.03 + 2 * 0.002] + 2 * 0.01 * 23$

= 0.818141 m

Heat transfer perimeter (P_h) = $\pi\,(d + 2t) + 2\,H_f\,N_f$

= $\pi *$ (0.03+2*0.002) + 2*0.01*23

= 0.56681415 m

Net flow area in the annulus (A_c) = $\frac{\pi}{4} * D^2 - \frac{\pi}{4} * (d + 2t)^2 - \delta * H_f * N_f$

$= \frac{\pi}{4} * 0.08^2 - \frac{\pi}{4} * (0.03 + 0.002 * 2)^2 - 0.001 * 0.01 * 23$

= 0.003888628 m^2

Hydraulic diameter (D_h) = $4 * \frac{A_c}{P_w} = 4 * \frac{0.003888628}{0.818141} = 0.019012005$ m

Equivalent diameter (D_e) = $4 * \frac{A_c}{P_h} = 4 * \frac{0.003888628}{0.56681415} = 0.027441996$ m

Unfinned outer surface area of inner tube (A_u) = $2[\pi(d + 2t)L - \delta L N_f]$

$= 2[\pi * 0.034 * 1 - 0.001 * 1 * 23]$

$= 0.1676283\ m^2$

Finned surface area (A_f) = $2[2 * H_f * L * N_f + \delta * L * N_f]$

$= 2[2 * 0.01 * 1 * 23 + 0.001 * 1 * 23]$

$= 0.506\ m^2$

Total area for heat transfer (A_t) = $A_u + A_f$ = (0.1676283 + 0.506) m^2 = 0.6736283 m^2

Velocity of the cold fluid in the annulus (V_c) = $\frac{\dot{m}_c}{\rho_c * A_c} = \frac{0.3}{997.5 * 0.0038886} = 0.07734\ m/s$

Reynold's number of cold fluid (Re_c) = $\frac{\rho_c * V_c * D_h}{\mu_c} = \frac{997.5 * 0.07734 * 0.019012005}{0.0009465}$

$= 1549.644831$

To calculate Nusselt's number of cold fluid (Nu_c), applying Sieder-Tate correlation,

$Nu_c = 0.027 * Re^{0.8} * Pr^{1/3} * (\mu_b/\mu_s)^{0.14}$ …….(I)

Where, μ_b = dynamic viscosity of cold fluid at average temperature (T_c) = 22.5°C = 0.0009465 kg/m.s

μ_s = dynamic viscosity of cold fluid at temperature T_s

$T_s = \frac{1}{2}\left(\frac{T_{h1} + T_{h2}}{2} + \frac{T_{c1} + T_{c2}}{2}\right) = \frac{1}{2}\left(\frac{60 + 51}{2} + \frac{20 + 25}{2}\right) = 39°C$

At a temperature of 39°C, μ_s = 0.000664 kg/m.s

From equation (I),

$$Nu_c = 0.027 * 1549.644831^{0.8} * 6.575^{\frac{1}{3}} * \left(\frac{0.0009465}{0.0006664}\right)^{0.14} = 18.94590734$$

$$h_c = \frac{Nu_c * k_c}{D_e} = \frac{18.94591 * 0.6025}{0.027441996} = 415.9649685\ W/m^2.°C$$

Fin parameter(m) = $\sqrt{\frac{2*h_c}{\delta*k_f}} = \sqrt{\frac{2*415.9649685}{0.001*45}} = 135.9681284$

Fin efficiency (η_f) = $\frac{\tanh(m*H_f)}{m*H_f} = \frac{\tanh(135.9681*0.01)}{135.9681*0.01} = 0.644503338$

Overall surface efficiency (η_o) = $1 - (1 - \eta_f) * \frac{A_f}{A_t} = 0.732966517$

Overall heat transfer coefficient based on outer area (U_o) = $\frac{1}{\frac{A_t}{A_i*h_h} + A_t*R_w + \frac{1}{\eta_o*h_c}}$

$$= \frac{1}{\frac{0.6736283}{2*\pi*0.03*1*1838.35} + \frac{0.6736283*\ln(\frac{0.03+0.002*2}{0.03})}{2*\pi*45*2*1} + \frac{1}{0.733*415.964}} = 186.1169\ W/m^2.°C$$

No of hairpins required (N_{hp}) = $\frac{Q}{U_o*A_t*LMTD} = \frac{6300}{186.12*0.674*32.96} \approx 1.5$

Total length of heat exchanger with fins (L_f) = 2*L_h *N_{hp} = 3 meters

Fin effectiveness (ε) = $\frac{\text{Heat transfer per unit length with fin}}{\text{Heat transfer per unit length without fin}} = \frac{(6300/3)}{(6300/10)} = 3.333$

Hence, the number of hairpins required is 1.5 and the total length of heat exchanger has been reduced from 10 meters to 3 meters by the addition of fins.

4.2.2 Final design and verification via simulation

The second stage of our finned heat exchanger design involved the creation of a CAD model using SolidWorks. The design includes 1.5 hairpins, is comprised of three inner and outer tubes each, with each hairpin extending to a length of 1.02 meters. On the surface of each inner tube, 23 straight radial fins were attached according to the theoretical calculations preformed. The inner finned tubes were enveloped by outer pipes.

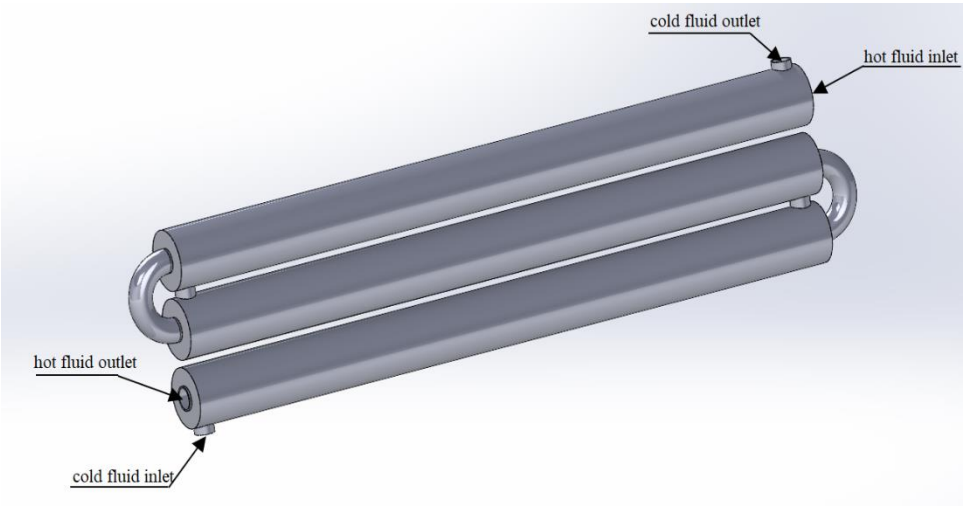

Figure 4.15: CAD model of the finned heat exchanger

The sectional front and side views were generated from the CAD model. These views offer a detailed representation of the arrangement of the inner and outer tubes, showing the position of the radial fins on the inner tube surfaces. The generated sectional views helps to visualize how the model would look like from the inside.

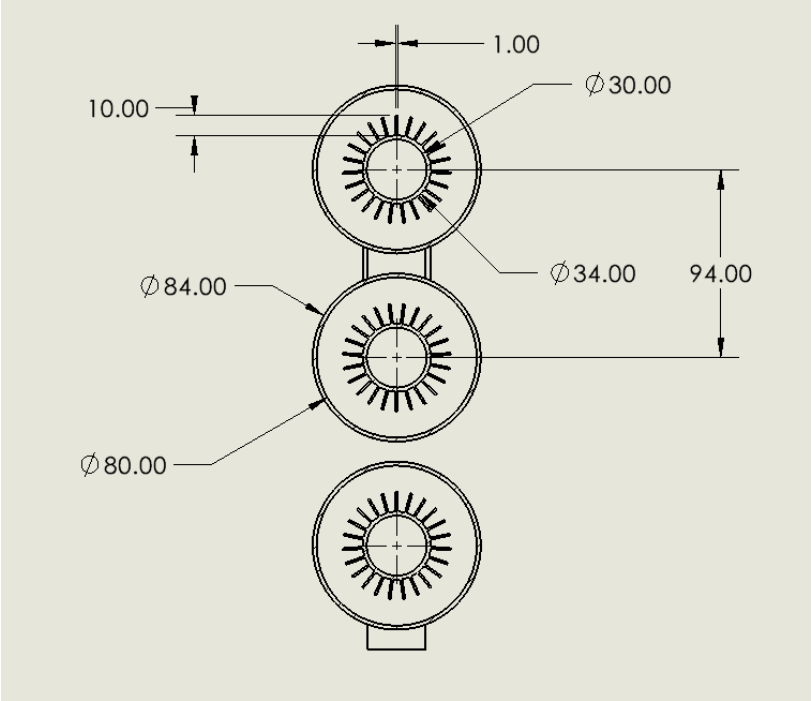

Figure 4.16: Side view of the finned heat exchanger

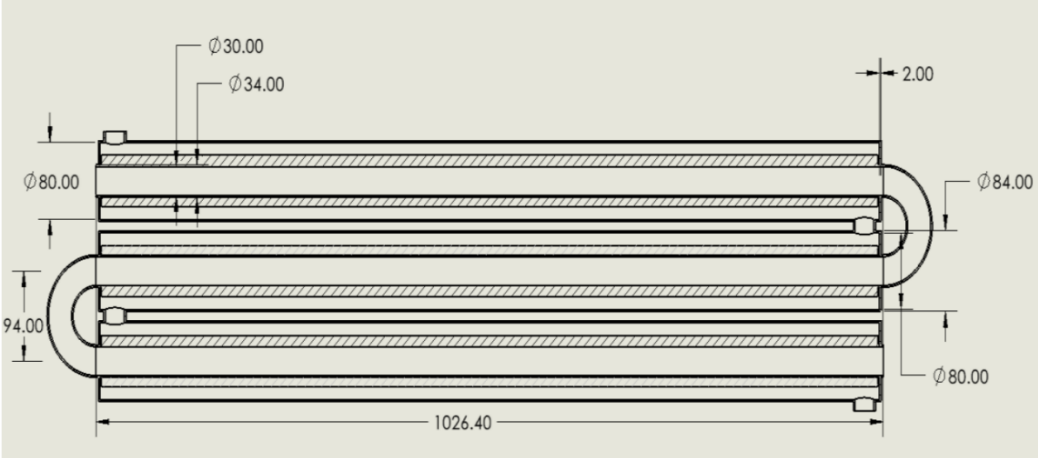

Figure 4.17: Sectional front view of the finned heat exchanger

After the completion of detailed theoretical calculations and making a CAD model, Computational Fluid Dynamics (CFD) simulations were performed to validate our theoretical calculations. The simulations were conducted using ANSYS Fluent and SolidWorks Flow Simulation. The simulation results were close the theoretical calculations. Minor deviations were present which were attributed to factors such as mesh size and turbulence effects within the fluid flow.

Similarly, temperature contours and flow trajectories were obtained from the simulation which are shown below. These contours show how the fluid flows throughout the heat exchanger and how the temperature of fluid is distributed throughout the entire heat exchanger setup.

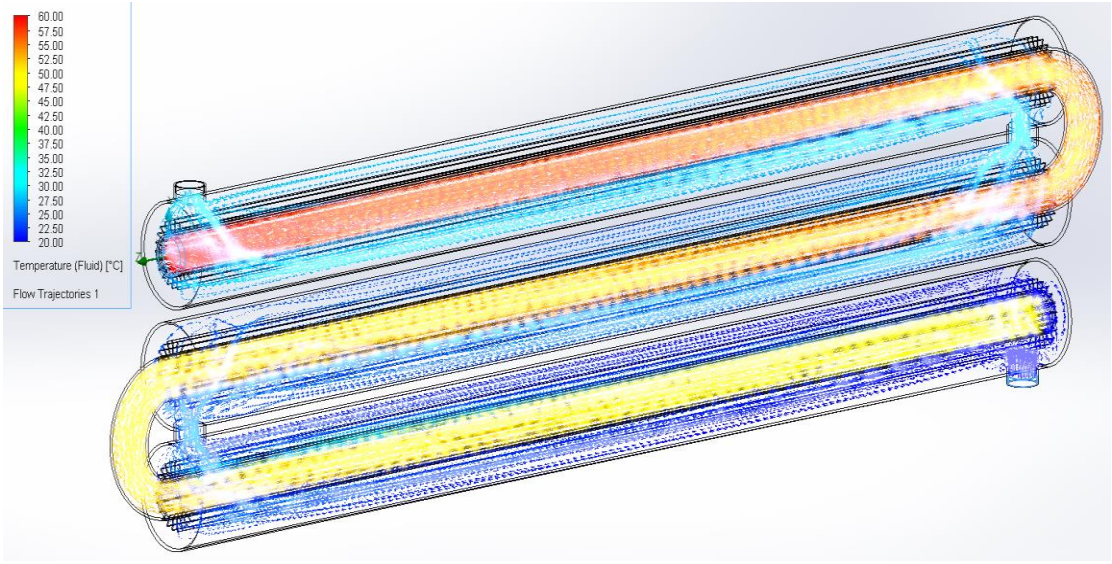

Figure 4.18: Flow trajectories representing the temperature of fluid

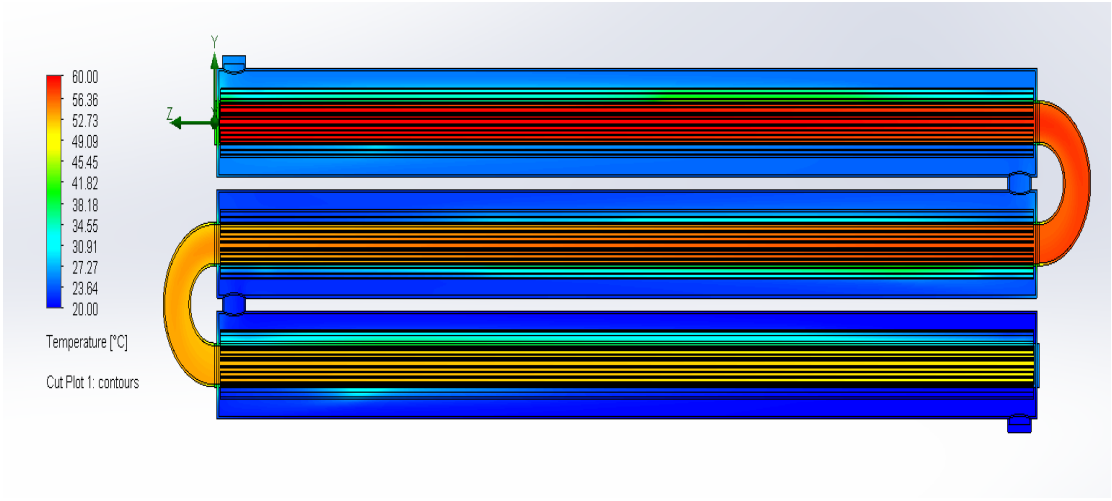

Figure 4.19: Temperature contour of the finned heat exchanger

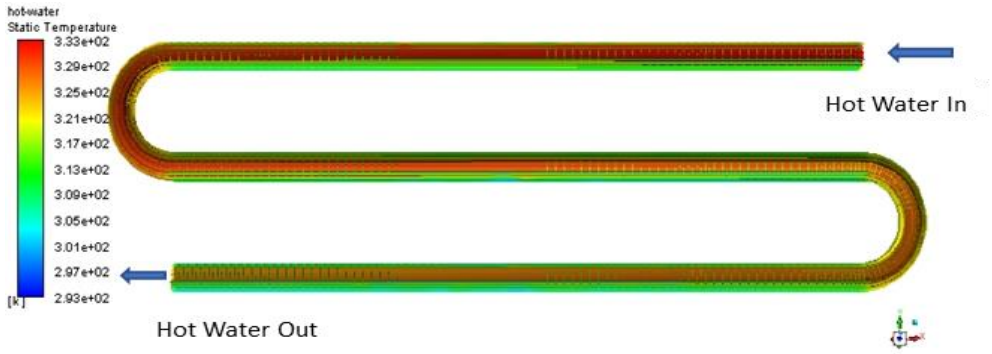

Figure 4.20: Temperature contour of hot water in the finned heat exchanger

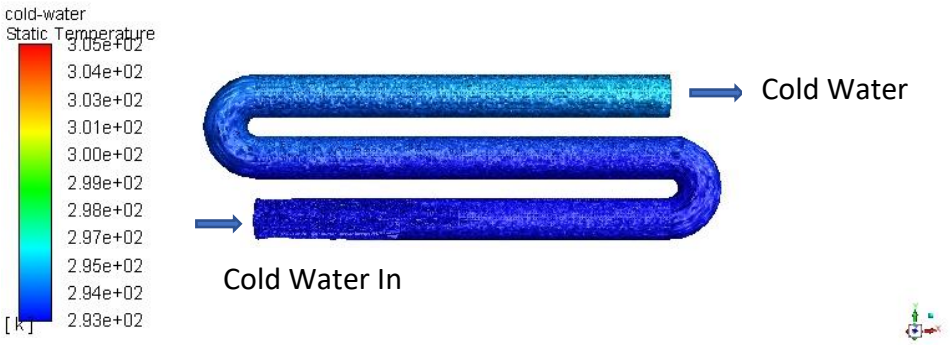

Figure 4.21: Temperature contour of cold water in the finned heat exchanger

The comparison of theoretical calculation and the results from the CFD simulation is shown in the following table:

Sections	Temperature (^{o}C)		Percentage Error
	Theoretical Calculation	CFD Simulation	
Hot Inlet	60	60 (BC)	--
Cold Inlet	20	20 (BC)	--
Hot Outlet	51	52.21	2.37254902
Cold Outlet	25	24.035	3.86

* BC = Boundary Condition

Table 4.7: Theoretical calculation versus CFD simulation results in case of finned heat exchanger

4.3 Design of Quadruple Pipe PCM Heat Storage Setup

The design of the finned double pipe heat exchanger was further enhanced into a quadruple pipe configuration with a Phase Change Material (PCM) heat storage facility. This design comprises four distinct regions of fluids:

- hot water within the inner tube,
- PCM within the annular space of the fins,
- an air insulation layer separating PCM from cold water, and
- cold water within the annular space of the outer pipe.

The quadruple pipe PCM heat storage setup stores excess heat in the Phase Change Material (PCM) during high supply periods. This surplus thermal energy, stored as latent heat, is then retrieved when required.

The working of a quadruple pipe PCM heat storage setup is explained below in three distinct cases:

- **Case-I (Charging):** During the charging phase, the Phase Change Material (PCM) within the annular space of the fins is initially solid at room temperature. Only the hot fluid, flowing through the inner tube, interacts with the PCM. As the hot fluid passes through the inner tube, it transfers heat to the solid PCM, causing the PCM to absorb this thermal energy and undergo a phase change, transitioning from a solid to a liquid state. This phase change occurs at a constant temperature, known as the melting point. The process of absorbing heat and storing it in the form of latent heat is referred to as charging. To preserve the stored heat, an air insulation layer is strategically placed outside the PCM layer.

- **Case-II (Discharging):** During the discharging phase, the objective is to retrieve the stored heat from the melted PCM. To achieve this, the cold fluid is introduced into the annular space of the outer pipe. As the cold fluid flows through this region, the PCM starts to solidify, releasing the stored latent heat. The released heat is then transferred to the cold fluid, heating it in the process.

Also, the air insulation layer utilized during charging process is replaced by a thermally conductive liquid (nanofluid) to enhance heat transfer efficiency between the solidifying PCM and the cold fluid. This process of releasing stored heat is referred to as discharging.

- **Case-III (Simultaneous Charging & Discharging):** In certain scenarios, the hot fluid and cold fluid can be allowed to flow simultaneously through their respective regions. This enables simultaneous transfer of heat from the hot fluid to the cold fluid.

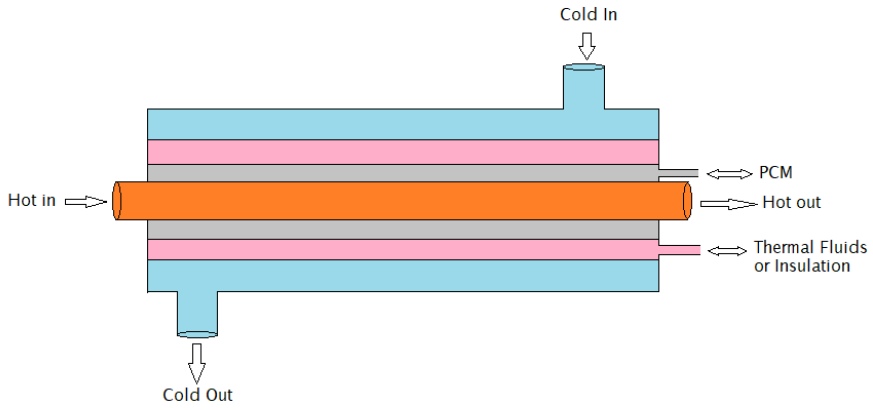

Figure 4.22: Preliminary schematic of the quadruple pipe PCM heat storage setup

4.3.1 PCM Selection

Several factors were considered to determine the best PCM material for our requirements and after careful evaluation, paraffin wax was chosen for its well-balanced properties.

- **Specific Heat (High Desirable):** Specific heat measures a material's ability to store thermal energy. Paraffin wax exhibits a relatively high specific heat, making it effective in absorbing and releasing significant amounts of heat per unit mass.
- **Latent Heat (High Desirable):** The latent heat of fusion is crucial for storing heat during the phase change. Paraffin wax possesses a high latent heat,

indicating its ability to absorb and release substantial energy during melting and solidification.

- **Thermal Conductivity (High Desirable):** Efficient heat transfer within the PCM is facilitated by high thermal conductivity. Although paraffin wax has a lower thermal conductivity compared to some other materials, its overall performance is acceptable due to the addition of fins.
- **Melting Point (Low Desirable):** A lower melting point ensures that the PCM transitions between solid and liquid phases within the desired temperature range. Paraffin wax has a relatively low melting point, contributing to its applicability in various thermal storage applications.
- **Density (High Desirable):** Higher density allows for more heat to be stored within a given volume. Paraffin wax exhibits a desirable density, enabling efficient use of available space for heat storage.
- **Chemical Stability:** Paraffin wax demonstrates chemical stability, ensuring its longevity and reliability in repeated phase change cycles.
- **Cost (Low Desirable**): Paraffin wax is cost-effective, making it a practical choice for applications where economic considerations are essential.
- **Thermal Expansion (Low Desirable):** Low thermal expansion minimizes the risk of structural damage during repeated phase transitions. Paraffin wax exhibits low thermal expansion, contributing to its durability.
- **Availability:** Paraffin wax is readily available, making it a practical choice for large-scale applications.

The various thermo-physical properties of Paraffin wax as a PCM are:

- **Specific Heat:** Approximately 2.1 - 2.5 kJ/kg°C
- **Latent Heat of Fusion:** Around 200 kJ/kg
- **Thermal Conductivity:** Approximately 0.2 W/(m·K)
- **Melting Point:** Typically, between 37°C and 70°C (depending on the specific type of paraffin wax)
- **Density:** Approximately 900 kg/m^3

4.3.2 Theoretical Calculation

4.3.2.1 Mass of PCM required

The initial step involves determining the necessary mass of Phase Change Material (PCM) required to store a defined quantity of heat. This calculation relies on the fundamental heat equation.

Phase Change Material: Paraffin Wax

Latent heat of fusion of PCM (L_f) = 190000 J/kg

Specific heat of solid PCM (c_{ps}) = 2000 J/kg °C

Specific heat of liquid PCM (c_{pl}) = 2150 J/kg °C

Density of solid PCM (ρ_{ps}) = 910 kg/m^3

Density of liquid PCM (ρ_{pl}) = 790 kg/m^3

Melting temperature of PCM (T_m) = 53.7°C

Thermal conductivity solid PCM (k_s) = 0.24 W/m°C

Thermal conductivity liquid PCM (k_l) = 0.22 W/m°C

Initial temperature of solid PCM (T_i) = 20°C

Final temperature of liquid PCM (T_f) = 70°C

Heat load of the heat exchanger (Q) = 6300 W

Time for which the heat is to be stored (t_s) = 120 s

Amount of heat stored in the above time (Q_s) = Q * t_s = 756000 J

The mass of PCM required to store Q_s amount of heat in time t_s can be determined as,

$$Q_s = m_p * c_{ps} * (T_m - T_i) + m_p * L_f + m_p * c_{pl} * (T_f - T_m)$$

$$756000 = m_P * [\ 2000*(53.7-20) + 190000 + 2150*(60-53.7)]$$

$$m_p = 2.79023418 \text{ kg}$$

Hence, the calculated mass of PCM required for effective heat storage in the system is determined to be 2.7902 kg.

4.3.2.2 Required diameter of the pipe enclosing PCM

After that, calculations were performed to determine the diameter of the pipe enclosing the PCM within the annular space of the fins. Initially, the maximum volume of the PCM is computed by dividing the previously determined mass by the density of the liquid PCM. An equation for the volume of the PCM, expressed in terms of the required diameter of the PCM pipe, is then formulated. This equation is solved to determine the diameter of the PCM pipe.

Similarly, another approach involves calculating the diameter by determining the volume of solid PCM, utilizing the density of the solid phase. The difference between these two calculated diameters gives us the necessary diametral clearance to allow for thermal expansion during the phase change from solid to liquid. These calculations are crucial in ensuring the appropriate sizing of the PCM pipe.

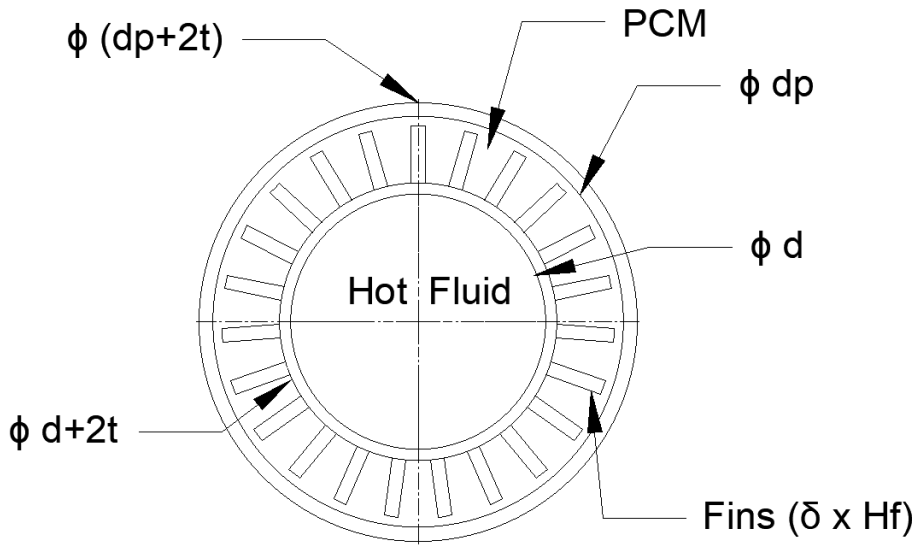

Figure 4.23: Diameter calculation PCM pipe

Volume of PCM (V_p) is given by,

$$V_p = 2 * L * N_{hp} * [\frac{\pi * d_p^2}{4} - \frac{\pi * (d+2t)^2}{4} - \delta * H_f * N_f] \text{.....(I)}$$

Where, d_p= inner diameter of pipe enclosing PCM

Equation (I) can be solved for d_p as,

$$d_p = \sqrt{\frac{4}{\pi} * [\frac{V_p}{2 * L * N_{hp}} + \frac{\pi * (d+2t)^2}{4} + \delta * H_f * N_f]} \text{.....(II)}$$

The volume of PCM can be calculated as,

$V_p = m_p / \rho_p$

Where, ρ_p= density of PCM

For solid PCM,

density of solid PCM (ρ_{ps}) = 910 kg/m^3

Volume of solid PCM (V_{ps})= $\frac{m_p}{\rho_{ps}} = \frac{2.79}{910} = 0.00306619\ m^3$

On substitution, equation (II) becomes,

$$d_{ps} = \sqrt{\frac{4}{\pi} * [\frac{0.00306619}{2*1*1.5} + \frac{\pi*(0.034)^2}{4} + 0.001 * 0.01 * 23]} = 52.4421\ mm$$

For liquid PCM,

density of liquid PCM (ρ_{pl}) = 790 kg/m^3

Volume of liquid PCM (V_{pl})= $\frac{m_p}{\rho_{pl}} = \frac{2.79}{790} = 0.003531942\ m^3$

On substitution, equation (II) becomes,

$$d_{pl} = \sqrt{\frac{4}{\pi} * [\frac{0.003531942}{2*1*1.5} + \frac{\pi*(0.034)^2}{4} + 0.001 * 0.01 * 23]} = 54.294\ mm$$

To allow for thermal expansion during phase change from solid to liquid, the diameter of PCM pipe is chosen as the maximum value between d_{pl} and d_{ps}. That is,

$d_p = d_{pl}$

Radial clearance to allow for phase change expansion (r_c):

$r_c = (d_{pl}-d_{ps})/2 \quad r_c = \frac{d_{pl}-d_{ps}}{2} = \frac{54.294-52.4421}{2} = 0.92595\ mm$

4.3.2.3 Pump sizing and selection

In the pump sizing and selection process, the determination of head loss in the heat exchanger is a critical step. This involves calculating both major and minor head losses for both the hot and cold fluids.

Major Head Loss: The major head loss includes the frictional head loss along the length of the pipe, and is calculated using the Darcy-Weisbach equation. This equation is applied for both hot and cold fluids.

For hot fluid,

$$\Delta P_{h,frictional} = \frac{f_h * L_t * v_h^2 * \rho_h}{2 * d_{hi}} = \frac{0.031035 * 3 * 0.23937^2 * 985.01}{2 * 0.03} = 89.019 \text{ Pa}$$

For cold fluid,

$$\Delta P_{c,frictional} = \frac{f_c * L_t * v_c^2 * \rho_c}{2 * d_{ci}} = \frac{0.019686 * 3 * 0.215613^2 * 997.5}{2 * 0.012} = 117.7085 \text{ Pa}$$

Minor Head Loss: The minor head loss includes considerations for the head loss in the pipe bend of the hot pipe, entry loss from the reservoir to the pipeline, and exit loss from the pipes in the heat exchanger to the atmosphere. These are calculated individually and summed up for both hot and cold fluids.

For hot fluid,

$$\Delta P_{h,bends} = 1.3 * \frac{v_h^2}{2 * g} * 2 = 1.3 * \frac{0.23937^2}{2 * 9.81} = 73.37083 \text{ Pa}$$

$$\Delta P_{h,entry} = \frac{0.5 * v_h^2 * \rho_h}{2} = \frac{0.5 * 0.23937^2 * 985.01}{2} = 14.1098 \text{ Pa}$$

$$\Delta P_{h,exit} = \frac{v_h^2 * \rho_h}{2} = \frac{0.23937^2 * 985.01}{2} = 28.2196 \text{ Pa}$$

For cold fluid,

$$\Delta P_{c,entry} = \frac{0.5 * v_c^2 * \rho_c}{2}$$

Where, v_c = velocity of the cold fluid in the annular space $= \frac{4 * m_c}{\pi * \rho_c * (0.08^2 - 0.068^2)}$

$$= \frac{4 * 0.3}{\pi * 997.5 * (0.08^2 - 0.068^2)}$$

$$= 0.215613 \text{ m/s}$$

So, $\Delta P_{c,entry} = \frac{0.5 * 0.21613^2 * 997.5}{2} = 11.64 \text{ Pa}$

$$\Delta P_{c,exit} = \frac{v_c^2 * \rho_c}{2} = \frac{0.215613^2 * 997.5}{2} = 23.28 \text{ Pa}$$

To account for factors not considered in the above calculations, an additional head of 2m is added for both fluids. This includes the physical height of the reservoir, head losses due to factors such as frictional losses in the pipeline from the reservoir to the heat exchanger, and disturbances arising from the hairpin geometry of the heat exchanger. The corresponding pressure drops are calculated as,

For hot fluid,

$$\Delta P_{h,additional} = \rho_h * g * H = 985.01 * 9.81 * 2 = 19326 \text{ Pa}$$

For cold fluid,

$$\Delta P_{c,additional} = \rho_c * g * H = 997.5 * 9.81 * 2 = 19571 \text{ Pa}$$

The total pressure drops for both hot and cold fluids is determined by summing the major and minor head losses along with the additional considerations.

For hot fluid,

$$\Delta P_{h,total} = \Delta P_{h,frictional} + \Delta P_{h,bends} + \Delta P_{h,entry} + \Delta P_{h,exit} + \Delta P_{h,additional} = 19531 \text{ Pa}$$

For cold fluid,

$$\Delta P_{c,total} = \Delta P_{c,frictional} + \Delta P_{c,bends} + \Delta P_{c,entry} + \Delta P_{c,exit} + \Delta P_{c,additional} = 19724 \text{ Pa}$$

The calculated total pressure drops serve as the basis for determining the pumping power required for the application. The pumping power is a crucial parameter in the selection of an appropriately sized pump for optimal system performance whose calculations are shown below.

Assuming the pump efficiency(η_p) of both hot and cold fluids to be 0.5,

$$(\text{Pumping power})_{\text{hot}} = \frac{\Delta P_{h,total} * \dot{m}_h}{\eta_p * \rho_h} = \frac{19531 * 0.16667}{0.5 * 985.01} = 6.61\ \text{W}$$

$$(\text{Pumping power})_{\text{cold}} = \frac{\Delta P_{c,total} * \dot{m}_c}{\eta_p * \rho_c} = \frac{19724 * 0.3}{0.5 * 997.5} = 11.86\ \text{W}$$

Since there aren't any commercially available pumps that have an exact power of 11.86 watts, the next available size has to be selected which is 15 watts.

4.3.3 CAD Modelling and Simulation

4.3.3.1 CAD Modelling

The final design phase includes a detailed schematic diagram, which clearly shows the main parts of the quadruple pipe PCM heat storage setup and what they do. This visual representation shows how all the parts are organized systematically, giving us an idea of how each piece helps store and release thermal energy effectively.

- Inner Tube with Fins (Hot Fluid Flow)
- PCM Pipe Enclosing PCM
- Insulation Pipe (Air Enclosure for Insulation)
- Outer Pipe (Cold Fluid Flow)
- Water Pumps (Hot and Cold Fluids)
- Reservoirs (Hot and Cold Fluids)
- Cooling Tower

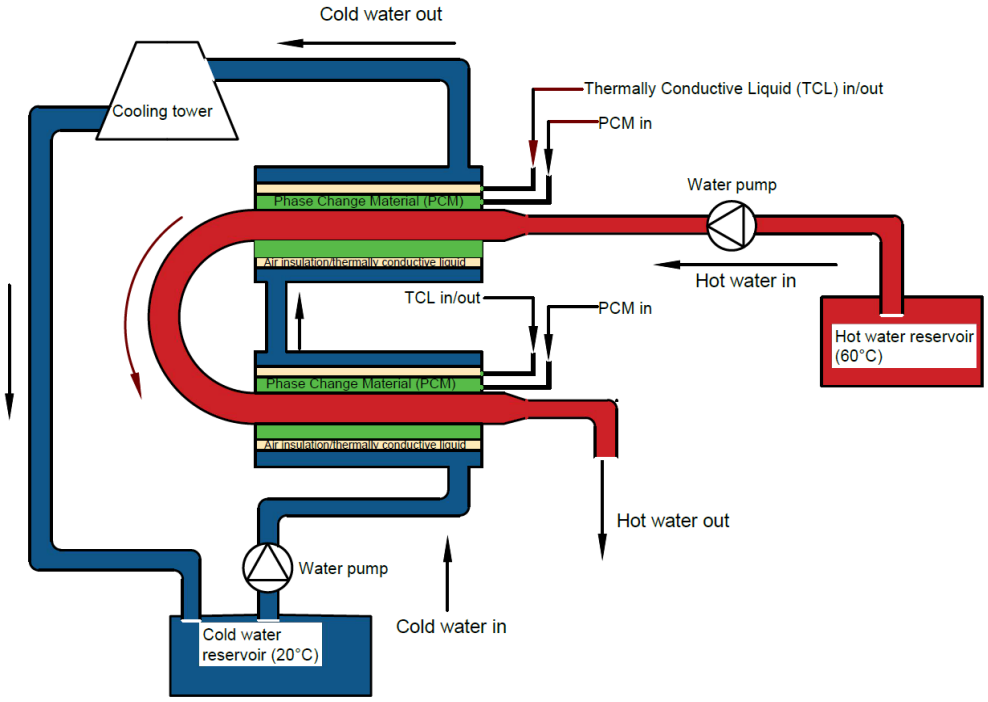

Figure 4.24: Schematic diagram of the quadruple pipe/concentric tube PCM heat storage setup

The theoretical calculations are turned into a real design by making a detailed Computer-Aided Design (CAD) model. This model, created with CAD software, includes all the measurements and details we figured out earlier in the project.

The two-dimensional side and sectional front views produced from the CAD model, gave a detailed look at how the PCM heat exchanger is set up and its important measurements. These views are crucial for making sure the real prototype matches the planned specifications during fabrication.

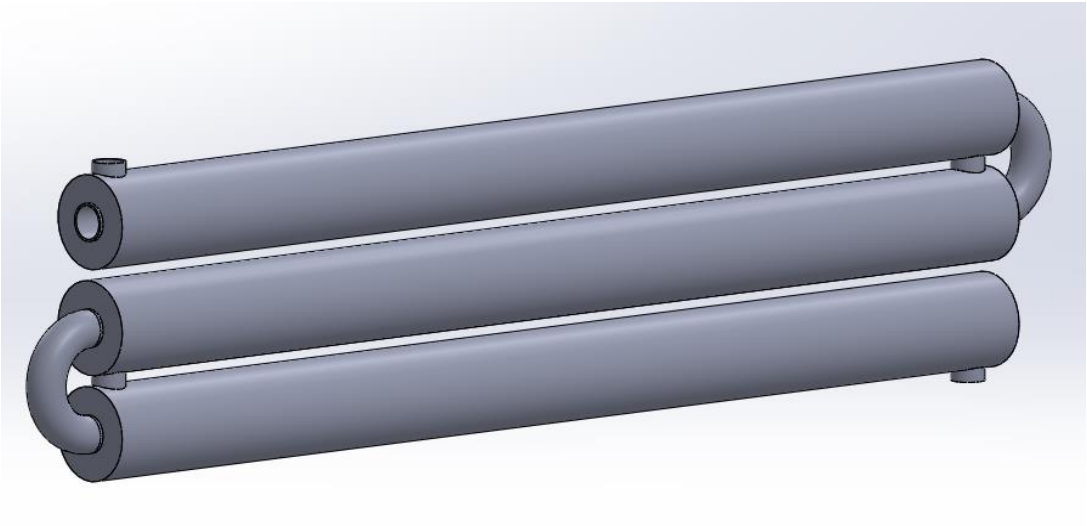

Figure 4.25: CAD Model of the concentric tube PCM heat storage setup

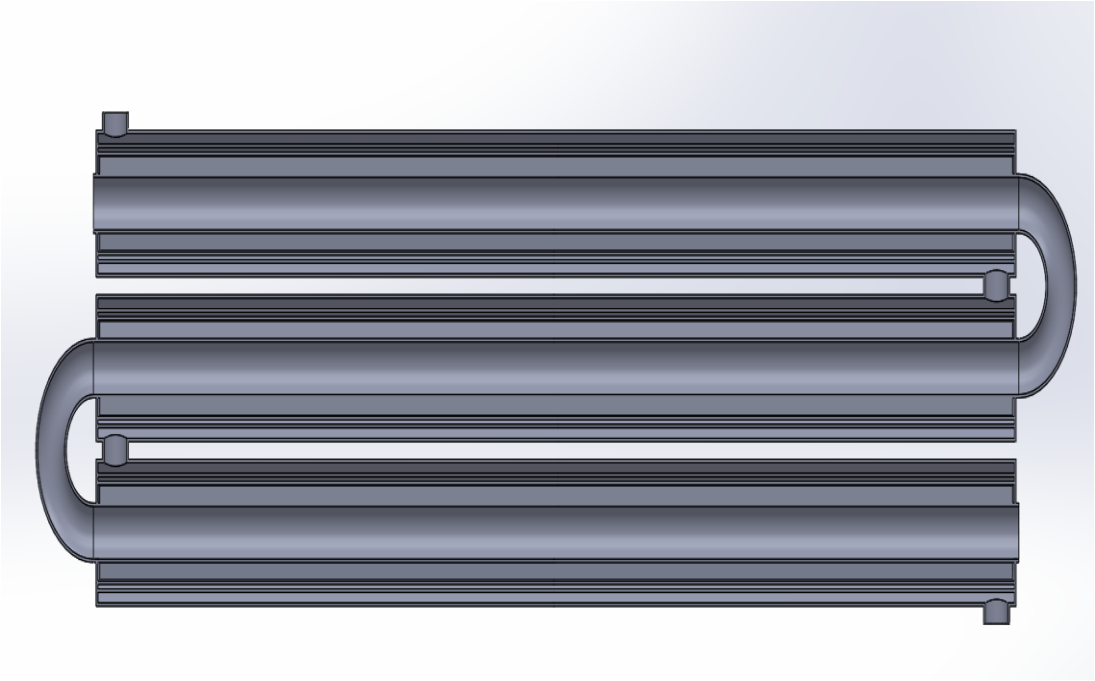

Figure 4.26: Side view of the concentric PCM heat storage setup

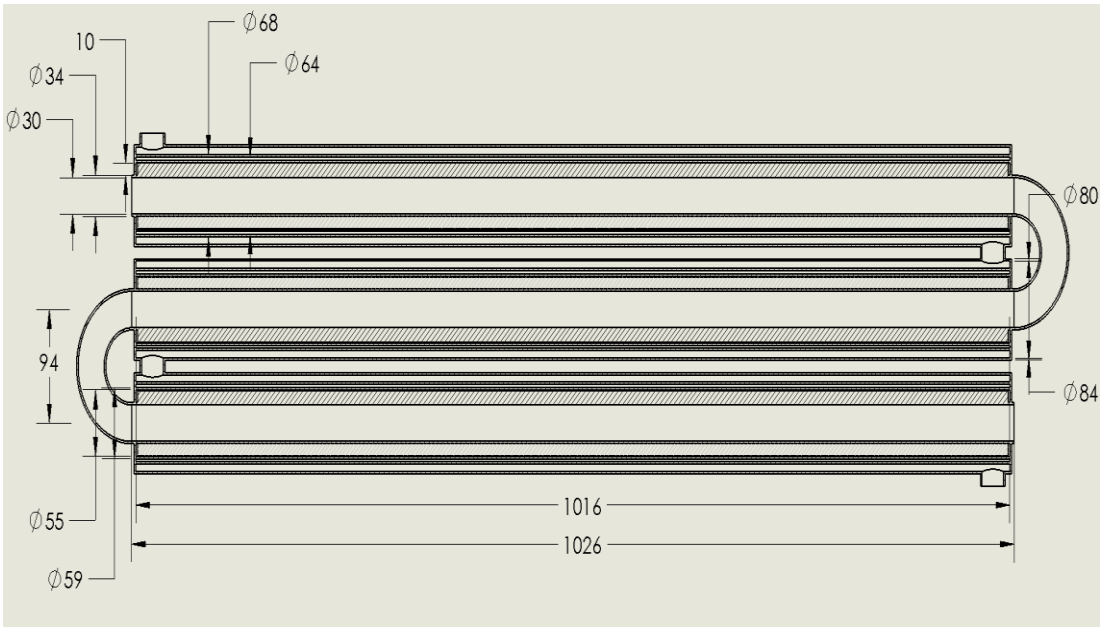

Figure 4.27: Sectional front view of the concentric tube PCM heat storage setup

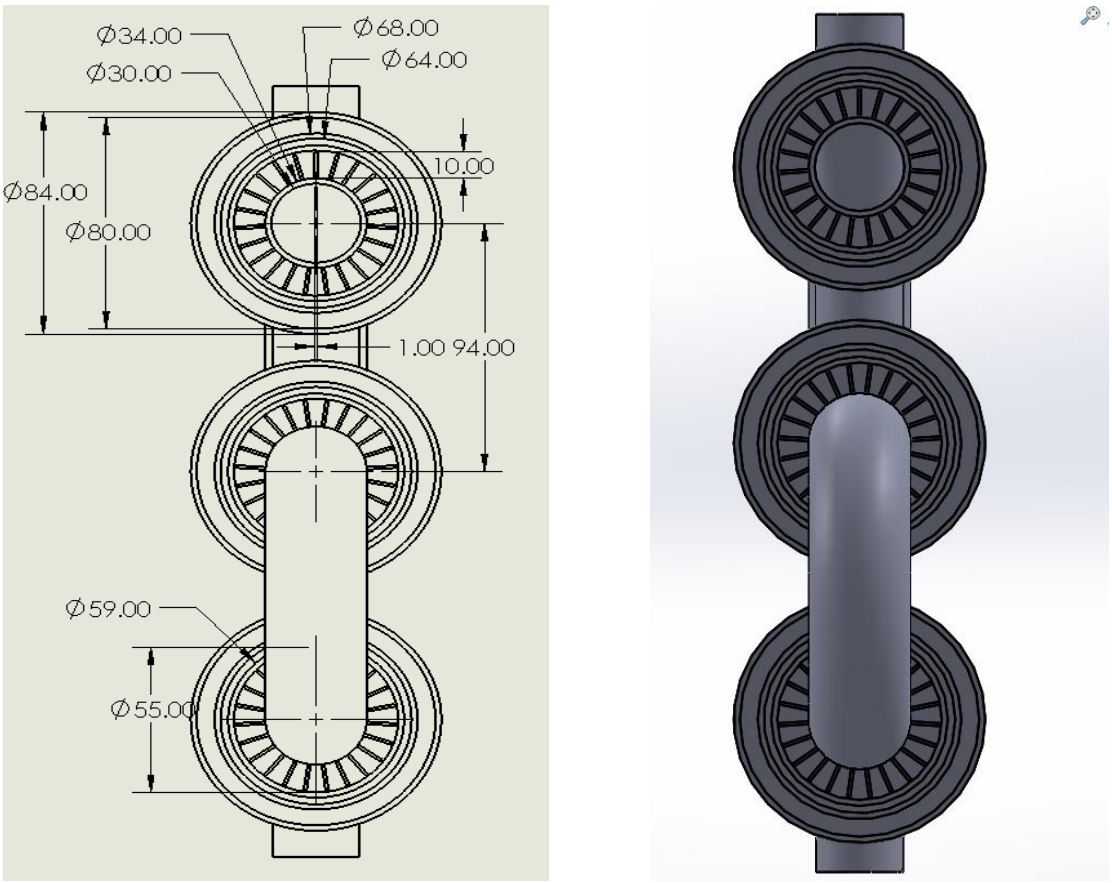

Figure 4.28: Side view of the concentric tube PCM heat storage setup

4.3.3.1 Simulation of melting/solidification of PCM

Initially the simulation of melting of PCM was performed by passing hot water at a temperature of 60^{o}C with a flow rate of 10 LPM. The liquid fraction, outlet temperature of hot water, and PCM average temperature were noted at every time step of the transient simulation. Then the heat transfer rate was calculated using the equation,

$$Q = \dot{m} * c_p * (T_o - T_i)$$

Where, $\dot{m}$ = mass flow rate of hot fluid

c_p = specific heat capacity of water

$T_o - T_i$ = Temperature difference between inlet and outlet

Inlet temperature of hot water (T_i) = 60^{o}C = 333 K

Then, the logarithmic mean temperature difference (LMTD) was also calculated using,

$$LMTD = \frac{(\text{Hot water outlet temp} - \text{average PCM temperature}) - (T_i - \text{average PCM temperature})}{\ln\left(\frac{\text{Hot water outlet temp} - \text{average PCM temperature}}{T_i - \text{average PCM temperature}}\right)}$$

Finally, the overall heat transfer coefficient was calculated using, $h = \frac{Q}{A_f * LMTD}$

Where, A_f = Net finned area of the tube

Flow time(sec)	PCM liquid fraction	Outlet temperature (K)	PCM average temperature (K)	Heat transfer rate (W)	LMTD (K)	Overall heat transfer coefficient ($W/m^2.K$)
0	0	-	318	-	-	-
100	0.0055	330.67	318.127	1631.3262	13.6749	177.0979471
200	0.0869	331.164	322.03	1285.45704	10.0239	190.3771291
300	0.21107	331.399	323.1546	1120.92414	9.02123	184.4625255
400	0.3255	331.572	323.947	999.79992	8.31858	178.4274693
500	0.4267	331.7211	324.6455	895.409046	7.69735	172.6943437
600	0.5164	331.851	325.26	804.46086	7.15011	167.02809
700	0.5962	331.96	325.815	728.1456	6.65145	162.5172706
800	0.6678	332.059	326.309	658.83174	6.20861	157.5351223
900	0.73182	332.1451	326.76	598.549686	5.80205	153.1497023
1000	0.78867	332.2948	327.1793	493.738728	5.46051	134.2337419
1100	0.83833	332.3662	327.58126	443.748732	5.09527	129.2908193
1200	0.8786	332.4375	328.002	393.82875	4.71115	124.1017726
1300	0.91	332.5088	328.441	343.908768	4.30873	118.4926545
1400	0.93564	332.5801	328.621	293.988786	4.16552	104.7753493
1500	0.95849	332.6514	329.11	244.068804	3.71297	97.58619966
1600	0.9769	332.7227	329.282	194.148822	3.57755	80.56490009
1700	0.99531	332.794	329.454	144.22884	3.44197	62.20748127
1750	1.00	332.82965	329.54	119.268849	3.37410	52.47662899

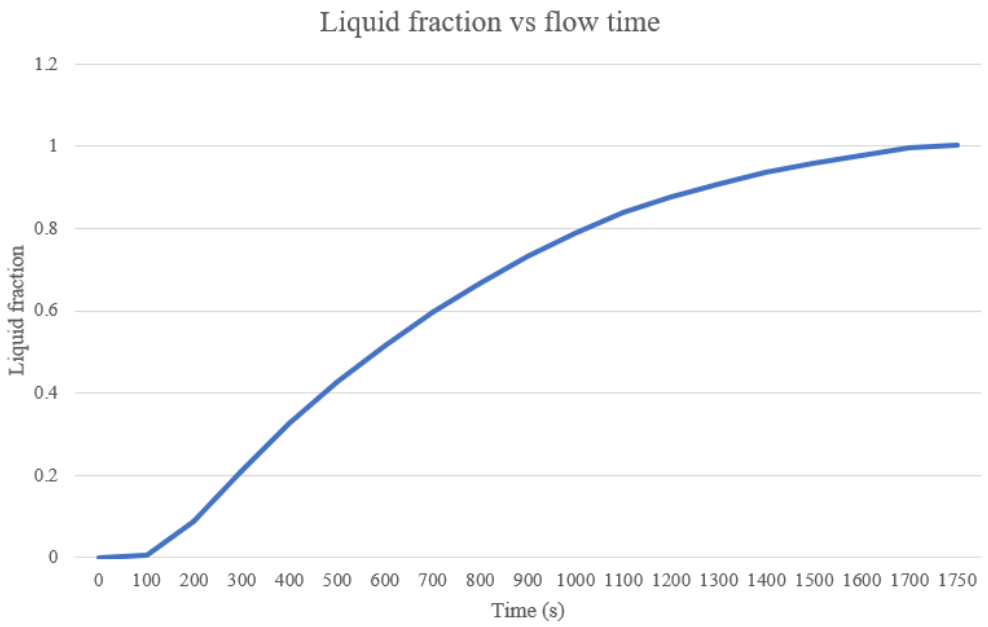

Figure 4.29: Variation of liquid fraction vs. Time during the melting of PCM in concentric tube heat storage setup

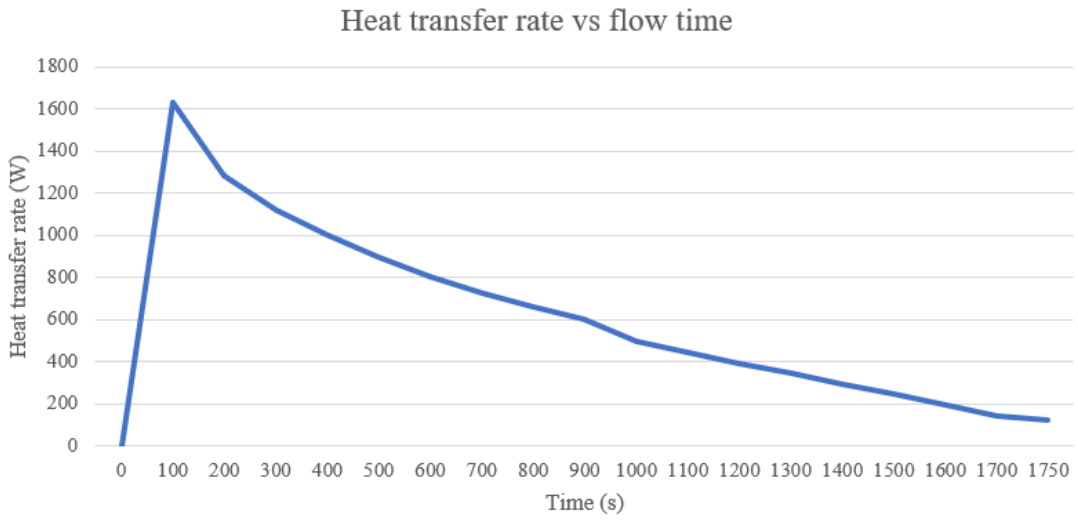

Figure 4.30: Heat transfer rate vs. Time during the melting of PCM in concentric tube heat storage setup

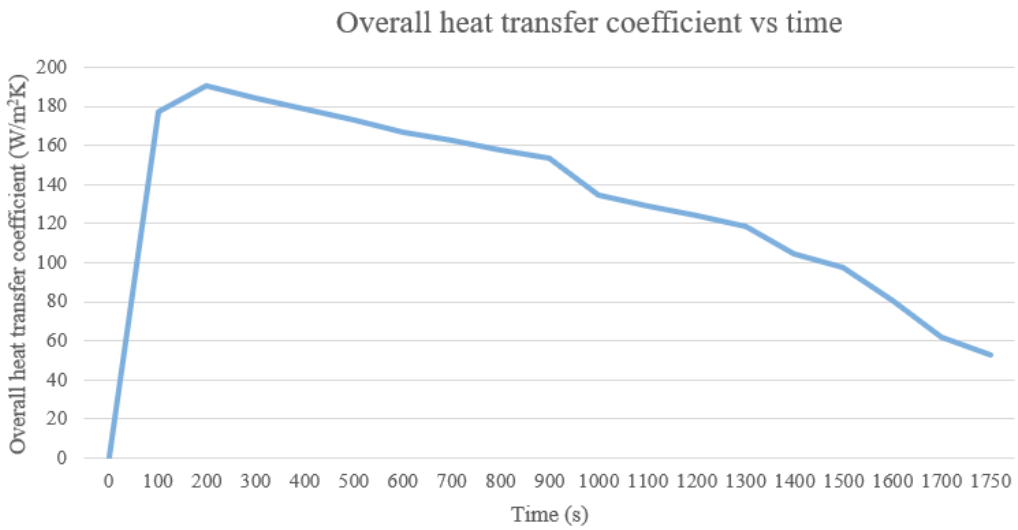

Figure 4.31: Variation of overall heat transfer coefficient vs. Time during the melting of PCM in concentric tube heat storage setup

Initially, the graph showcasing liquid fraction vs. time indicates that approximately 1750 seconds are required to fully melt 2.8 kilograms of PCM. Also, the graph illustrating heat transfer rate vs. time shows a rapid increase in heat transfer for the initial 150 seconds, followed by a gradual decrease over time. This decrease in heat transfer rate can be attributed to several factors. Firstly, as the PCM undergoes phase change from solid to liquid, there is a decreasing temperature difference between the hot water and the PCM, leading to a decline in the rate of heat transfer. Additionally, during the phase change process, the thermal conductivity of the PCM decreases, further contributing to the reduction in heat transfer efficiency. Also, the overall heat transfer coefficient demonstrates a decreasing trend over time, indicative of a declining effectiveness in the heat transfer process.

The amount of heat lost by the hot water can be calculated from the area under the heat transfer rate vs. time graph. This area includes the total heat transferred from the hot water to both the PCM and the pipes.

Conducting a heat balance analysis enables estimation of the heat stored within the PCM and the pipes. The heat stored in the PCM comprises both sensible heat, associated with temperature rise before phase change, and latent heat absorbed during the phase change process and the heat stored in the pipes corresponds to the increase in

their temperature as a result of heat transfer from the hot water. The distribution of heat reveals that approximately 65.5% of the heat lost by the hot water is absorbed by the PCM as latent heat during the phase change, with the remaining portion being stored in the pipes.

Amount of heat stored in PCM = $Q_s = m_p*c_{ps}*(T_m - T_i) + m_p*L_f + m_p*c_{pl}*(T_f - T_m)$ = 726.889 KJ

Amount of heat lost by hot water throughout the melting of PCM = Area under the heat transfer rate graph = 1126.832 KJ

By heat balance, Heat lost by hot water = Heat stored in PCM + Heat lost from the system and heat stored in pipes

Therefore, Heat lost from the system and heat stored in Pipes = 1126.832-726.889 = 399.94 KJ

Heat	**Amount (KJ)**	**Percentage**
Stored in PCM	726.889	64.55%
Stored in Pipes & lost from the system via natural convection	399.94	35.45%
Total	**1126.832**	**100%**

Table 4.8: Heat transfer distribution in concentric tube arrangement

Similarly, the simulation of solidification of PCM was also performed by following the similar procedure whose results are shown below:

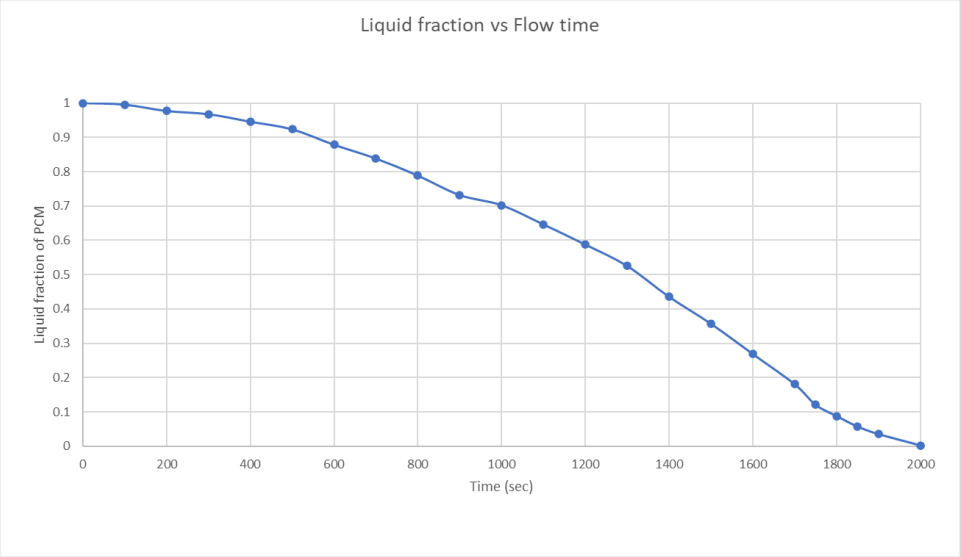

Figure 4.32: Variation of liquid fraction vs. Time during the solidification of PCM in quadruple pipe arrangement

The graph showcasing liquid fraction vs. time indicates that approximately 2000 seconds are required to fully solidify 3.4 kilograms of liquid PCM.

4.4 Design of a finned shell and tube arrangement

4.4.1 Material Selection

In the design of the shell and tube heat exchanger for the PCM heat storage system, the selection of appropriate materials was a critical first step. A decision matrix, similar to the one used for the double pipe heat exchanger design, was employed to systematically evaluate and choose the most suitable material.

In contrast to the double pipe heat exchanger, the shell and tube arrangement required fewer components and materials. Therefore, thermal conductivity was given the highest priority in the decision-making process, prioritizing performance over cost.

A decision matrix was created with rows representing different materials and columns representing evaluation criteria such as thermal conductivity, cost, corrosion resistance, and availability. Each material option was assessed based on its thermal conductivity,

cost-effectiveness, corrosion resistance, and availability, and scores were assigned accordingly for each criterion.

		Weight factor of					
		Thermal Conductivity	**Cost**	**Strength**	**Corrosion Resistance**	**Light Weight**	**Total Weighted Score**
		5	4	3	2	1	
Materials	Stainless Steel	0.2	1.9	2.2	5	2	27.2
	Mild Steel	0.6	5	4	2	3	42
	Carbon Steel	0.6	4	3.3	1	4	34.9
	Copper	5	0.7	2	4	1	42.8
	Aluminum	2.9	1.6	1	3	5	34.9

Table 4.9: Decision Matrix for material selection in shell & tube heat exchanger arrangements

After careful evaluation, copper emerged as the top choice with the highest overall score of 42.8. Its outstanding thermal conductivity outweighed concerns about cost, corrosion resistance, and availability. Therefore, copper was chosen for both the pipes and fins in the shell and tube heat exchanger. Its excellent thermal conductivity matches the needs of our PCM heat storage system perfectly.

4.4.2 Hydraulic Design

In the hydraulic design phase of the shell and tube heat exchanger project, the aim was to determine the optimal diameter that strikes a balance between material cost and power loss due to head loss.

Similar to the approach taken in the double pipe heat exchanger design, frictional head loss was computed for the tube of the optimum diameter using established equations such as the Darcy-Weisbach equation. Using appropriate equations, such as Haaland's

equation for determining the friction factor, and considering factors like relative roughness, head loss per unit length for both hot and cold fluid flows through the shell and tube arrangement were calculated.

The results of all the hydraulic design of shell & tube arrangement are tabulated below:

Optimum pipe diameter = 28 mm

Total pipe length = 1.963 m

Parameters	**Hot Water**	**Cold Water**
Flow rate	10 LPM	18 LPM
Mass flow rate	0.16667 kg/s	0.3 kg/s
Reynold's number	17477.0706	13906.87762
friction factor for that diameter (f)	0.02671793	0.028331744
Head loss per length (H/L)	0.00533805	0.017787969
Head loss (in m of water)	0.01047859	0.034917783

Table 4.10: Hydraulic design of shell & tube arrangement

4.4.3 Thermal Design

The thermal design followed the same procedure used for the double pipe heat exchanger. Calculations involved finding the Nusselt number and the heat transfer coefficient due to convection. The results of these calculations are shown in the table below.

Parameters	**Hot Water**	**Cold Water**
Thermal conductivity (k) (W/m.K)	0.654	0.5944
Prandtl's number (Pr)	2.99	7.442
Nusselt's number (Nu)	91.95505514	108.851229
Convection heat transfer coefficient ($W/m^2.K$)	2313.02331	2488.506558

Table 4.11: Thermal design of shell & tube arrangement

4.4.4 Structural Design

The structural design of the shell and tube arrangement followed a similar approach to that of the double pipe heat exchanger. Maximum allowable water pressures were found using hoop stress and axial stress equations for a pipe with an optimal internal diameter of 28 mm and a wall thickness of 1 mm.

Parameters	**Values**
Yield strength of copper	150 Mpa
Pipe thickness	1 mm
Inner diameter of pipe	28 mm
Outer diameter of pipe	30 mm
Factor of safety	2
Allowable hoop stress	75 Mpa
Maximum allowable pressure to withstand hoop stress	2.631 Mpa
Allowable axial stress	100 Mpa
Maximum allowable pressure to withstand axial stress	7.27 Mpa

Table 4.12: Structural design of the shell & tube arrangement

The values calculated, shown in the table below, reveal that the maximum allowable pressures are much higher than the actual internal pressure in the pipe. Therefore, it's concluded that a pipe with a 1 mm wall thickness is suitable for the intended use.

4.4.5 Pump sizing and selection

The pump was selected following the same careful steps used for the double pipe heat exchanger. Detailed calculations were done to figure out how much pressure the water loses as it moves through the system. This included looking at different factors like how the water enters and exits, how it flows around bends, how rough the pipes are inside, and how high the water needs to go. All these losses were added up to find the total pressure loss of the water. Then, using this total pressure loss, the exact power needed for the pump was determined. The results of the pump sizing and selection are shown in the table below:

Number of 90° elbows = 10

Efficiency of the pump = 50%

Parameters	**Hot water**	**Cold water**
Velocity of fluid (m/s)	0.313915075	0.565047135
Frictional head loss (h_f) (m)	0.010131531	0.034808925
Diversions and bends loss (h_d) (m)	0.050225624	0.162731022
Static head/height of the setup (h_s) (m)	0.35	0.35
Additional head (h_a) (m)	2	2
Entry loss (h_{entry}) (m)	0.002707216	0.008771381
Entry loss (h_{exit}) (m)	0.005414433	0.017542762
Total head (h_t) (m)	2.418478804	2.573854089
Total pressure (Pa)	23329.06494	25210.11938
Pump power (W)	7.77635498	15.12607163

Table 4.13: Pump sizing and selection

Since there aren't any commercially available pumps that have an exact power of 15.126 watts that can handle hot water of 60°C, the next available size has to be selected which is 186.425 W or 0.25 HP.

4.4.6 CAD Modeling and Simulation

After finalizing the design of the PCM shell and tube heat exchanger arrangement for heat storage, a CAD model was developed using SolidWorks CAD software. The model was then subjected to Computational Fluid Dynamics (CFD) simulation in ANSYS Fluent.

4.4.6.1 Shell & tube setup with fin

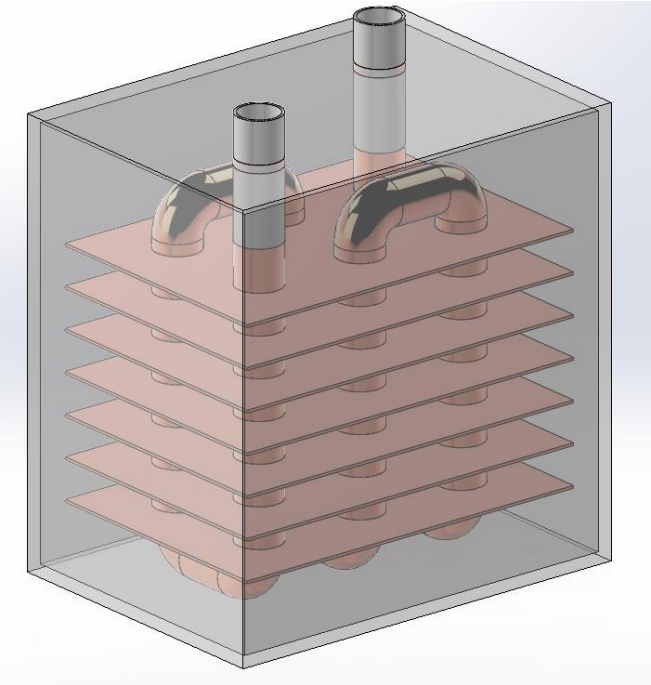

Figure 4.33: CAD Model of the finned shell & tube setup

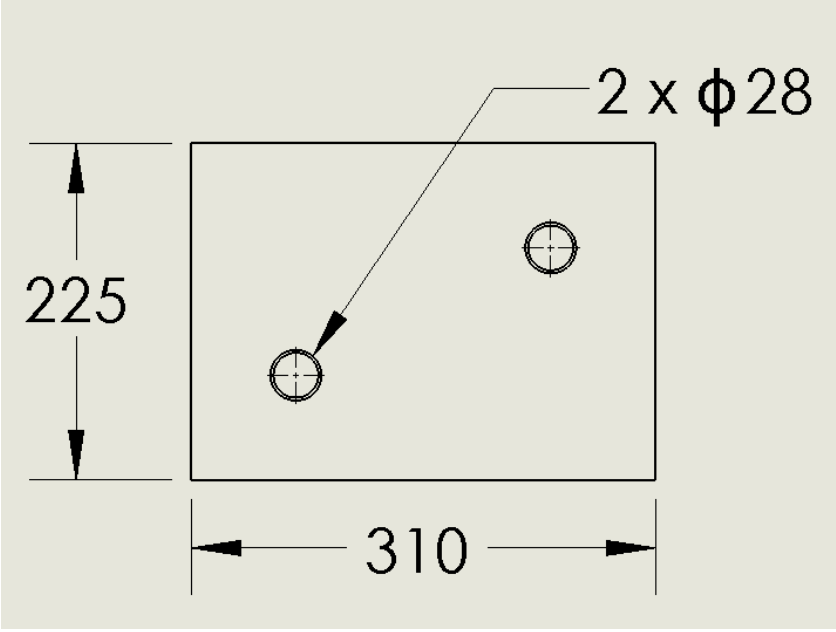

Figure 4.34: Top view of the finned shell & tube setup

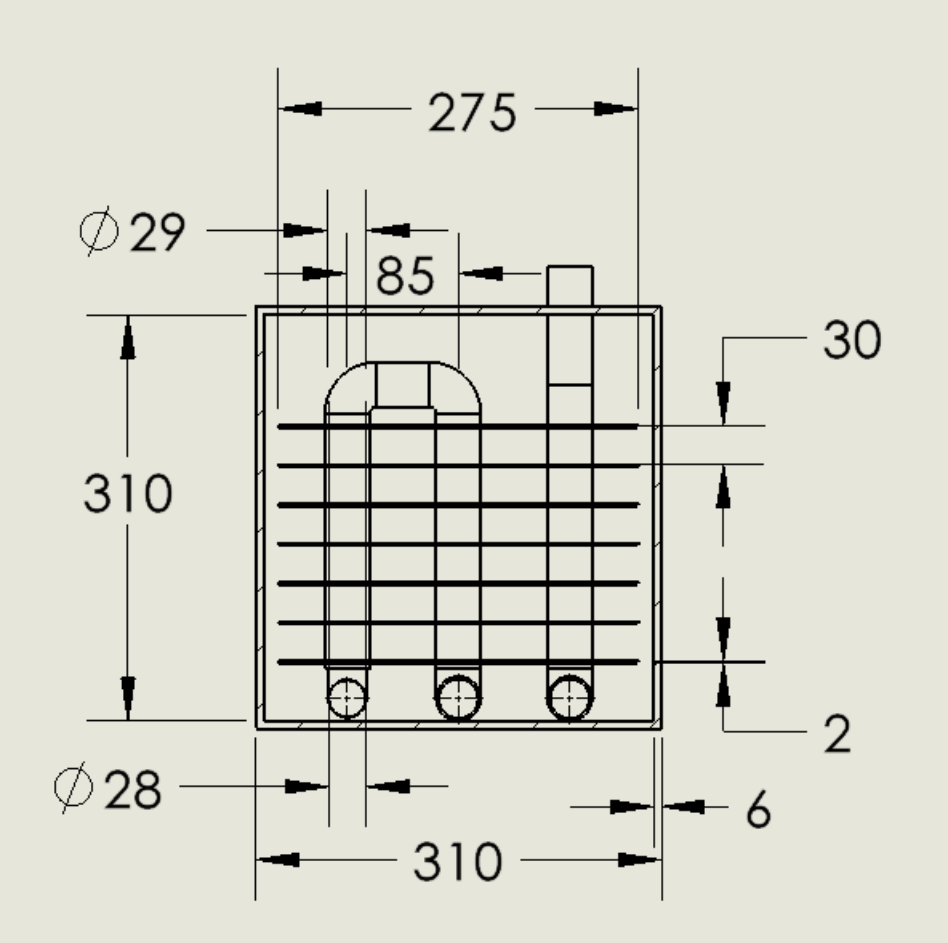

Figure 4.35: Sectional front view of the finned shell & tube setup

a) Melting of PCM

The simulation aimed to understand how different things changed over time as the phase change material (PCM) melted in a finned shell and tube setup. It looked at things like how much of the PCM turned into liquid, the temperature of the water, the temperature of the PCM, how fast heat moved, how well heat transferred, and a number called Nusselt's number.

Graphs and contours were used to show these changes visually. These pictures helped see how the system behaved as the PCM changed from solid to liquid. Important things noticed included how much of the PCM turned into liquid and how its temperature changed, along with changes in water temperature and heat transfer characteristics.

The various contours are shown in the pictures below:

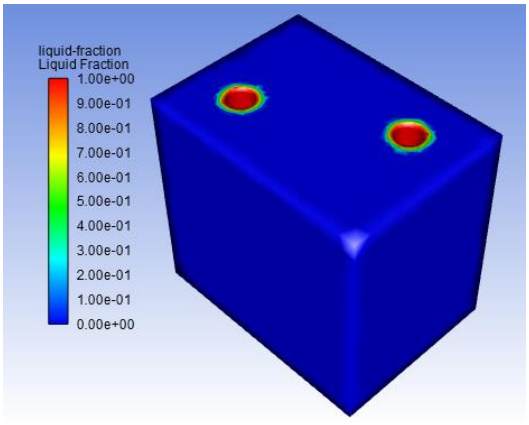

Flow Time: 610 sec

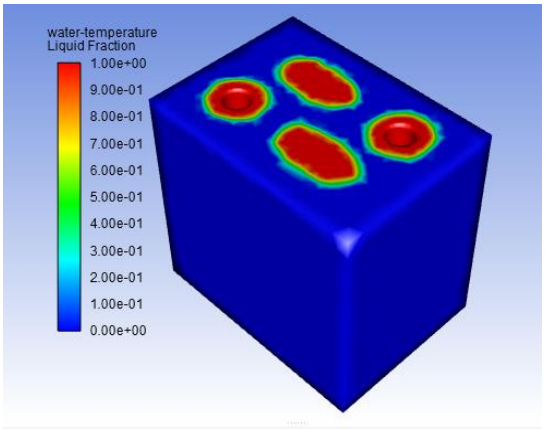

Flow Time: 2110 sec

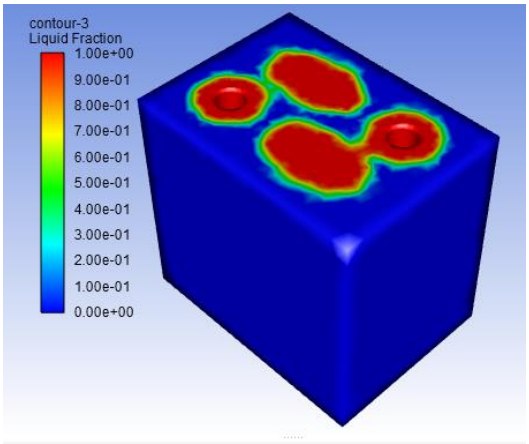

Flow Time: 3318 sec

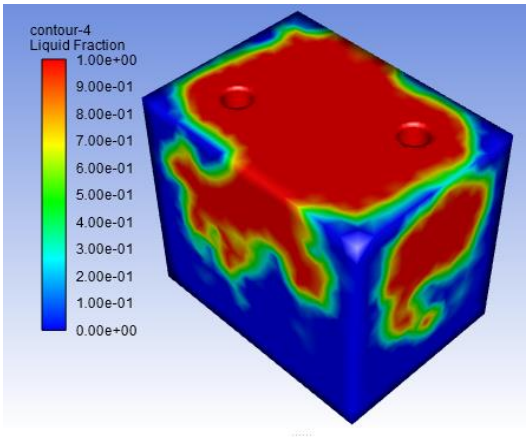

Flow Time: 4640 sec

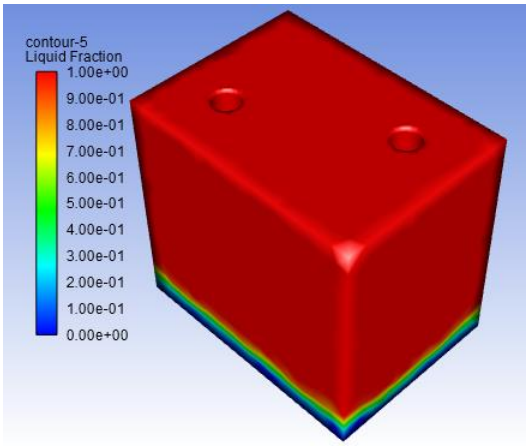

Flow Time: 7722 sec

Figure 4.36: Liquid fraction contours during the melting of PCM in finned shell & tube arrangement

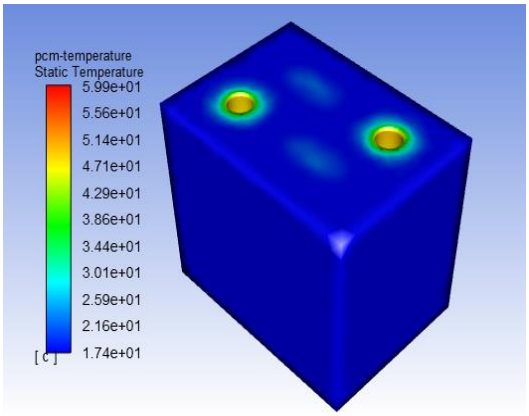

Flow Time: 610 sec

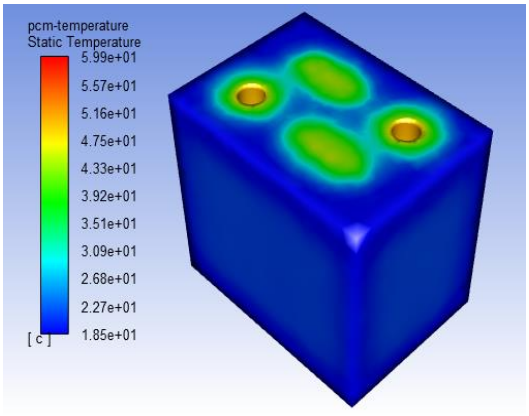

Flow Time: 2110 sec

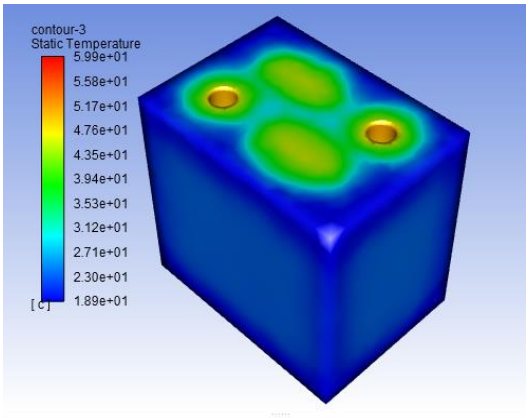

Flow Time:3318 sec

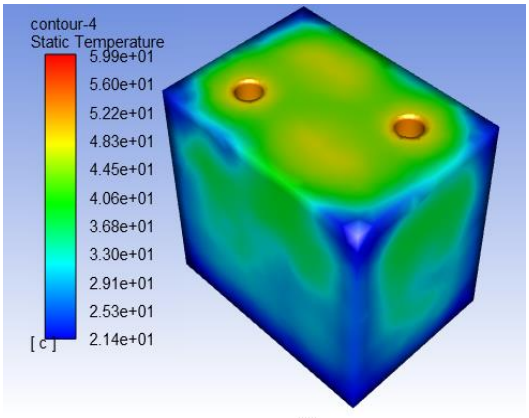

Flow Time: 4640 sec

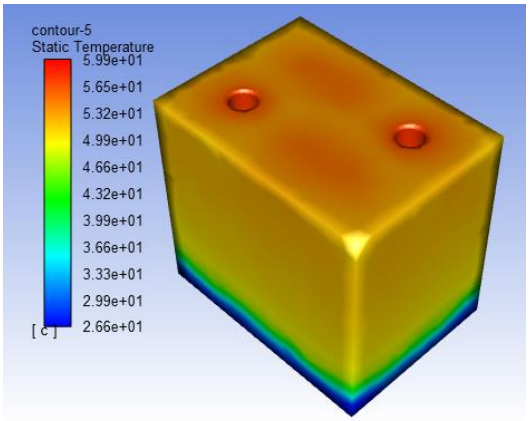

Flow Time: 7722 sec

Figure 4.37: PCM average temperature contours during the melting of PCM in finned shell & tube arrangement

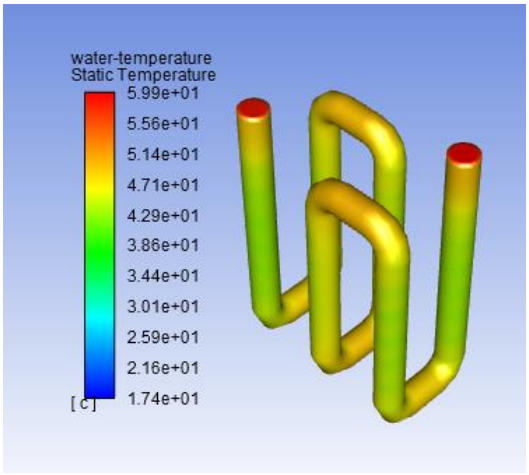

Flow Time: 610 sec

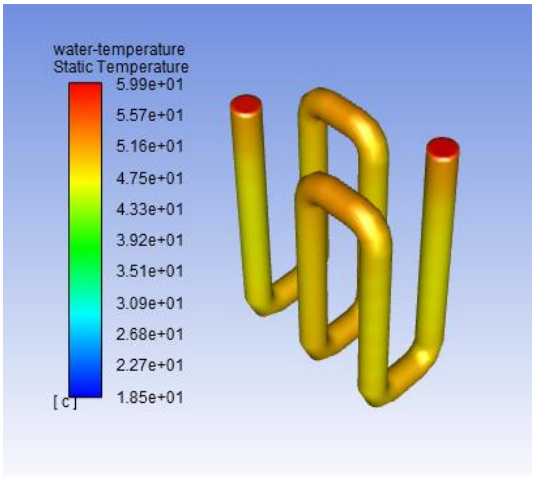

Flow Time: 2110 sec

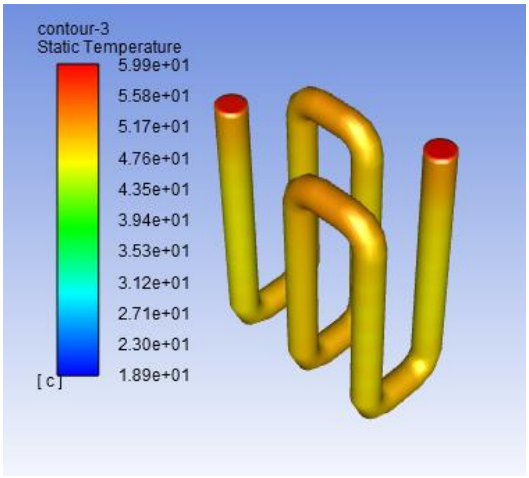

Flow Time: 3318 sec

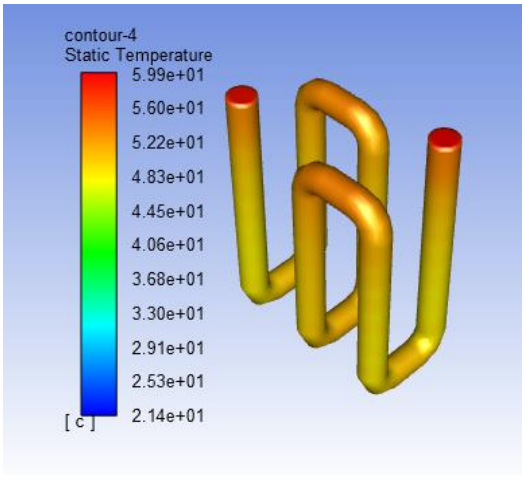

Flow Time: 4640 sec

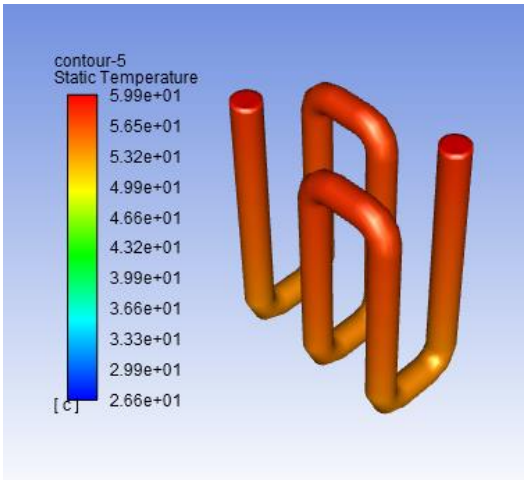

Flow Time: 7722 sec

Figure 4.38: Water temperature contours during the melting of PCM in finned shell & tube arrangement

The various graphs and charts are shown in the pictures below:

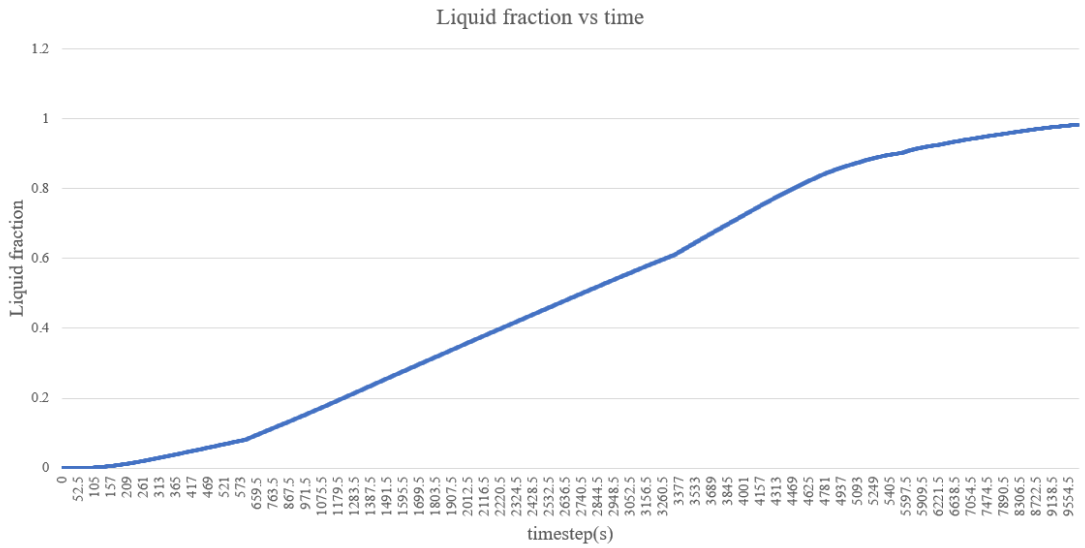

Figure 4.39: Liquid fraction plot during melting of PCM in finned shell & tube arrangement

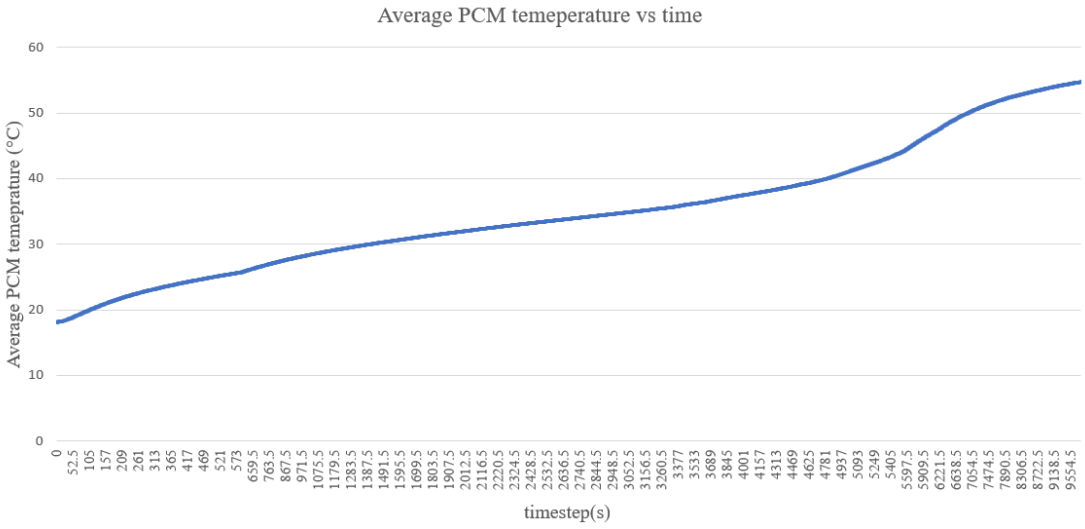

Figure 4.40: Average PCM temperature vs flow time during melting of PCM in finned shell & tube arrangement

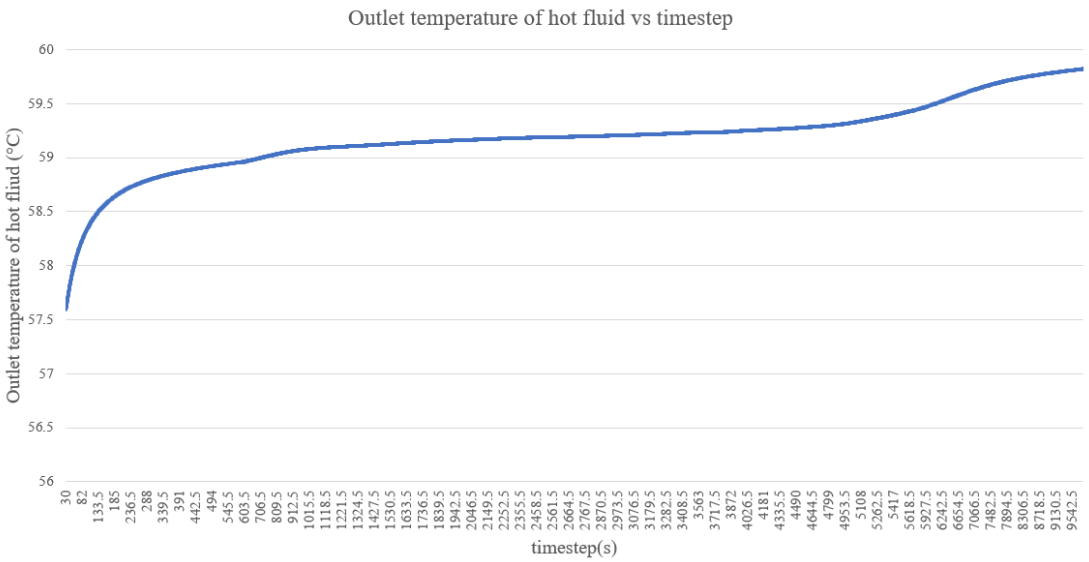

Figure 4.41: Hot water outlet temperature vs flow time during melting of PCM in finned shell & tube arrangement

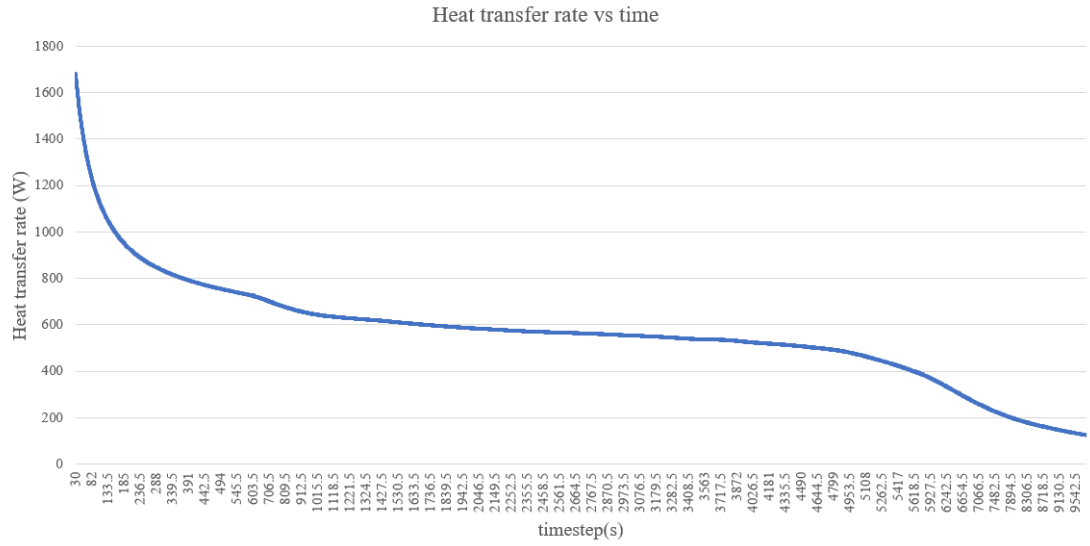

Figure 4.42: Heat transfer rate vs flow time during melting of PCM in finned shell & tube arrangement

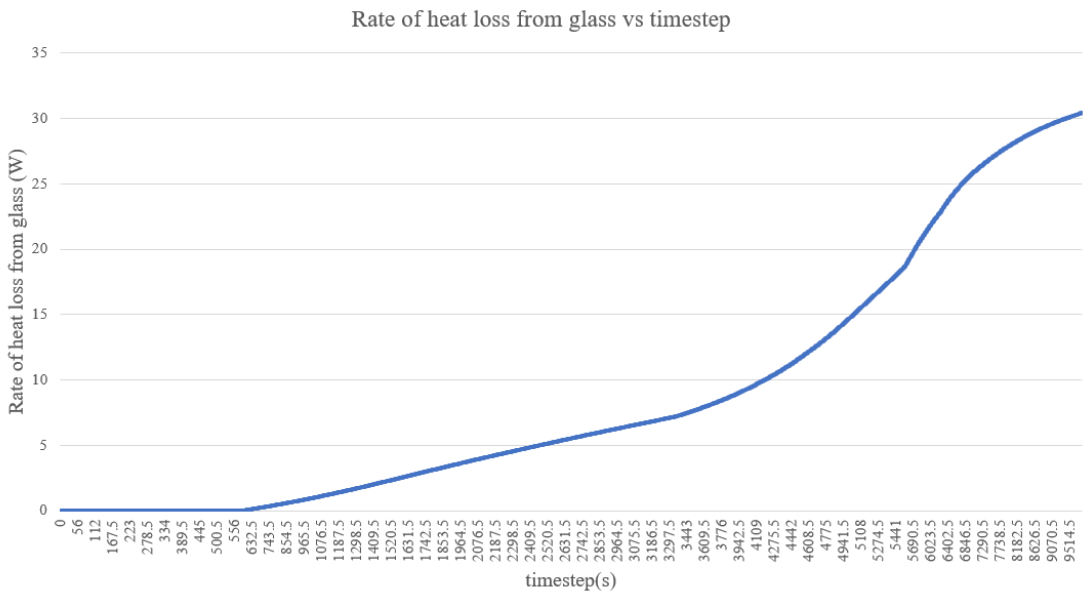

Figure 4.43: Heat loss rate from the glass surface vs flow time during melting of PCM in finned shell & tube arrangement

The graph showing how much of the PCM turned into liquid over time tells us that it takes about 2.73 hours for around 16 kg of PCM to melt completely. At the same time, the graphs for the PCM temperature and the temperature of the hot water going out show a steady rise and fall, which is what we expected.

But the graph for the heat transfer rate shows a steady decrease over time. This happens because as the PCM changes from solid to liquid and gets closer in temperature to the fluid around it, there's less of a difference in temperature, so heat transfers more slowly.

To figure out how much heat is exchanged, we can look at the area under the graph for the heat transfer rate and time. This shows us the total heat transferred from the hot water to the PCM and surroundings. And to find out how much heat is lost from the glass surface, we can look at the area under the graph for heat loss rate versus time.

Theoretical amount of heat stored in PCM = $m_p * c_{ps} * (T_m - T_i) + m_p * L_f + m_p * c_{pl} * (T_f - T_m)$ = 4218.632278 kJ

From the graphs, Heat lost by the hot water = 4391.04 kJ

Heat lost from the glass outer surface = 149.383 kJ

By heat balance, Heat lost by hot water= Heat stored in PCM + Heat loss from the glass + Heat stored in glass and pipe

So, heat stored in glass and pipe = 4391.04 - 4218.632 - 149.383 = 23.02 kJ

The overall distribution of the heat can be visually represented by the pie-chart shown below:

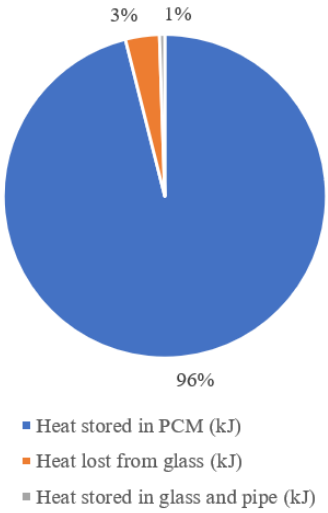

Figure 4.44: Overall distribution of the heat lost by the hot water

b) Solidification of PCM

The study on PCM solidification in a finned shell and tube setup, similar to the PCM melting simulation, aimed to look at things like how much of the PCM turned into liquid, the temperatures of the water and PCM, how fast heat moved, how well heat transferred, and a number called Nusselt's number over time. By watching how these things changed, we could understand how the system behaved as the PCM changed from liquid to solid while absorbing heat from cold water passing through the tubes.

Graphs and contours were used to show these changes visually, helping to see how the liquid fraction, PCM temperature, water temperature, and heat transfer characteristics changed over time.

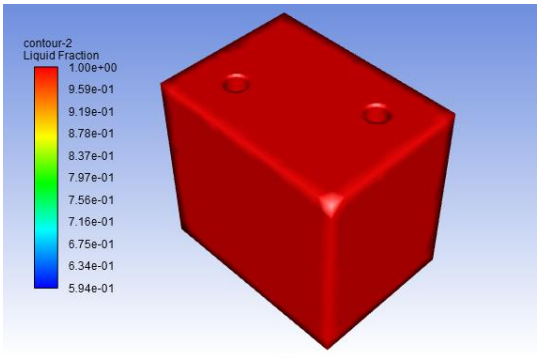

Flow Time: 195 sec

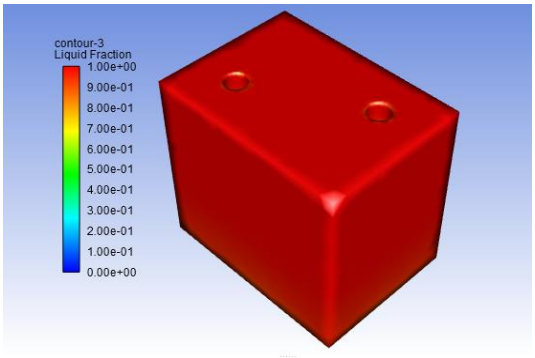

Flow Time: 1245 sec

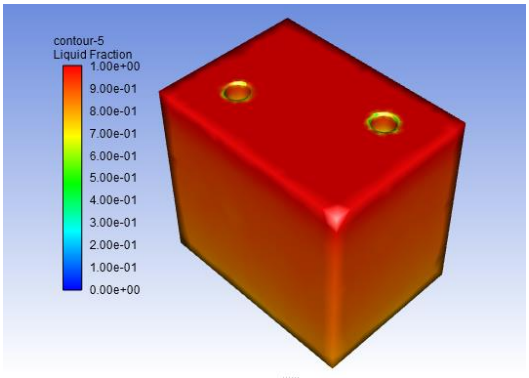

Flow Time: 2136 sec

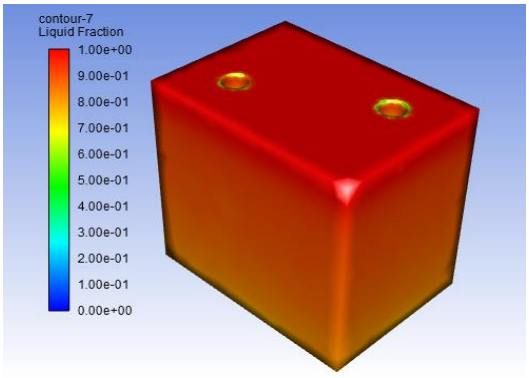

Flow Time: 4725 sec

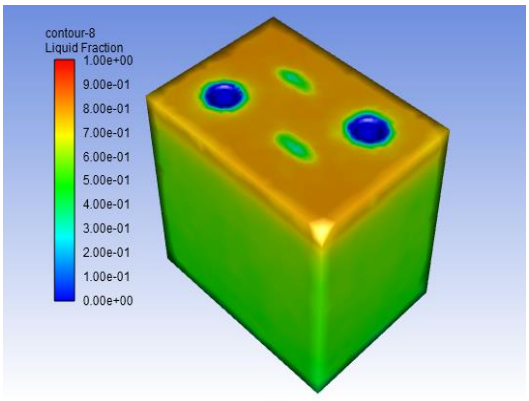

Flow Time: 7706 sec

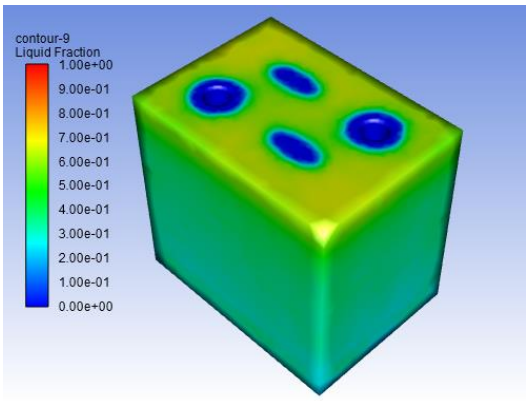

Flow Time: 11503 sec

Figure 4.45: Liquid fraction contours during the solidification of PCM in finned shell & tube arrangement

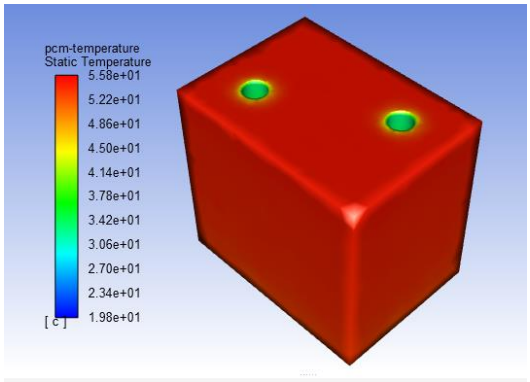

Flow Time:195 sec

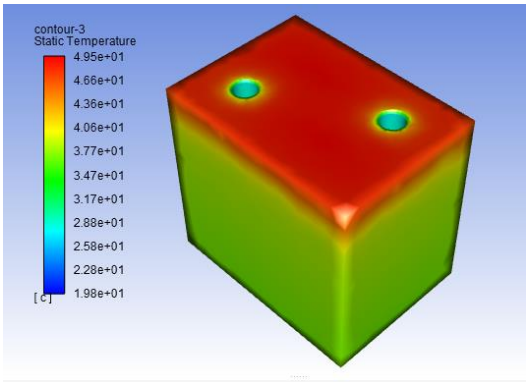

Flow Time: 1245 sec

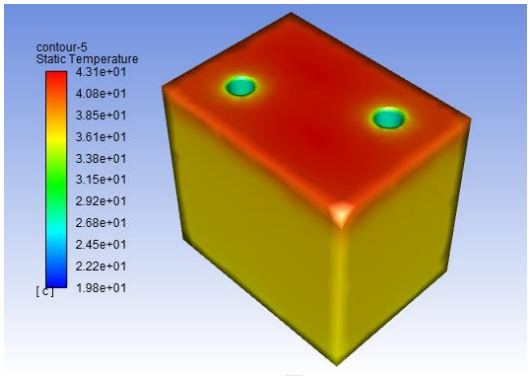

Flow Time:2136 sec

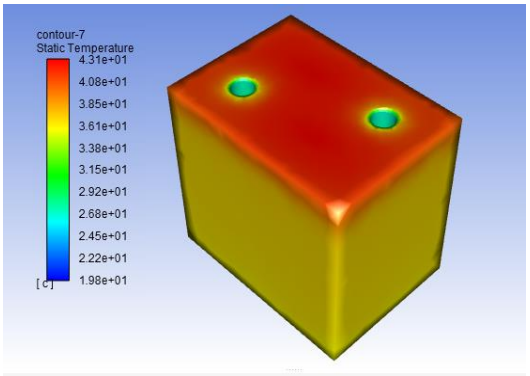

Flow Time: 4725 sec

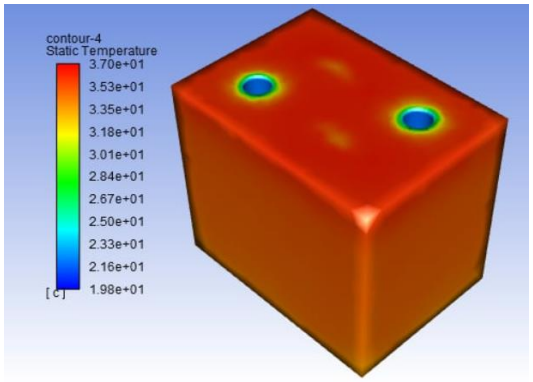

Flow Time: 7706 sec

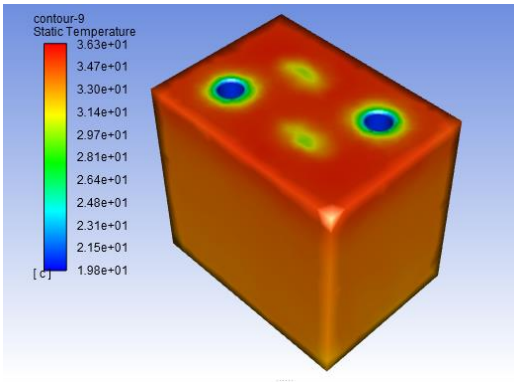

Flow Time: 11503 sec

Figure 4.46: PCM average temperature contours during the solidification of PCM in finned shell & tube arrangement

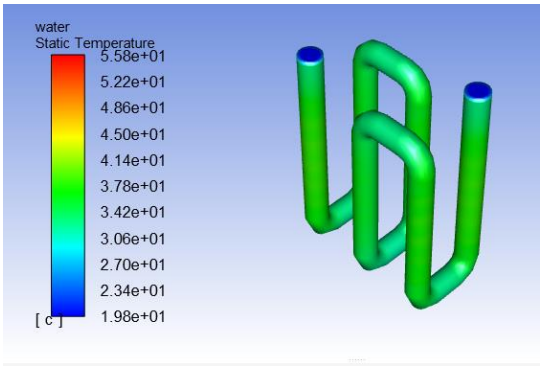

Time Step:195 sec

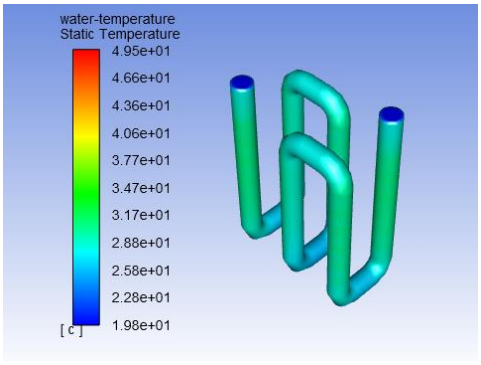

Time Step:1245 sec

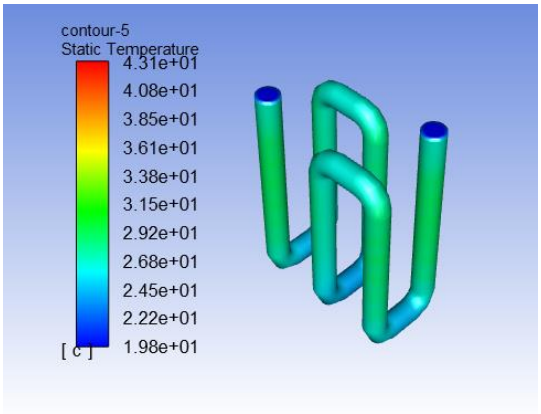

Flow Time: 2136 sec

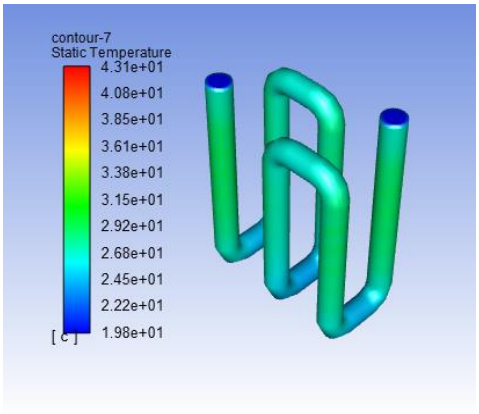

Flow Time: 4725 sec

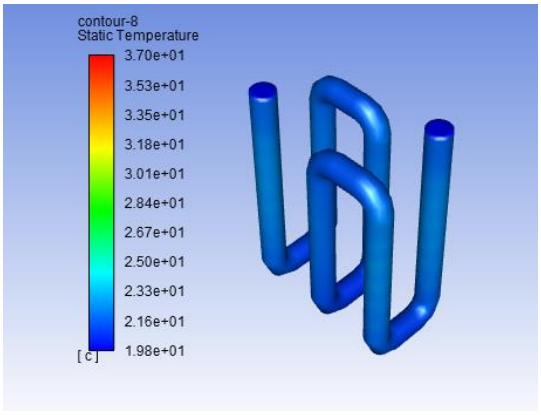

Flow Time: 7706 sec

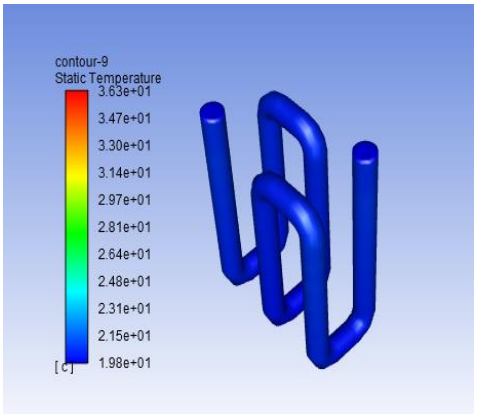

Flow Time: 11503 sec

Figure 4.47: Water temperature contours during the solidification of PCM in finned shell & tube arrangement

The various graphs and charts are shown in the pictures below:

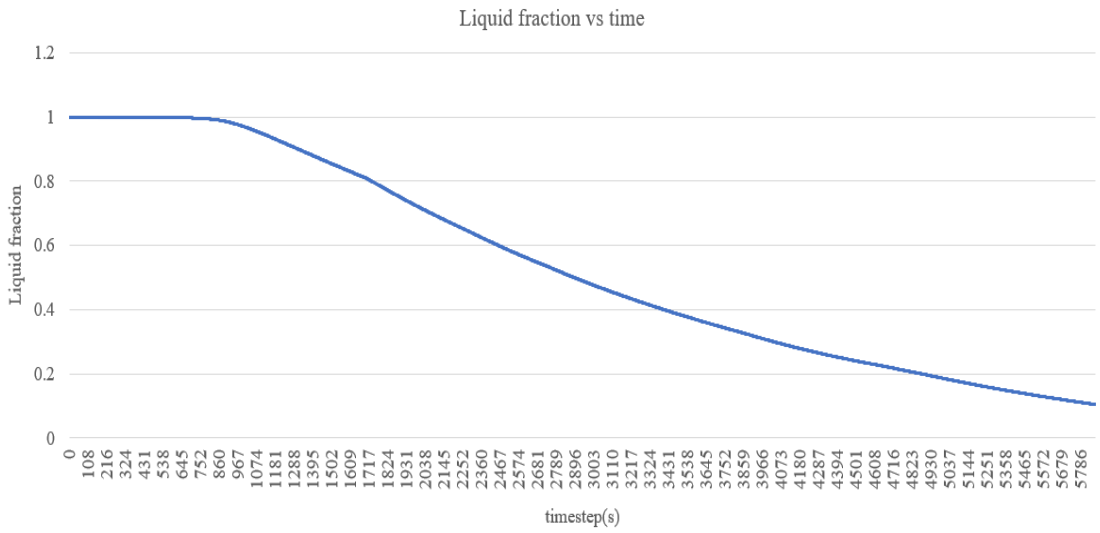

Figure 4.48: Liquid fraction plot during solidification of PCM in finned shell & tube arrangement

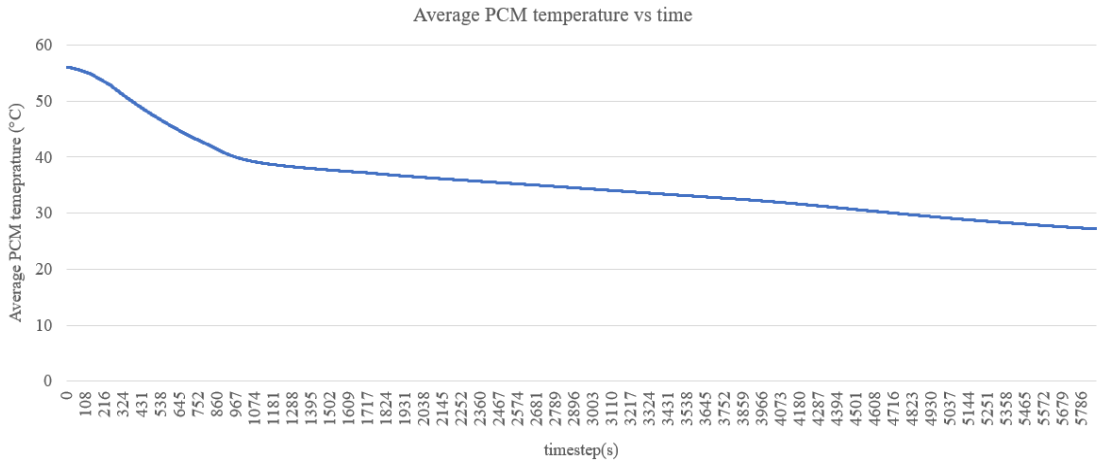

Figure 4.49: Average PCM temperature vs time during solidification of PCM in finned shell & tube arrangement

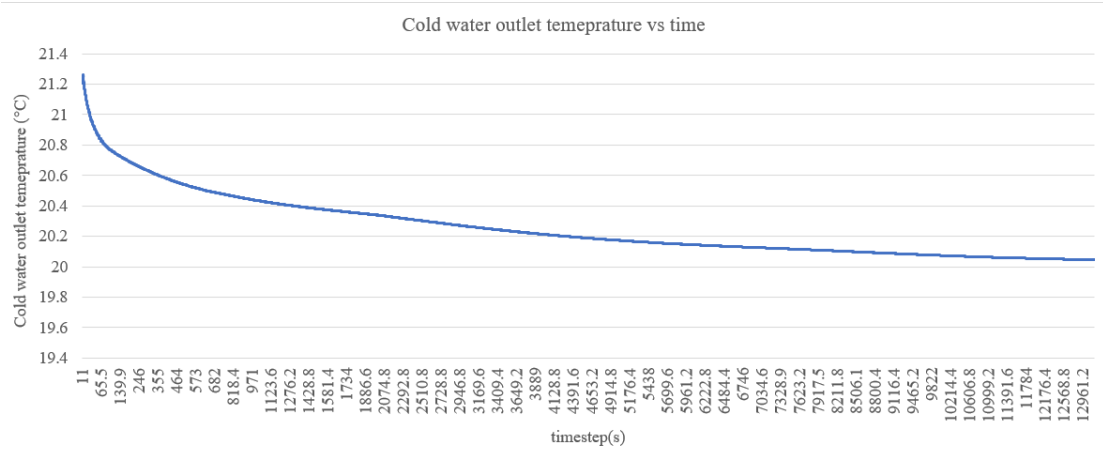

Figure 4.50: Cold water outlet temperature vs time during solidification of PCM in finned shell & tube arrangement

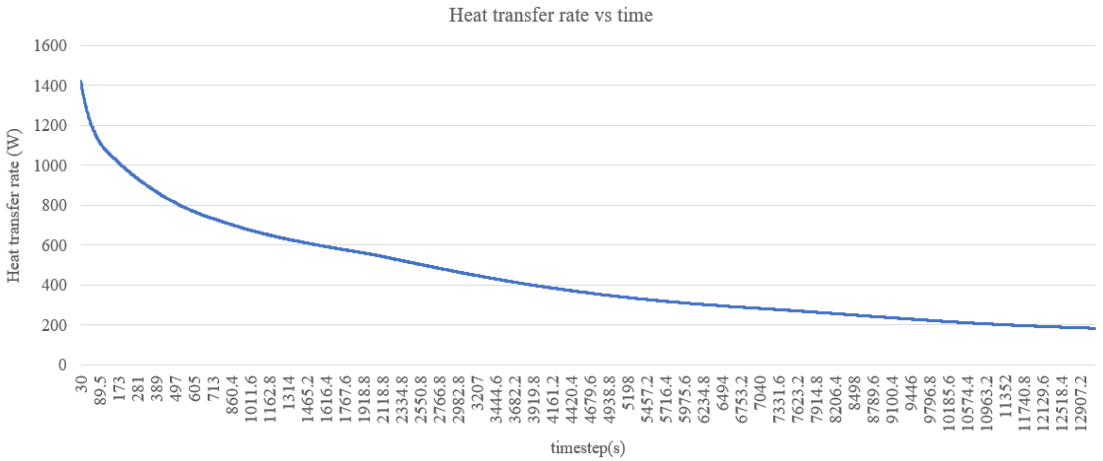

Figure 4.51: Heat transfer rate vs time during solidification of PCM in finned shell & tube arrangement

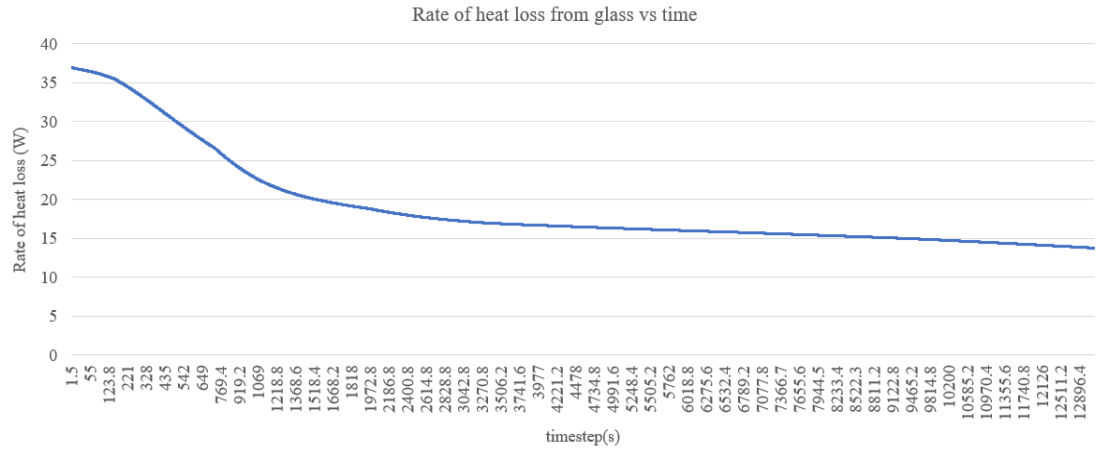

Figure 4.52: Heat loss rate from the glass surface vs time during solidification of PCM in finned shell & tube arrangement

Just like when the PCM melted, the graphs showed that the heat transfer rate decreased over time as the PCM solidified. This happened because as the PCM turned from liquid to solid and got closer in temperature to the cold water, there was less of a difference in temperature, so heat transferred more slowly. This also meant that less heat was lost from the glass surface over time.

To understand how much heat was exchanged, we could look at the area under the graph for the heat transfer rate and time. This would tell us how much heat the cold water gained, and we could use a similar method to figure out how much heat was lost from the glass surface.

Calculating the amount of heat released from the PCM during solidification is similar to what we did when it melted. We consider sensible heat, latent heat, and changes in temperature over time.

Heat released by PCM = $m_p * c_{ps} * (T_m - T_i) + m_p * L_f + m_p * c_{pl} * (T_f - T_m)$

$= 3925.19$ kJ

From graphs, Heat absorbed by cold water =3713.67 kJ

Heat lost from the glass = 225.267 kJ

Through a heat balance analysis, the distribution of heat could be determined as,

Heat released by PCM + Heat released by the Pipes & glass = Heat loss from the glass + Heat absorbed by the cold water

Therefore, Heat released by the pipes & glass = 225.267+3713.67-3925.19 = 13.747 kJ

The overall distribution of the heat can be visually represented by the pie-chart shown below:

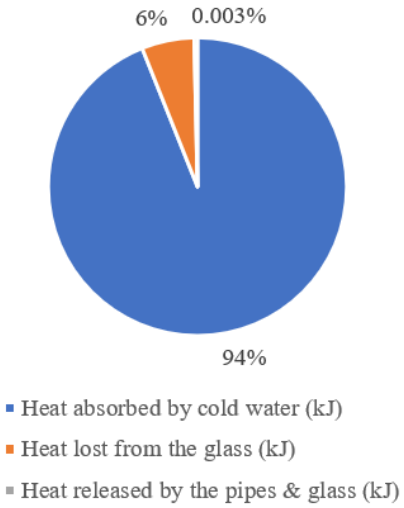

Figure 4.53: Overall heat distribution of the heat released by PCM

Hence, the simulation of PCM solidification provided valuable insights into the thermal behavior of the system and allowed for the assessment of heat transfer processes during the transition from liquid to solid state.

4.5 Comparison of performance of quadruple concentric tube and shell-tube arrangement

After completing the design and simulation of both PCM quadruple pipe concentric tube and PCM shell and tube heat exchangers, an analysis of their performance was done.

Setup Type	Mass of PCM (kg)	Amount of heat stored during melting (KJ)	Time required to melt (min)	Rate of heat storage (KJ/min)	Design complexity	Cost
Quadruple concentric tube	3.4	726.889	29.16667	24.92190	High	High
Shell & Tube	16	4218.632	163.2	25.849	Low	Low

Table 4.14: Comparison of parameters of concentric tube and shell and tube heat exchangers

The results showed that both setups could store heat, but the shell and tube design could hold more heat. However, they both stored heat at nearly the same rate. Despite this, the concentric tube setup's complicated design and higher cost made it less practical to make compared to the shell and tube one.

Also, the analysis found that the shell and tube setup absorbed about 95% of the heat from the hot water, while the concentric tube setup only absorbed around 65%. This big difference shows that the shell and tube setup is better than the concentric tube one.

As a result, only the shell and tube setup was made and tested in the experiment because it's simpler and cheaper to make, which matches the project's goal of using resources efficiently.

4.6 Fabrication and Experimentation

4.6.1 Fabrication & Experimentation procedure

The detailed fabrication procedure followed during the project is explained below:

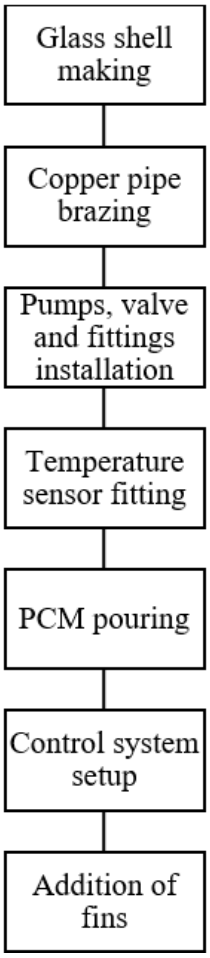

Figure 4.54: Fabrication procedure

i) Making the glass shell: First, the process started by putting together the glass shell, which holds the PCM. Clear glass plates, each 6mm thick, were carefully joined using a special heat-resistant glue. Then, holes were drilled on the top and sides of the glass box for temperature sensors to keep track of how well it works.

ii) Brazing the copper pipes: After finishing the glass shell, attention moved to building the pipes for the heat exchanger. Different sections of copper pipes and bends

were carefully joined together using a special kind of welding with air-acetylene gas. This precise welding ensured that the pipes were strong and wouldn't leak, which is really important for heat transfer to work well.

iii) Installing the pump, valves, and fittings: Once the pipe assembly was done, the focus shifted to putting in all the things needed to move the fluid around. A 0.25hp pump, along with valves like ball valves, fittings, and connecting pipes, were carefully installed. This setup helped make sure that the water flowed smoothly and in the right way through the copper pipes, which is crucial for the heat exchange to happen properly.

Figure 4.55: Pump used

iv) Installing temperature sensors: Making sure we could monitor temperatures accurately throughout the system was really important for evaluating and controlling how well it worked. To do this, temperature sensors were carefully placed in specific spots within the setup. Each sensor was fitted into holes that were pre-drilled on the surface of the glass shell, making sure they were positioned exactly right for dependable temperature readings. After that, to make sure there were no leaks and to keep everything in good shape for a long time, the holes were sealed permanently using a special adhesive called M-seal.

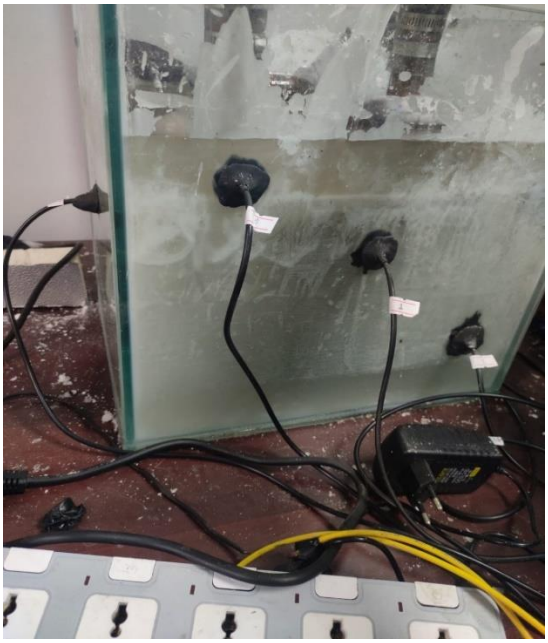

Figure 4.56: Temperature sensors attached to the glass surface

v) Pouring the PCM: After finishing the tube side assembly and installing temperature sensors, attention turned to getting the PCM ready. Paraffin wax, picked as the phase change material, was melted until it became liquid. Then, the melted PCM was poured carefully onto the shell side of the setup, filling up the inside of the glass box. This step made sure that the PCM was used effectively to store thermal energy within the heat exchanger system.

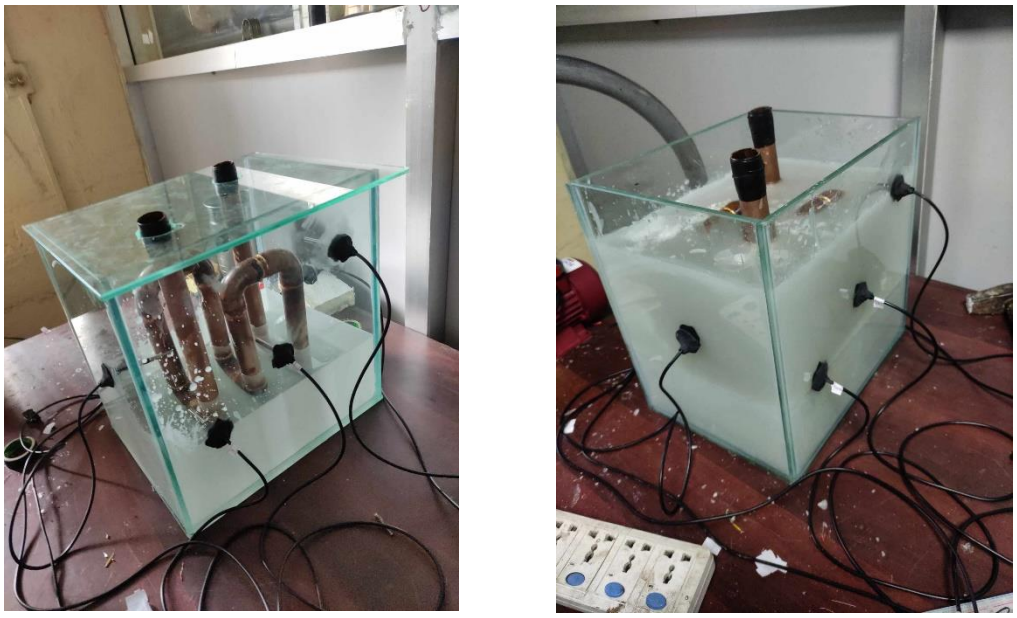

Figure 4.57: PCM being poured

vi) Setting up the control system: In the final stage of fabrication, a complete control system was put in place to monitor and control how the heat exchanger worked. A simple but effective control system, based on an Arduino board, was installed. This board connected to all nine temperature sensors placed around the setup, constantly gathering temperature readings. These readings were then shown in real-time on a computer screen, allowing for a detailed analysis of how the system's temperature changed over time. Additionally, a temperature control thermostat was added to keep the water temperature steady at 60°C during the melting or charging process of the PCM, ensuring that the system worked efficiently. This made sure the system worked well.

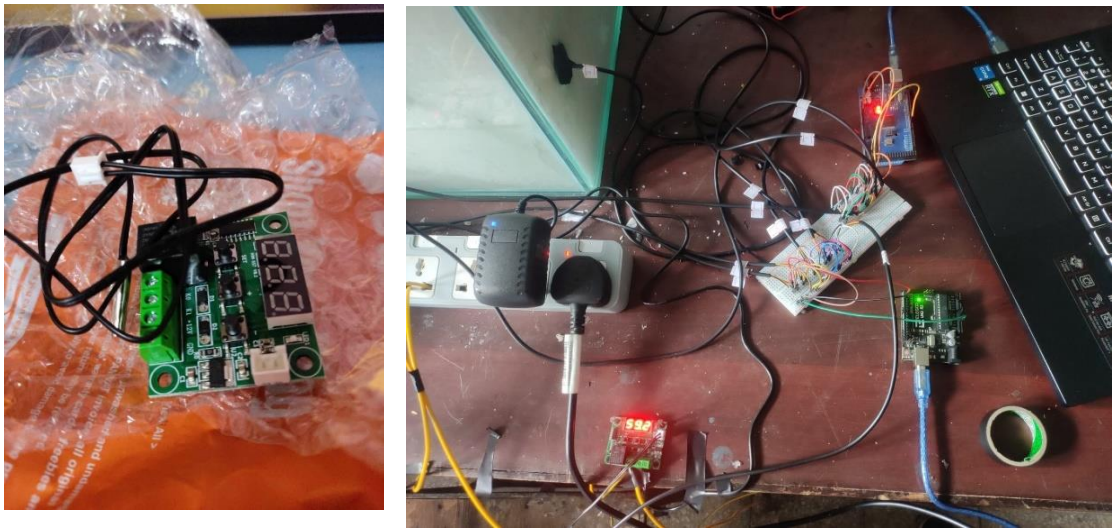

Figure 4.58: Temperature control thermostat and control system

Vi) Adding fins: Following the first test without fins, an improvement to the heat exchanger's performance was made by attaching six copper plate fins, each 2mm thick, to the copper tubes using brazing techniques. This addition aimed to increase the rate at which heat moves within the system. By making the surface area larger for heat exchange, the fins helped heat transfer better between the fluid in the tubes and the surrounding PCM. This change was made to make the heat exchanger work better and store more thermal energy effectively.

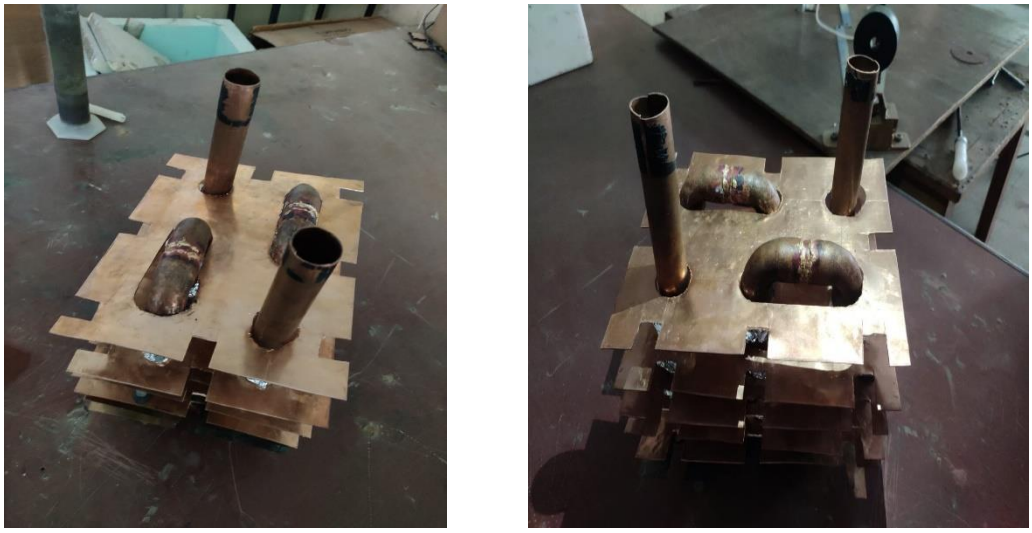

Figure 4.59: Copper tube with plate fins

The detailed experimentation procedure is explained below:

i) System checks and sensor calibration: First, the entire system was carefully inspected to find any possible leaks or damage. This was really important to make sure the setup was safe and working properly. Also, all temperature sensors were checked against known temperatures to make sure they were accurate and dependable. This checking process was crucial to get precise temperature readings during the experiment.

ii) Experiment of the setup: After finishing the experiment without fins, plate fins were added onto the copper tubes to make heat transfer faster. These plate fins were firmly attached to the tubes using brazing. Then, the experiment was done again, following the same steps as before. Hot water was sent through the pipe at a rate of 10 liters per minute, followed by cold water at 18 liters per minute to make the PCM solidify. During both parts of the experiment, temperatures at the inlet, outlet, and PCM locations were measured using digital temperature sensors connected to the Arduino board.

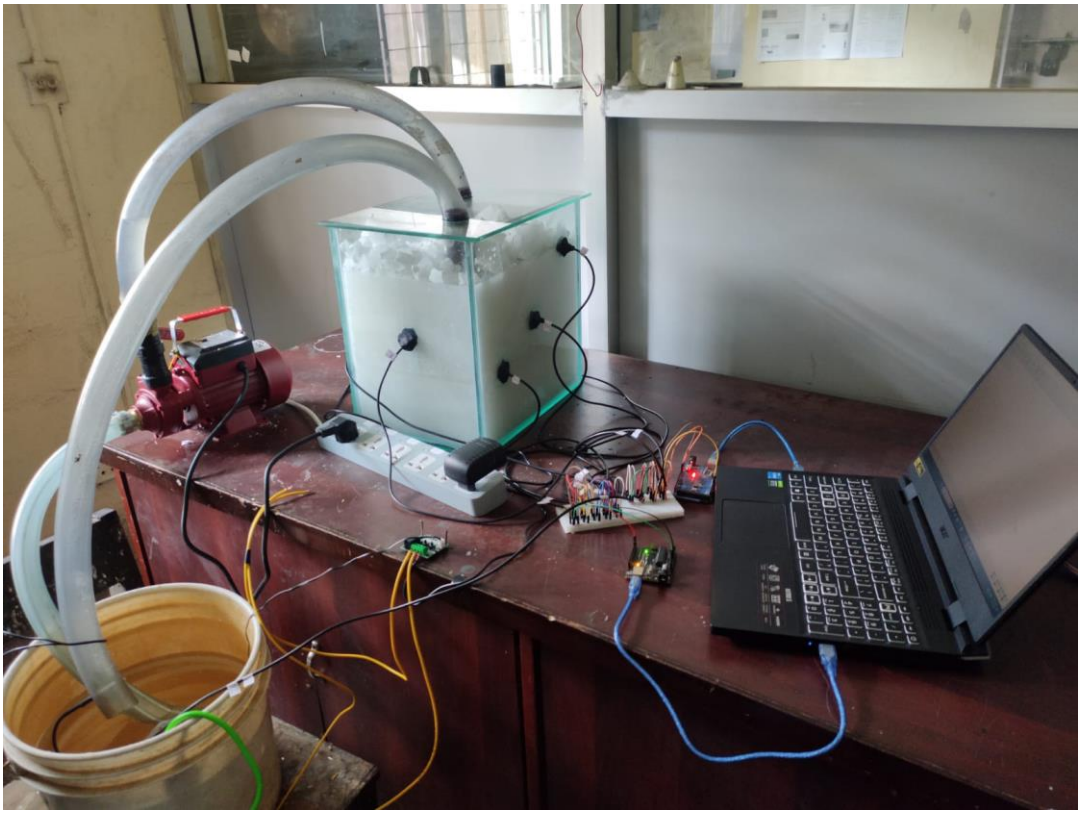

Figure 4.60: Overall experimental setup

4.6.2 Experimentation Results & Discussion

Once the fabrication and testing were done, the experiment moved on to the setup with fins. This involved two main phases: first, hot water flowed to melt the PCM, and then cold water flowed to solidify it.

4.6.2.1 Melting/charging

Hot water at 60^{o}C was passed through the tube at a uniform flow rate of 10 LPM for the melting of PCM. The temperature readings obtained from the sensors and the necessary calculations are shown in the graphs below.

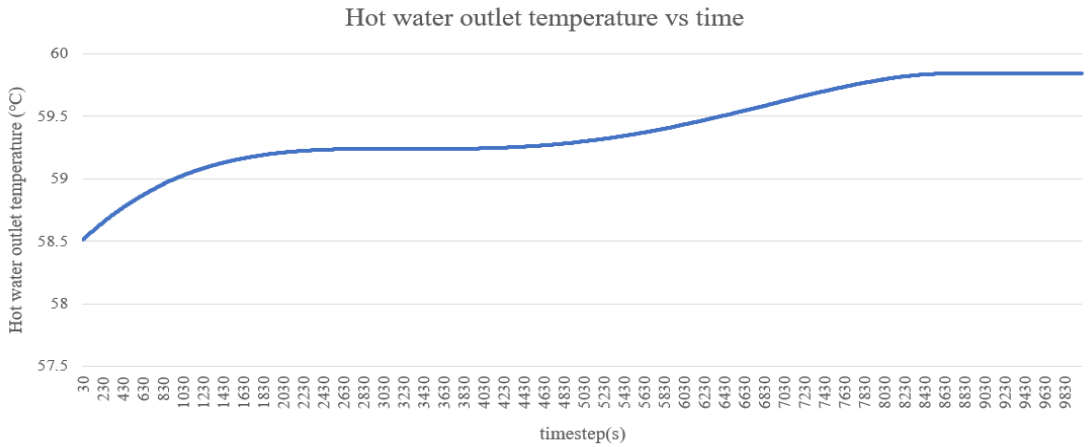

Figure 4.61: Experimental average PCM temperature variation over time during melting in finned shell & tube arrangement

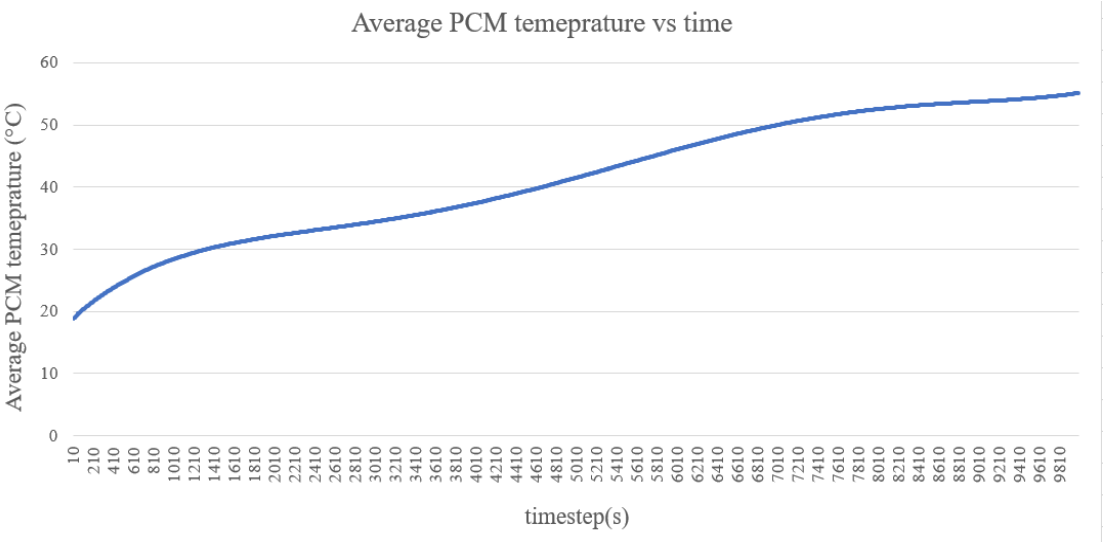

Figure 4.62: Experimental hot water temperature variation over time during melting in finned shell & tube arrangement

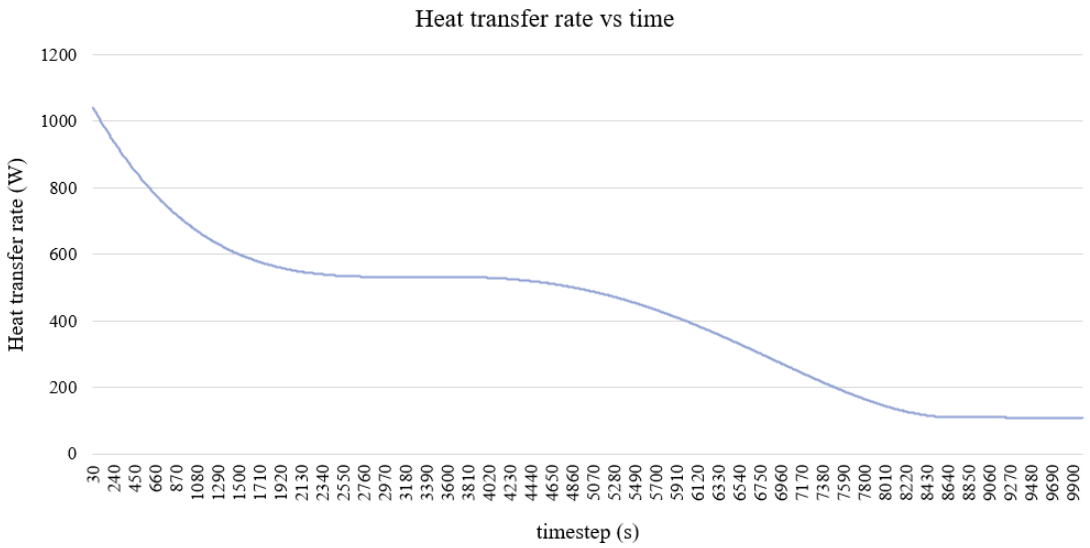

Figure 4.63: Experimental heat transfer rate variation over time during melting in finned shell & tube arrangement

As seen in the graphs above, the PCM temperature measured by the digital sensors keeps going up steadily as it absorbs heat from the hot water. Starting from a room temperature of 19°C, the PCM reached its melting point of about 53°C in around 10,000 seconds (or roughly 3 hours), which is a bit higher than what we expected from the simulation. This difference could be because of extra heat loss from the pipes and changes in how well heat transfers in the surroundings, which weren't included in the simulation.

Meanwhile, the temperature of the hot water going out started at 60°C and dropped to 58°C at first, with the difference getting smaller over time. This happened because the rate at which heat moved between the PCM and the hot water slowed down. Also, the graph showing the heat transfer rate over time shows that the rate of heat transfer decreased as time went on. This was because the difference in temperature between the PCM and hot water got smaller, and the heat transfer ability of the PCM decreased over time.

To figure out how much heat the hot water lost and how much heat the PCM stored, we can use the area under the graph showing the heat transfer rate over time. We can also calculate the heat stored in the pipes using a basic heat equation. By adding up all these numbers, we can find out how much heat was lost and how much was stored in the system.

Theoretical heat stored in PCM = $m_p*c_{ps}*(T_m - T_i) + m_p*L_f + m_p*c_{pl}*(T_f - T_m)$
= 4186.63 KJ

From the graph, Heat lost by the hot water = 4423.667 KJ

By heat balance,

Heat lost by hot water = Heat stored in PCM + Heat lost from the glass and stored in glass and pipe

So, heat lost from the glass and stored in glass and pipe =4423.667 - 4186.63 = 237.03 KJ

The overall distribution of the heat can be visually represented by the pie-chart shown below:

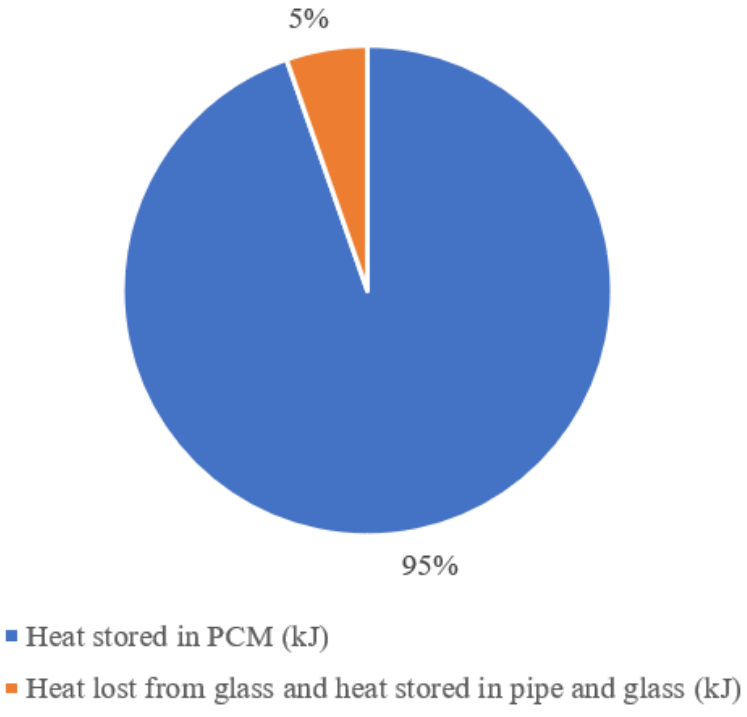

Figure 4.64: Overall heat distribution of the heat lost by hot water

4.6.2.2 Solidification/discharging

Cold water at 18°C was passed through the tube at a uniform flow rate of 18 LPM for the solidification of PCM. The temperature readings obtained from the sensors and the necessary calculations are shown in the graphs below.

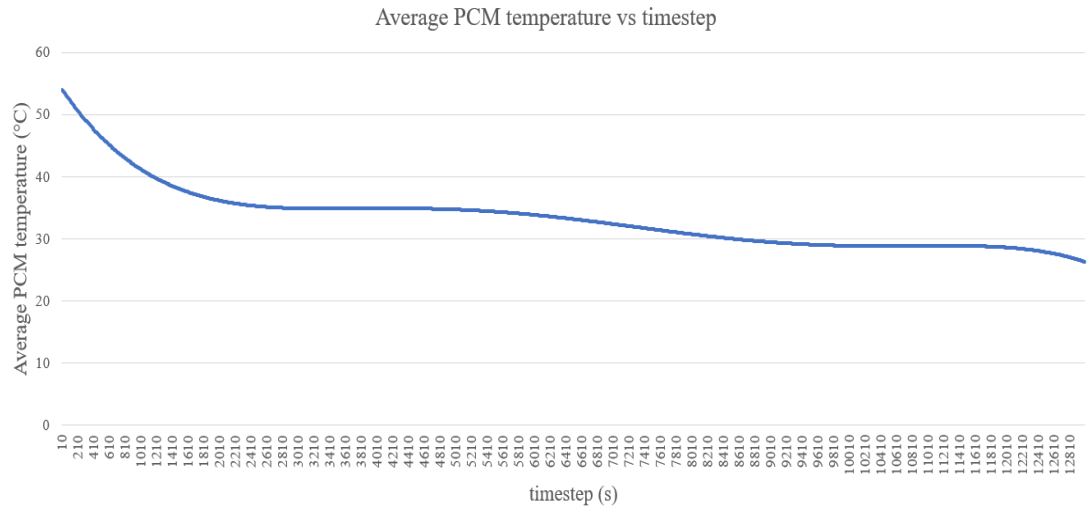

Figure 4.65: Experimental average PCM temperature variation over time during solidification in finned shell & tube arrangement

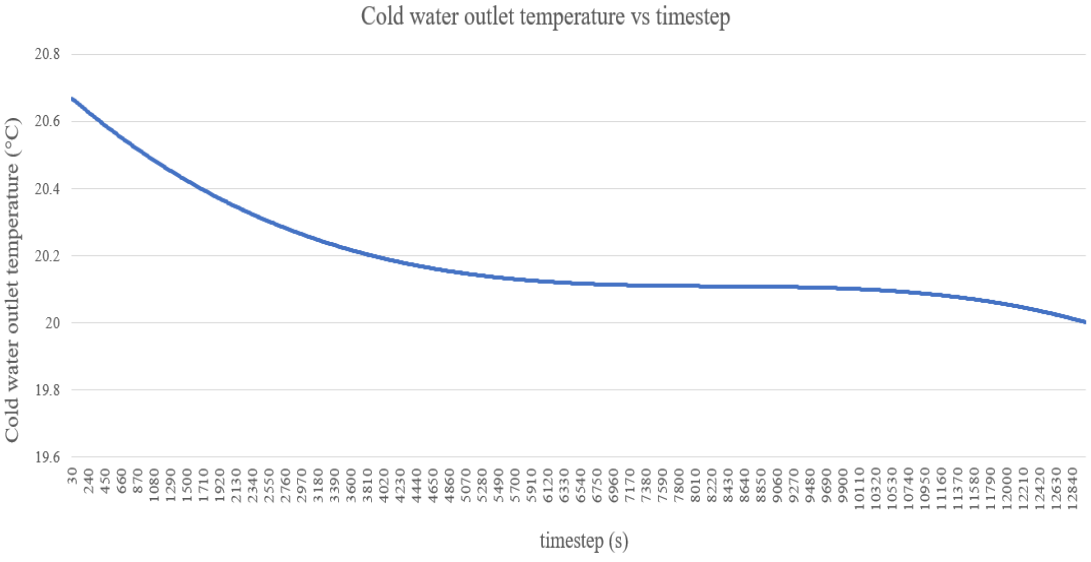

Figure 4.66: Experimental cold water outlet temperature variation over time during solidification in finned shell & tube arrangement

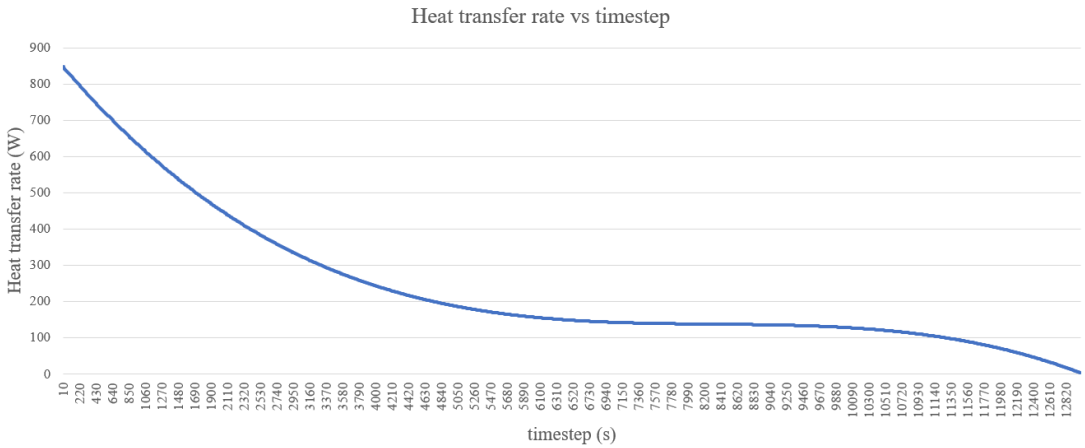

Figure 4.67: Experimental heat transfer rate variation over time during solidification in finned shell & tube arrangement

During the solidification of the PCM, the average PCM temperature went down gradually because the heat stored in the PCM was being lost to the cold water. At first, the temperature of the cold water coming out went up from the room temperature of 18°C to 21°C, but this difference got smaller over time because the rate at which heat moved between the PCM and cold water slowed down. Looking at the graph showing the heat transfer rate over time, we can see that the rate of heat transfer decreased gradually, which happened because the temperature difference between the PCM and cold water got smaller.

By using a similar method to the heat balance we used before, we can create a chart that shows how heat is distributed within the system accurately.

Heat released by PCM = $m_p*c_{ps}*(T_m - T_i) + m_p*L_f + m_p*c_{pl}*(T_f - T_m)$ = 3962.632 KJ

From graphs, Heat absorbed by cold water = 3524 KJ

Through a heat balance analysis, the distribution of heat could be determined as,

Heat released by PCM + Heat released by the Pipes & glass = Heat loss from the glass + Heat absorbed by the cold water

Therefore, Heat loss from the glass - Heat released by the pipes & glass = 3962.632 - 3524.327 = 438.305 KJ

4.7 Challenges and Limitations

Throughout this project, there are several restrictions and issues that arises, some of which are stated below:

a) This project required specialized materials such as phase change materials (PCMs), which were difficult to obtain in large quantities.
b) The design simulation required computers with high computational power due to the complicated geometry and analysis of the system.
c) The PCM layer and additional pipes made this heat exchanger more expensive than a conventional heat exchanger.
d) Accessing specific tools or machinery required for fabrication or testing, particularly for intricate components like the PCM layer, posed a challenge due to their limited availability or high cost.
e) Combining various parts like fins and PCM layers in a heat exchanger design was tricky to put together. Ensuring everything fitted correctly and sealed tightly to avoid leaks was a challenge during assembly.

4.8 Problems Faced

- Difficulty in generating an appropriate mesh for complex geometries, especially in the case of finned surfaces.
- Limited availability of high-performance computing resources for running simulations might have prolonged the simulation process
- Specifying accurate and realistic boundary conditions for different parts of the heat exchanger, such as contact interfaces.
- Obtaining accurate thermophysical properties for materials, including the phase change properties of PCM, was challenging due to experimental uncertainties or limited data availability.
- Setting up experiments to accurately measure temperature, flow rates may have encountered technical difficulties such as system instability, affecting the reliability of the collected data.

4.9 Budget Analysis

Particulars	Rate (Rs.)	Quantity	Price (Rs.)
Copper Pipes	5,700	-	5,700
Water Pumps and fittings	4,700	-	4,700
PCM	4,604	-	4,640
Glass	3,950	-	3,950
Glass silicon joining	1,000		1,000
Temperature controller, sensors and Arduino	5,685	-	5,685
Heating rod	700	-	700
Copper Plates	1,500		1,500
Documentation	5,000/-	-	5,000
Man Hour	-	-	-
Miscellaneous	5,000/-	-	5,000
Total			37,875

Table 4.15: Budget Analysis

4.10 Work schedule

Task	Start date	End date	Duration (Days)
Literature Review	19-Jun-23	4-Apr-24	290
Proposal Writing	22-Jun-23	27-Jun-23	5
Design and calculation of Double Pipe Heat Exchanger	12-Jul-23	5-Aug-23	24
Simulation of Double Pipe Heat Exchanger	6-Aug-23	22-Aug-23	16
Design and Calculation of Finned Double Pipe Heat Exchanger	25-Aug-23	18-Sep-23	24
Simulation and Analysis of Finned Double Pipe Heat Storage	19-Sep-23	25-Nov-23	67
Design and Calculation of PCM Pipe Heat Exchanger	26-Nov-23	20-Dec-23	24
Simulation and Analysis of PCM	20-Dec-23	10-Jan-24	21
Design and calculation of Shell and Tube Heat Exchanger	5-Jan-24	10-Jan-24	5
Simulation and Analysis of Shell and Tube Heat Storage	10-Jan-24	2-Feb-24	23
Accumulating Material	1-Feb-24	1-Mar-24	29
Fabrication	5-Feb-24	2-Mar-24	26
Experimentation and Data Collection	20-Feb-24	4-Mar-24	13
Documentation	19-Jul-23	5-Apr-24	292
Final Report Preparation	1-Apr-24	6-Apr-24	5

Table 4.16: Time scheduling

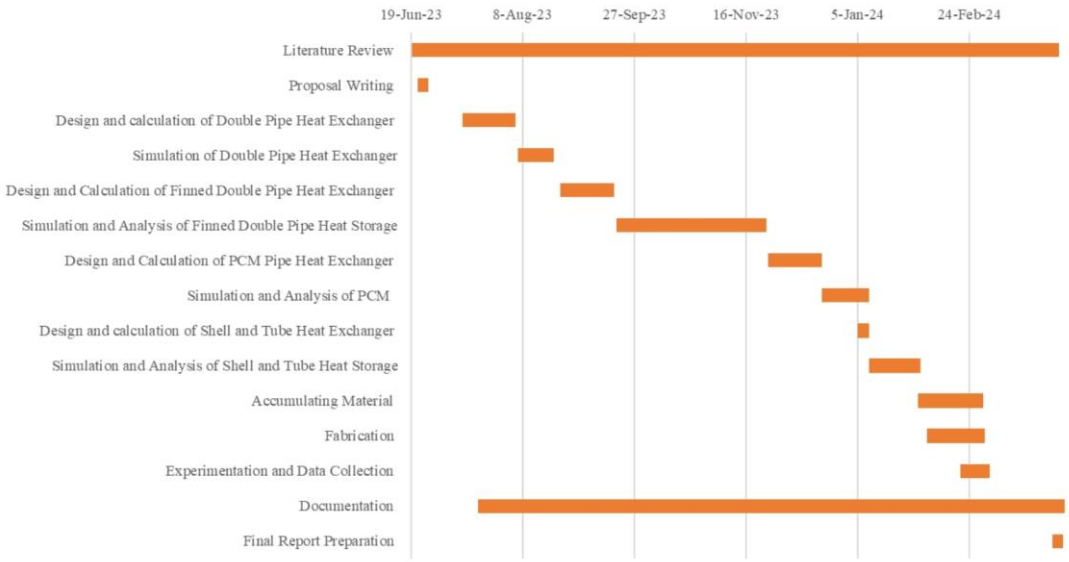

Figure 4.68: Gantt chart

CHAPTER FIVE: CONCLUSION AND FUTURE ENHANCEMENT

5.1 Conclusion

The project aimed to create and test thermal energy storage systems using heat exchangers with phase change materials (PCMs). It started by designing traditional double pipe and shell & tube heat exchangers, adding features like fins and PCM integration to improve their efficiency and storage capacity. These designs considered material choice, optimizing water flow, and making sure the structure was strong enough to build on later. Detailed computer simulations were done for both designs using ANSYS Fluent to see how they performed in different situations, including when the PCM changed phases. After making sure the simulations were accurate, we built and tested the shell & tube PCM heat storage system. We compared the results with what we expected to see how well the system worked in real-life conditions.

Here are some key findings from the project:

1. Both double pipe and shell & tube designs stored heat at similar rates.
2. The shell & tube design was simpler, cheaper, and stored heat more efficiently than the double pipe design.
3. Small differences between what we expected and what we saw in experiments were because of things like changes in properties of the PCM and heat transfer characteristics.
4. Theoretical models and computer simulations were confirmed to be effective.
5. These designs could be used in solar thermal systems, HVAC systems, and industrial processes because they can be scaled up and adapted.
6. Future work might focus on making the designs even better, trying different PCM materials, and connecting them to renewable energy systems to use energy more efficiently and make the power grid more stable.

5.2 Scope for Future Enhancement

To enhance thermal energy storage systems, future improvements can focus on several key areas. Exploring alternative phase change materials (PCMs) offers the potential to customize the system to specific requirements by using different thermo-physical properties. By incorporating different PCMs, such as salts or fatty acids, we can increase heat storage capacity and the range of operating temperatures. Additionally, adding nanofluids to the PCM matrix could improve thermo-physical properties and heat transfer characteristics, boosting overall system performance.

Optimizing fin geometries within the heat exchangers shows promise for increasing heat transfer rates. Experimenting with alternative fin configurations, like pin fins or vortex generators, could enhance heat exchange efficiency by promoting turbulence and disrupting boundary layers. Integrating these advanced thermal energy storage systems with renewable energy sources, such as solar heating systems, also presents an exciting opportunity. By combining the storage systems with solar collectors, excess thermal energy can be efficiently captured and stored for later use, contributing to improved energy utilization and grid stability. Similarly, connecting with HVAC systems offers opportunities for load shifting and demand management, leading to energy savings and environmental sustainability. Through these avenues of exploration and innovation, the future of thermal energy storage systems promises significant advancements towards a more sustainable energy future.

REFERENCES

Y. A. Çengel and A. J. Ghajar, *Heat and Mass Transfer: Fundamentals and Applications*. 2019.

L. Kalapala and J. K. Devanuri, "Influence of operational and design parameters on the performance of a PCM based heat exchanger for thermal energy storage – A review," *Journal of Energy Storage*, vol. 20, pp. 497–519, Dec. 2018, doi: 10.1016/j.est.2018.10.024.

H. Garg, B. K. Pandey, S. Chakraborty, S. Singh, and R. Banerjee, "Design and analysis of PCM based radiant heat exchanger for thermal management of buildings," *Energy and Buildings*, vol. 169, pp. 84–96, Jun. 2018, doi: 10.1016/j.enbuild.2018.03.058.

A. H. N. Al-Mudhafar, A. Nowakowski, and F. C. G. A. Nicolleau, "Enhancing the thermal performance of PCM in a shell and tube latent heat energy storage system by utilizing innovative fins," *Energy Reports*, vol. 7, pp. 120–126, May 2021, doi: 10.1016/j.egyr.2021.02.034.

D. G. Lee and C. Kang, "A study on development of the thermal storage type plate heat exchanger including PCM layer," *Journal of Mechanical Science and Technology*, vol. 33, no. 12, pp. 6085–6093, Dec. 2019

Y. Tao and Y.-L. He, "A review of phase change material and performance enhancement method for latent heat storage system," *Renewable & Sustainable Energy Reviews*, vol. 93, pp. 245–259, Oct. 2018

M. Sheikholeslami, R. U. Haq, A. Shafee, and Z. Li, "Heat transfer behavior of nanoparticle enhanced PCM solidification through an enclosure with V shaped fins," *International Journal of Heat and Mass Transfer*, vol. 130, pp. 1322–1342, Mar. 2019, doi: 10.1016/j.ijheatmasstransfer.2018.11.020.

G. Wei *et al.*, “Selection principles and thermophysical properties of high temperature phase change materials for thermal energy storage: A review,” *Renewable & Sustainable Energy Reviews*, vol. 81, pp. 1771–1786, Jan. 2018, doi: 10.1016/j.rser.2017.05.271.

D. Laing, T. W. Bauer, N. Breidenbach, B. Hachmann, and M. Johnson, “Development of high temperature phase-change-material storages,” *Applied Energy*, vol. 109, pp. 497–504, Sep. 2013, doi: 10.1016/j.apenergy.2012.11.063.

N. L. Narasimhan, “Assessment of latent heat thermal storage systems operating with multiple phase change materials,” *Journal of Energy Storage*, vol. 23, pp. 442–455, Jun. 2019, doi: 10.1016/j.est.2019.04.008.

C. Voelker, O. Kornadt, and M. Ostry, “Temperature reduction due to the application of phase change materials,” *Energy and Buildings*, vol. 40, no. 5, pp. 937–944, Jan. 2008, doi: 10.1016/j.enbuild.2007.07.008.

J. M. P. Da Cunha and P. C. Eames, “Thermal energy storage for low and medium temperature applications using phase change materials – A review,” *Applied Energy*, vol. 177, pp. 227–238, Sep. 2016, doi: 10.1016/j.apenergy.2016.05.097.

M. R. Hosseini, M. Rahimi, and R. Bahrampoury, “Experimental and computational evolution of a shell and tube heat exchanger as a PCM thermal storage system,” *International Communications in Heat and Mass Transfer*, vol. 50, pp. 128–136, Jan. 2014, doi: 10.1016/j.icheatmasstransfer.2013.11.008.

A. Trp, K. Lenić, and B. Franković, “Analysis of the influence of operating conditions and geometric parameters on heat transfer in water-paraffin shell-and-tube latent thermal energy storage unit,” *Applied Thermal Engineering*, vol. 26, no. 16, pp. 1830–1839, Nov. 2006, doi: 10.1016/j.applthermaleng.2006.02.004.